SYNTHESIS, CHARACTERISATION AND CATALYTIC REACTIONS OVER METALPHOSPHATE MOLECULAR SIEVES

A THESIS

SUBMITTED TO THE

UNIVERSITY OF POONA

FOR THE DEGREE OF

DOCTOR OF PHILOSOPHY

(IN CHEMISTRY)

BY

Mrs. KANCHAN RAMCHANDRA KAMBLE

M. Sc.

INORGANIC CHEMISTRY DIVISION

NATIONAL CHEMICAL LABORATORY

PUNE - 411 008 (INDIA)

JANUARY 1989

DEDICATED

TO

MY HUSBAND

Certified that the work incorporated in the thesis titled " SYNTHESIS, CHARACTERISATION AND CATALYTIC REACTIONS OVER METAL PHOSPHATE MOLECULAR SIEVES ", submitted by Mrs. Kanchan Ramchandra Kamble, was carried out under my supervision. Such materials as has been obtained from other sources are duly acknowledged in the thesis.

DR PAUL RATNASAMY

ACKNOWLEDGEMENT

I wish to record my deep sence of gratitude to Dr. P. Ratnasamy, for his meticulous planning of this investigation, inspiring guidance and encouragement which made this work possible.

I specially express my deep gratitude to Dr. (Miss) S.B. Kulkarni, and Dr. S.G. Hegde, for their valuable advise, suggestions, and constant encouragement. Without their help, I would not have been able to complete this work.

Thanks are due to Dr (Mrs) A.J. Chandwadkar and Dr. V.P. Shiralkar, colleagues and friends from the Catalysis and SIL groups, for their wholehearted cooperation during the course of this work.

I thank Mr. S.M. Kulkarni and Mr. P.K. Purushotham, who completed the typing work in a very short time. Also I thank Mr. N.C. Benjamin, for xeroxing this thesis.

I wish to offer my sincere thanks to the Director, National Chemical Laboratory, Pune, for allowing me to submit this investigation in the form of thesis to the University of Pune, for the Ph.D degree.

K.R. Kamble

(K.R. KAMBLE)

Place : Pune

Date : January 1989

C O N T E N T S

C H A P T E R – I

I N T R O D U C T I O N

1.1. INTRODUCTION

Molecular sieves comprising of the crystalline aluminosilicates (zeolites) are well known. More than 150 species of both naturally occurring and synthetic compositions of aluminosilicates have been reported (1). They are formed by corner sharing of AlO_4 and SiO_4 tetrahedra and are characterised by pore openings of uniform dimensions. They exhibit significant ion exchange capacity and reversible sorption capacities filling the internal voids of the crystals. Synthetic zeolites of the type A and X, discovered by Milton as early as 1940, are aluminium rich and were first introduced (2) commercially for adsorptive and catalytic applications, respectively. During the next 20 years more silicious zeolite framework structures such as zeolite Y and mordenite (zeolon) were reported (3,4) and commercialised. Further progress in the zeolite research was the introduction of Beta and ZSM-5 by Wadlinger et al. (5) and Argauer and Landolt (6), respectively. The total elimination of aluminium in the framework led to the silica molecular sieves typified by silicalite.

1.2 MICROPOROUS ALUMINIUM PHOSPHATE MOLECULAR SIEVES

The Union Carbide laboratories have discovered and reported (7) a new generation of molecular sieves having framework compositions comprising of AlO_2^- and PO_2^+ tetrahedra. Based on the known crystal chemistry of framework oxides aluminium and phosphorous were the first elements explored as the tetrahedral framework cations in phosphate molecular sieves. Initial success

resulted in the discovery of the aluminium phosphate molecular sieves (AlPO-n) reported in 1982 by Wilson et al. (8,9,10). The substitution of silicon for aluminium and phosphorous in the framework resulted in the silico alumino phosphate (SAPO-n) molecular sieves which were disclosed in a patent by Lok et al. (11) in 1984. The metal aluminophosphate (MeAPO-n) molecular sieves with frameworks containing aluminium, phosphorous and metal cations where Me is Mg^{2+}, Mn^{2+}, $Fe^{2+,3+}$, Co^{2+} and Zn^{2+} were patented by Messina et al. (12) and Wilson et al. (13) in 1985 and 1986. Recently, Flanigen et al. (14) in an extensive review have reported incorporation of fourteen elements viz. Li, Be, B, Mg, Si, Ti, Mn, Fe, Co, Cu, Zn, Ga, Ge and As into the aluminophosphate framework. The resulting new generation of crystalline microporous molecular sieves comprise nearly 200 compositions with more than two dozen known as well as some of the new structures.

Aluminophosphate molecular sieves are the first reported novel class of crystalline microporous oxide framework structures synthesised without silica (8,9,15,16). These molecular sieves are similar to zeolites in some properties and it has been claimed that these may be used as adsorbents, catalysts and catalyst supports. The new AlPO-n family currently includes about twenty three-dimensional framework structures (Table 1.1) of which at least fourteen are microporous and six are two-dimensional layer type materials. Most of the three-dimensional structures are novel (e.g. $AlPO_4$-5, 11, 14,16,18,31 and 33). However, they appear to be structurally related to the zeolite

TABLE 1.1

TYPICAL STRUCTURES IN $AlPO_4$ BASED MOLECULAR SIEVES

Species	Structure type	Pore size nm	Sat. H_2O vol.cc/gm.	Species	Structure type	Pore size nm	Sat. H_2O vol.cc/gm.
Large pore				Very small pore			
5	Novel(d)	0.80	0.31	16	Novel	0.30	0.34
36	Novel	0.80	0.31	20	Sodalite	0.30	0.24
37	Faujasite	0.80	0.35	25	Novel	0.30	0.17
40	Novel	0.70	0.33	28	Novel	0.30	0.21
46	Novel(d)	0.70	0.28				
Intermediate pore				Small pore			
11	Novel(d)	0.60	0.16	14	Novel(d)	0.40	0.19
31	Novel	0.65	0.17	17	Erionite	0.43	0.28
41	Novel	0.60	0.22	18	Novel	0.43	0.35
				26	Novel	0.43	0.23
				33	Novel	0.40	0.23
				34	Chabazite	0.43	0.30
				35	Leugnite	0.43	0.30
				39	Novel	0.40	0.23
				42	Linde type A	0.43	0.30
				43	Gismondine	0.43	0.30
				44	Chabazite	0.43	0.34
				47	Chabazite	0.43	0.30

(d) = Determined, Ref: 14.

family with framework topologies of erionite offertite ($AlPO_4$-17), the sodalite type ($AlPO_4$-20) and the analcime type ($AlPO_4$-24). One of the novel three-dimensional structures namely $AlPO_4$-5 has hexagonal symmetry with a=1.37 nm and c=0.847 nm and contains unidimensional channels oriented parallel to the c axis and bounded by 12-membered rings of AlO_4 and PO_4 tetrahedra (16) as shown in Fig.1.1.

1.3. HISTORICAL BACKGROUND

Silicon and aluminium are not unique in their ability to form tetrahedrally coordinated oxide net works. The element phosphorous at the right of silicon in the Periodic Table frequently assumes tetrahedral coordination with oxygen. Aluminium phosphate possesses many structural similarities to silica with phosphorous in the +5 oxidation state: (1) $AlPO_4$ is isoelectronic with Si_2O_4, (2) The average ionic radii of Al^{3+} (0.39 nm) and P^{5+} (0.17 nm) is 0.28 nm, very close to the ionic radius of Si^{4+} (0.26 nm) (17), (3) $AlPO_4$ and SiO_2 form isomorphic dense phases with Al^{3+} alternating with P^{5+} in a tetrahedral oxide framework. There are dense phases of $AlPO_4$ corresponding to seven structural forms of SiO_2, alfa, beta-quartz, alfa, beta and gama tridymite and alfa and beta cristobalites (18). These structural similarities between $AlPO_4$ and SiO_2 served as a stimulus for examining alumino phosphates as a potential source of microporous framework structures. The second stimulus was the availability of extenive literature and easy method of hydrothermal synthesis for many aluminosphosphate materials. Two hydrated meta stable forms of

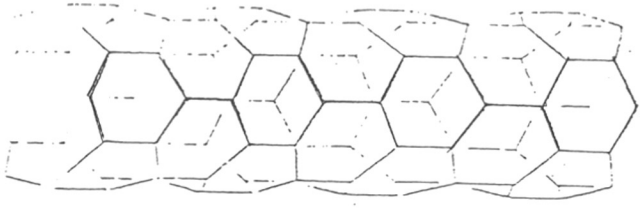

Cylindrical channel of $AlPO_4$-5

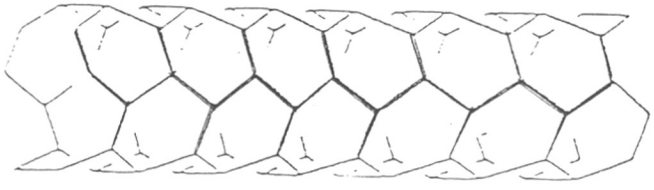

Cylindrical channel of cancrinite

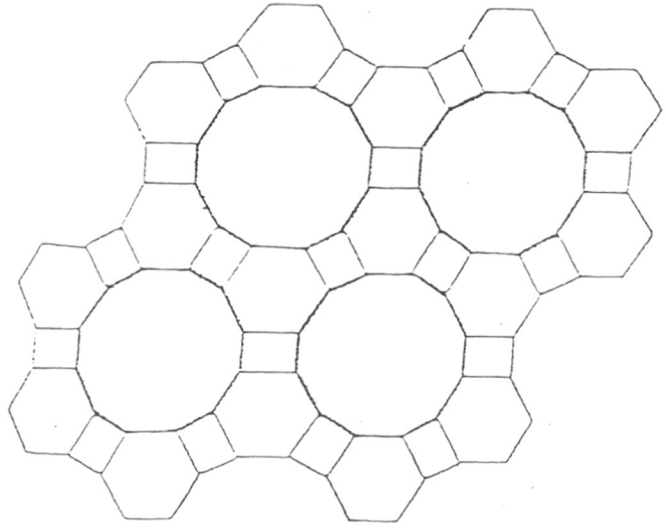

Framework (001) projection of $AlPO_4$-5.

FIG. I·I TUBULAR UNITS IN $AlPO_4$-5 (AFI) AND CANCRINITE (CAN)

Ref. (16).

$AlPO_4-2H_2O$ are variscite and meta variscite composed of alternating aluminium and phosphorous are exibiting octahedral and tetrahedral coordination (19,20) respectively.

1.4. SYNTHESIS OF MICROPOROUS ALUMINO-PHOSPHATE MOLECULAR SIEVES

These novel materials are synthesised hydrothermally in the temperature range 373-523 K from a reaction mixture containing sources of alumina, phosphate and an organic amine or quarternary ammonium salt (R) which gets entrapped or clathrated within the crystalline products. The oxide mole composition is

$$XR:Al_2O_3:1.0 \pm 0.2\ P_2O_5:YH_2O$$

The quantities X and Y represent the amounts of organic compound and water needed to fill the microporous voids within the neutral aluminophosphate framework. The species R listed in Table 1.2 appears to fulfil an essential templating or structure directing role in the synthesis of these novel microporous phases. Without R, dense aluminophosphate structures of known hydrates ($AlPO_4.nH_2O$) are formed. Microporous alumino phosphates designated as $AlPO_4$-5 can be synthesised with 23 different amines and quaternary ammonium compounds (21, Table 1.2). It is believed that the large unidimensional cylindrical pore system imposes fewer constraints on the template fit. Since the aluminophosphate framework is electrically neutral, the template is not needed as a charge balancing agent, therefore its incorporation into the structure is a function of its size and shape relative to the channel-volume to be filled. The entrapped

TABLE 1.2

STRUCTURE-TEMPLATE RELATIONSHIP FOR $AlPO_4$-n

Structure type	Template (R)	To_2/R	Structure type	Template (R)	To_2/R
5	$(C_3H_7)_4N^+$	26	8	$(n\text{-}C_4H_9)N^+$	
	$(C_6H_{11})_2NH$			$(n\text{-}C_5H_{11})_4N^+$	
	$(C_2H_5)_2NCH_2CH_2$ $-N(C_2H_5)_2$			$(n\text{-}C_4H_9)_2NH$ $(n\text{-}C_5H_{11})_2NH$	
	$(C_3H_7)_3N$	26	11	$(n\text{-}C_3H_7)_2NH$	21
	$(CH_3)_2NCH_2C_6H_5$			$(1\text{-}C_3H_7)_2NH$	19
	$(HOCH_2CH_2)_3N$			$(n\text{-}C_4H_9NHC_2H_5)$	
	$(CH_3CH_2)_4N^+$	23		$(n\text{-}C_5H_{11})_2NH$	
	NN'-dimethyl piperazine	18	14	$1\text{-}C_4H_9NH_2$	8.2
				$1\text{-}C_3H_7NH_2$	8.2
	$C_6H_{11}NHCH_3$		16	1-azabicyclo(2,2,2) Octane	14
	1,4-diazabicyclo-[2,2,2] octane.	13	17	1-azabicyclo(2,2,2) Octane	8.7
	$(C_2H_5)_2N\ CH_2CH_2OH$	19		2,2 dimethylpropyl Amine	7.7
	$CH_3N\ [CH_2CH_2OH]_2$			Cycohexylamine	8.8
	Cyclohexylamine			Piperdine	
	$(C_2H_5)_3N$	20		$(C_2H_5)_4N^+$	13
	$(CH_3)_3N\ CH_2CH_2$ OH^+		18		

contd ... 2/-

Structure type	Template (R)	To_2/R	Structure type	Template (R)	To_2/R
5	2-methylpyridine	18	20	$(CH_3)_4N^+$	9.9
	3-methylpyridine		21(25)*	Pyrrolidine	6.1
	4-methylpyridine			$(CH_3)_3N$	
	N-methylpiperdine	19		NN'-dimethyl	
	3-methylpiperdine			Piperazine	
	Piperdine			$(n\text{-}C_4H_9NH)_2CHCH_2^-$	
	$(CH_3)_2NCH_2CH_2OH$			$-CH_2NH_2$	
	$CH_3NCH_2CH_2OH$			$(CH_3)_2NCH_2.CH_2CH_2N-(CH_3)_2$	18
21(25)*	$(CH_3)_2NCH_2CH_2OH$	10			
	$n\text{-}C_3H_7NH_2$				
	$(CH_3)_2NCH_2.CH_2N(CH_3)_2$				
	$CH_3NHCH_2CH_2OH$				
2.2	N,N'-dimethyl 1-4 diazobicyclo (2,2,2) octane dihydroxide	13.1			
23(28)*	Pyrrolidine	6.4			
31	$(n\text{-}C_3H_7)_2NH$	22			
33	$(CH_3)_4N^+$	6.1			

* = Designation for organic free framework.

n = Structure type in nomenclature.

Ref. 21.

organic species are removed by thermal decomposition. Moreover, these novel structures exhibit excellent thermal stability. Most of these remain crystalline after calcination around 673-873 K which is necessary for the removal of organic template and make the intracrystalline void volume free for adsorption and catalysis. It has been reported (10) that the $AlPO_4$-n retain their structures after calcination at 1273 K and also show hydrothermal stability without structural collapse when heated in presence of water vapour at 873 K.

The aluminophosphate molecular sieves exhibit intracrystalline pore volumes for H_2O from 0.04 to 0.35 cm^3/g and adsorption pore sizes from 0.3 to 0.8 nm covering the entire range of pore volumes and pore sizes known in zeolites and silica molecular sieves. The uniform pore dimensions defined by the crystal structure enable the use of these new materials for size and shape selective separation and catalysis. Properties of selected $AlPO_4$ molecular sieves are summarised (10) in Table 1.3.

$AlPO_4$-5 is a large pore molecular sieve with 12-ring channels which allow adsorption of molecules as large as 2,2 dimethyl propane (0.62 nm). Nearly all the aluminophosphate molecular sieves with pore sizes from 0.4 to 0.8 nm (8, 10 or 12-rings) exhibit a characteristic adsorption pore volumes of 0.10 to 0.37 cc/g for oxygen whereas the pore volume for hydrocarbons is found to be 50-80% of that for water. This indicates that their framework structures contain both large voids and voids accessible through small pores (6-rings) which admit only water. In $AlPO_4$-5

TABLE 1.3

ADSORPTION PROPERTIES OF SOME $AlPO_4$-n M.S.

Structure type[c]	Pore size[a] nm	Ring size[b]	Intracrystalline pore vol. cc/gm. O_2	H_2O
$AlPO_4$-5 (Novel)	0.8	12	0.18	0.30
$AlPO_4$-11 (Unknown)	0.61	10 or 12	0.11	0.16
$AlPO_4$-14 (Unknown)	0.41	8	0.19	0.28
$AlPO_4$-16 (Unknwon)	0.30	6	0.0	0.30
$AlPO_4$-17 (Erionite offertite type)	0.46	8	0.20	0.28
$AlPO_4$-18 (Unknown)	0.46	8	0.27	0.35
$AlPO_4$-20 (Sodalite)	0.30	6	0.0	0.24
$AlPO_4$-31 (Unknown)	0.80	12	0.09	0.17
$AlPO_4$-33 (Unknown)	0.41	8	0.23	0.23

Ref: 10

a = Determined by the standard McBain-Beker gravimetric techniques.

b = Number of tetrahedral atoms Al or P in ring that controls pore size.

c = Structure distinguished by their characteristic XRD patterns.

the excess water volume is associated with small voids outlined by columns of twisted chains of 4-rings and 6-rings parallel to the c axis.

The pure silica molecular sieve, silicalite with neutral SiO_2 framework and no extra framework cations is hydrophobic. In contrast the neutral aluminophosphate frameworks with no extra framework cations are moderately hydrophilic. This difference may probably be due to the difference in electronegativity between Al(1.5) and P(2.1). They exhibit less affinity for H_2O than the hydrophilic zeolites such as type A and type X but substantially more than the hydrophobic silicalite. Their framework composition with an Al/P ratio of 1 has a wide structural diversity. $AlPO_4$-5 framework is neutral and therefore does not possess ion exchange capacity and exhibits only very weak acidity. The unit cell contains 24 tetrahedral oxide units 12 Al and 12 P with strict alternation of Al and P throughout the framework. $AlPO_4$-5 is unique in that a large variety of organic templates facilitate its synthesis. On the contrary $AlPO_4$-20 with sodalite structure has been synthesised with only one template, namely, tetramethyl ammonium (TMA) cation. Elemental analysis of this reveals approximately one TMA per sodalite cage(15).

1.5. SILICOALUMINO PHOSPHATE

Another novel class of crystalline microporous framework oxide molecular sieve viz. silicoaluminophosphate with properties similar to zeolites and aluminophosphates have been reported by

Lok et al (22). The new class of silicoaluminophosphate molecular sieves (SAPO-n) also exhibit structural diversity with some 13 three dimensional microporous framework structures. These include novel stuctures, SAPO-40, SAPO-41 and SAPO-44 structures topologically related to the zeolites, Chabazite (SAPO-34), Levynite (SAPO-35), Faujasite (SAPO-37) and Zeolite A (SAPO-42). Novel structure types topologically related to the aluminophosphates are SAPO-5, SAPO-11, SAPO-16 and SAPO-31 and topologically related structures found in both zeolites and silicoaluminophosphates are erionite (SAPO-17) and Sodalite (SAPO-20). SAPO-n molecular sieves have tetrahedral oxide frameworks containing silicon, aluminium and phosphorous. Mechanistically their composition can be visualized in terms of silicon substitution into hypothetical aluminophosphate frameworks, the substitution can occur (22) via (i) silicon for aluminium, (ii) silicon for phosphorous or (iii) simultaneous substitution of two silicon atoms for aluminium and phosphorous. The net framework charge per framework silicon atom resulting from each mode of substitution would be +, − and 0, respectively. Thus, some of these materials will have anionic framework with a net negative charge coupled with exchangeable cations and Brönsted acid sites. SAPO-n molecular sievs exhibit a range of moderate to high hydrophilic surface properties because of variable presence of cations and hydroxyl groups and the local electro-negativity differences between framework Si, Al and P as shown by $AlPO_4$ molecular sieves and by low silica to alumina ratio zeolites respectively. These

materials can be used as adsorbents, catalysts and ion exchangers. The anhydrous composition of SAPO is represented as

$$0\text{-}0.3R(Si_X:Al_Y:P_Z)O_2$$

where X, Y and Z are the mole fractions of the silicon, aluminium and phosphorous, the value of R typically varies from 0.04-0.3 depending upon synthesis conditions and structure type. Their adsorption properties, pore sizes, thermal and hydrothermal stability resemble those of the $AlPO_4$ molecular sieves. Their acidic properties vary from mild to strong acidity depending on the silicon concentration and structure type.

1.6. METAL ALUMINOPHOSPHATES (MeAPO-n)

As aluminosphophate molecular sieves have a neutral framework structure, they do not exhibit ion exchange ability or strong acidity. Pyke et al. (23) have attempted to produce useful catalytic activity in microporous aluminophosphates by chemical modification, adsorption or entrapment of catalytic species within the pore system. However, direct lattice substitution of equivalent or altervalent cations offers a mechanism for fine tuning the dimensions at diffusion paths within the crystals for introducing ion exchange ability and acidic or basic centres. Hence di, tri and tetravalent cations which can adopt tetrahedral coordination have been incorporated during hydrothermal synthesis. Similar attempts were made (24) to introduce catalytically active centres in the neutral aluminophosphate framework by incorporating (Si^{4+}, Ti^{4+}, Sn^{4+}, Fe^{3+}, B^{3+}, Ni^{2}, Co^{2+}, Mg^{2+}, Sr^{2+}, La^{3+} and V^{5+}) during hydrothermal synthesis.

The novel modified microporous crystalline aluminophosphates have a pore diameter from 3-10A^{o}. The substitution causes the formation of acid sites after calcination. The framework composition of MeAPOS-n contains metal, aluminium and phosphorous. They exhibit a wide range of composition within the general formula 0-0.3R($Me_XAl_YP_Z$)O_2. The value of X, the mole fraction of Me, typically varies from 0.01 to 0.25. The introduction of divalent ions into a lattice made up of tetrahedral units of AlO_2^- and PO_2^+ is novel and creates acid sites and ion exchange ability. In this mode of substitution in the MeAPO, the metal appears to substitute exclusively for Al rather than P. Divalent or trivalent metal for trivalent aluminium results in a net negative or neutral framework charge respectively. Like SAPO-n the negatively charged MeAPO frameworks possess ion exchange properties and the potential Brönsted acid sites.

MeAPO-n also show structural diversity and compositional variation as regards isomorphous substitution. Thirteen structure types crystallised in the MeAPO family include framework topologies related to the zeolites and novel structures related to $AlPO_4$-5 and $AlPO_4$-11.

Adsorption, pore size, pore volume and hydrophilic surface selectivity of the MeAPOs are similar to those of SAPOs and AlPOs. The observed catalytic properties are dependent on both metal and structure type. The thermal and hydrothermal stability of the MeAPO-n material is somewhat less than that of the AlPO and SAPO materials.

1.6.1. METAL ALUMINO-SILICOPHOSPHATES-(MeAPSO)

MeAPSO (25,26) structure types include framework topologies observed in binary ($AlPO_4$) and ternary (SAPO and MeAPO) compositional systems of MeO_2, AlO_2, PO_2 and SiO_2 tetrahedral units. The empirical chemical composition on an anhydrous basis for these molecular sieves is expressed as

$$mR:(Me_wAl_xP_ySi_z)O_2$$

where w, x, y and z represent molar fractions of Me, Al, P and Si, respectively, present as tetrahedral oxides.

Molecular sieves with ZnO_2, AlO_2, PO_2 and SiO_2 and other molecular sieves with TiO_2, AlO_2, PO_2 and SiO_2 oxide framework structures have been reported by Lok et al. (27). When additional elements such as Li, Be, B, Ga, Ge, As and Ti, are incorporated into the framework structures, many large, intermediate and small pore size molecular sieves are formed. These molecular sieves are designated as ElAPO-n(28-30) and ElAPSO-n (25-27). Quinary and senary framework compositions have been synthesized containing aluminium, phosphorous and silicon with additional combinations of divalent metals.

1.7. PHYSICOCHEMICAL CHARACTERIZATION

1.7.1. X-ray diffraction (XRD)

This is the most widely used important classical technique to identify species and also to understand the kinetics and mechanism of zeolite crystallization (32). Variations in the lattice parameters and framework symmetry (33, 34), collapse of crystal structure and presence of alien phases are also detected

by x-ray diffraction measurements.

$AlPO_4$-5 was the first aluminophosphate molecular sieve synthesized. It was noted that the x-ray diffraction pattern was unique and represented a novel structure (16). The pattern is quite simple and easily indexed in the hexagonal system.

Parise (35) has studied some gallium phosphate frameworks similar to $AlPO_4$-n family by x-ray diffraction. The structural characterization showed that the structure of $[Pr(NH_3)(Ga_4)(PO_4.OH].H_2O$ has been related to $AlPO_4$-12, -15 and -21. Rudolf (36) reported the x-ray structure of a novel molecular sieve aluminosphophate $(AlPO_4)_3.(CH_3)_4NOH$ designated as $AlPO_4$-12. Bennet and Marcus (36a) have reported the crystal structure of several metalaluminophosphate molecular sieves.

1.7.2. Infrared spectroscopy (IR)

Infrared spectroscopy is an important technique for the investigation of zeolite framework vibrations and is complementary to x-ray structure analysis. The fundamental vibrations of AlO_4/SiO_4 tetrahedra are in the mid infrared region (200-1300 cm^{-1}) and these have been used in conjunction with XRD to identify the zeolite structure (37). It is found that the main Si-O, Al-O vibrational band occurs at about 1100 cm^{-1} and is related to the Si/Al ratio in the zeolite framework (37a).

Crystallization of the zeolite during the synthesis has been studied by monitoring the changes in the framework IR vibrational frequencies and comparing these with those of the reactants (38). It is also possible to study the progressive incorporation of the

organic cation into the zeolite lattice by measuring the intensity of peaks characteristic of the organic cation.

The IR technique has been extensively used to distinguish different types of structural hydroxyl groups from other types of hydroxyl groups, for instance, an OH group attached to a cation in cation exchanged zeolite formed by hydrolysis of water. The OH groups are characterized by the absorption bands in the region 3500-3750 cm^{-1}. IR (39) is also used for detection and estimation of acid sites by adsorption of bases and for the study of transformation of Brönsted to Lewis acid sites occurring at high temperature or under specified conditions.

The FTIR (Fourier Transform Infrared Spectroscopy) was used to show (40) that most of the templating species had been removed on heating the material leaving behind the degradation product in the inorganic matrix. Comparison of the IR spectra of ZnAlPO-5 and $AlPO_4$-5 showed considerable differences especially in the OH stretching bands normally associted with Brönsted acid sites. IR evidence indicated that triethyl amine was attached to the surface acid sites confirming their existance in both ZnAlPO-5 and $AlPO_4$-5. Hegde et al (41) have investigated the acidic sites of $AlPO_4$-5 and SAPO-5 by using the diffuse reflectance IR spectroscopy. They found that SAPO-5 contains stronger Brönsted acid sites than $AlPO_4$-5. The structrural OH groups differ in their accessibility to adsorbed molecules and demonstrate very high thermal stability. Qinhua et al.(54) also examined the hydroxyl groups and their acidic properties of AlPO-5 and SAPO-5 by

means of IR spectroscopy with adsorption of D_2O and pyridine as probe molecules.

1.7.3. Acid strength distribution

Acid strength distribution is studied by temperature programmed desorption technique which is very useful in characterising and estimating acid sites in zeolites. The various techniques used for acidity measurements have been reviewed by Tanabe (48), Jacobs (49) and Anderson et al (50). They have reported results on NaZSM-5, HZSM-5 and silicalite and suggested that sites of TPD maximum observed at 780 K are the probable sites used by hydrocarbon conversion process. Jacobs et al (51) have characterized acid sites as weak, medium and strong according to the release of ammonia over a large temperature range during acidity measurements on ultrastable Y and ZSM-5. The amount of ammonia released above 753 K was considered to represent the very strong acid sites on HZSM-5.

Topsoe et al (52) have investigated acidic properties of fresh and partially deactivated catalyst and reported three different states α, β, and γ, corresponding to the ranges of temperature of desorption of ammonia, 330-370, 423-473 and 693-773 K were distinguishable for fresh catalyst. The activation energies for desorption of ammonia from α, β, and γ, states were found to be 84.6, 96.7 and 162.3 K J $mole^{-1}$ respectively. In partially deactivated catalyst the beta state was absent and γ was strongly reduced.

Borade et al (53) have reported three desorption maxima in TPD spectrum of ammonia on HZSM-5 which shows that ZSM-5 has weak medium and strong acid sites. According to Qinhue et al (54) SAPO-5 contains only one type of medium acid site s and $AlPO_4$-5 contains very weak acid sites (54). Depending upon the amount of NH_3 held strongly on the surface above 673 K, Hegde et al (41) have ranked the four zeolites in the following oder of acid strength

HZSM-5 > HSAPO-5 > HY >> $AlPO_4$-5.

$AlPO_4$-5 contains both Lewis acid sites and Brönsted acid sites of which Brönsted acid sites are responsible for its catalytic activity (55). Accordingly it has higher acidity and catalytic activity than amorphous aluminophosphate but much lower as compared to zeolites (55). Metal substituted (23, 24) $AlPO_4$-5 molecular sieves show higher acidity than pure $AlPO_4$-5 and follows the sequence MeAPSO-5> MeAPO-5 > SAPO-5 >> $AlPO_4$-5.

1.7.4. Thermal analysis

This technique has been used (56, 57) to get information on the synthesis, mechanism as well as thermal behaviour of the synthesized zeolites. Various physicochemical changes occurring during the thermal treatment are reflected in the DTA/TG curves. Dehydration of adsorbed water, decomposition of occluded organic cations and dehydroxylation at higher temperatures to produce Lewis acid sites are reflected in these thermoanalytical curves. It is also useful in identifying the location of water molecules in hydrated zeolites from the splitting of the endothermal peak

due to hydration (58). Thermal analysis of molecular sieves find extensive applications in studying kinetics of water desorption (49, 60), oxidative thermal decomposition of organic templates occluded in the voids and thermal stability of zeolite structure.

The DTA curves for $AlPO_4$-5 do not exhibit exotherm at high temperatures indicative (24) of high thermal stability upto 1273 K and endotherm is a consequence of low temperature desorption of water molecules from zeolite cavity. An exotherm around 673-873 K is due to decomposition of the entrapped templates (47).

1.7.5. Sorption properties

The molecular sieving properties of zeolites are uniquely determined by their pore dimensions and characterized by their sorption capacities for various sorbate molecules. The molecular exclusion properties of these zeolites have been used to estimate their pore openings and shape selective properties. Sorption measurements can be used in estimating the size and shape of the pores in zeolites and compare them with those determined by XRD (50). Sorption studies often help in determining specific inter-actions between sorbate and sorbents. Isosteric heats of adsorption reflect the nature and strength of interactions (61, 62) such as the sorbate-sorbents and sorbate-sorbate. Void volume in zeolite can be measured by adsorption of molecules which have free access into the voids (63). Derouane (64) and Gabelica et al. (66) have studied adsorption of hexane to investigate the influence of zeolite modification on sorption properties. Barrer and coworkers (67, 68) have extensively studied sorption

of various gases and vapours on synthetic zeolites and evaluated various thermodynamic properties such as entropy and free energy of sorption.

Wilson (21) et al. have reported adsorption properties of $AlPO_4$-5 having essentially a unidimensional cylindrical pore bounded by 12-rings with a diameter of $\sim 8A^{\circ}$. Stach et al. (69) and Dworezkov et al. (70) have studied adsorption properties of aluminophosphate molecular sieves and reported that the microporous $AlPO_4$-n exhibits similar acid base properties as the amorphous aluminophosphates which showed that no new acid-base properties have been induced by the channel structure. $AlPO_4$-5 behaves in the adsorption of non-polar molecules as homogeneous adsorbent.

The void volume of porous zeolite solids is often determined by low temperature (77 K) nitrogen sorption. Analysis of such sorption isotherms have been found to be useful in determining the micropore volume and pore size distribution of composite materials containing molecular sieves (112-114).

1.8. CATALYTIC PROPERTIES OF $AlPO_4$-5, SAPO-5 AND MeAPO-5 MOLECULAR SIEVES

Crystalline aluminosilicates (zeolites) are outstanding heterogeneous catalysts and can be considered as solid acids capable of donating a proton or accepting an electron pair from the adsorbing molecule. Both functions play an important role in various catalytic processes (49, 74), such as cracking isomerization, alkylation, hydrogenation and dehydrogenation. The use of molecular sieve as a potential catalyst is a consequence of their

crystallographically well defined structure, high thermal and hydrothermal stability, acidity and molecular sieve action. The structural factors are of special interest in various hydrocarbon conversion reactions.

Weisz and coworkers (80) showed that the locus of the catalytic activity lies within the intracrystalline pores. Recently, several reviews discussing shape selectivity in catalysts have been published (80-82). Some industrially important aromatic processes are ethylation of benzene to produce ethylbenzene (83) (Mobil/Badger process) disproportionation of toluene and isomerization of xylenes.

The catalytic studies on cumene cracking and o-xylene isomerization on SAPO-5 have been investigated (54) and compared with those of $AlPO_4$-5 and HZSM-5. The catalyst poisoning has been carried out with pyridine. Results show that the SAPO-5 is catalytically active in these reactions, while $AlPO_4$-5 is inactive. The medium pore SAPO-5, -11, -31, -40 and -41 with unique pore structures and mild acidity were found to be outstanding catalysts with high selectivty to gasoline range, olefinic products in propylene reactions and high para-xylene yields by toluene methylation (87).

MeAPOs exhibit novel surface selectivity characteristics which render them useful as catalysts or catalyst bases in number of hydrocarbon conversion reactions. Among the hydrocarbon conversion reactions catalysed by MeAPO compositions are cracking, hydrocracking, alkylation for both the aromatic and

isoparaffin types, isomerization including xylene isomerization, polymerization, reforming,hyrogenation, dehydrogenation and transalkylation. Lok et al. (88) have disclosed molecular sieves containing TiO_2, SiO_2, AlO_2 and PO_2 tetrahedra units, used as adsorbents and catalysts for wide range of hydrocarbon conversion reactions. High conversion of methanol (87-96%) to olefins C2-C4 over aluminium phospho silicate molecular sieves were reported by Kaiser et al. (89). Pellet et al. (90-93) have used catalyst containing silicoaluminophosphate 7.5, NiO-5.0, WO_3-20.0 zeolite LZ-21.0-52.5 and Al_2O_3-15.00 wt. % for hydrocracking and dewaxing reactions.

Derouane et al. (94-97) have synthesized crystalline silico aluminophosphates having ion exchange and catalytic properties which are useful for various types of hydrocarbon conversions. Lok et al. (98-100) have studied butane cracking reactions over titanium containing aluminophosphate and silicoaluminophosphate molecular sieves. They have also synthesised (101) a novel class of molecular sieves containing ZnO_2, AlO_2, SiO_2 and PO_2 as tetrahedral units and have reported that they can be used as adsorbents and catalysts. They have also reported number of metal substituted (23) aluminophosphates and silicoaluminophosphates which can be used as catalysts for various types of hydrocarbon conversion reactions.

1.9. OBJECTIVES OF THE PRESENT WORK

The above literature survey shows that the $AlPO_4$ based molecular sieves are a landmark discovery in the area of molecular sieves. The remarkable crystal structure diversity and crystal chemistry offers a tremendous number of design parameters to tailor make molecular sieves with distinct adsorptive and catalytic properties. In the case of aluminophosphate molecular sieves the nature and the source of starting compounds are diverse and very little information is available in detail in these aspects.

The main objectives of the present work are (1) to study in detail the factors influencing the synthesis of $AlPO_4$-5 and SAPO-5 molecular sieves, (2) to understand the nature of the active sites in $AlPO_4$-5 SAPO-5 and MeAPO-5 molecular sieves which are useful in hydrocarbon conversion reactions. It has a scope mainly in the following areas. The study covers the following aspects :

(1) Synthesis of $AlPO_4$-5, SAPO-5 and MeAPO-5 molecular sieves.

(2) Characterization of the framework and pore structures as well as the surface acidity of these molecular sieves using XRD, IR, sorption, TPD and thermal analysis techniques.

(3) Correlation of the surface acidity of $AlPO_4$-5, SAPO-5 and MeAPO-5 with their catalytic activity in n-hexane cracking, o-xylene isomerization and toluene-methylation reactions.

CHAPTER - II

EXPERIMENTAL

2.1 INTRODUCTION

2.2 MATERIALS

2.2.1. PROCEDURE FOR THE PREPARATION OF REACTIVE ALUMINA

2.2.2. PREPARATION OF ALUMINIUM-ISOPROPOXIDE

2.2.3. SYNTHESIS OF $ALPO_4$-5

2.3. METHODS USED IN PHYSICOCHEMICAL CHARACTERIZATION

2.3.1. CHEMICAL ANALYSIS

2.3.2. X-RAY DIFFRACTION

2.3.3. THERMAL ANALYSIS

2.3.4. SCANNING ELECTRON MICROSCOPY

2.3.5. NITROGEN SORPTION

2.3.6. SORPTION OF WATER AND HYDROCARBONS

2.3.7. TEMPERATURE PROGRAMMED DESORPTION OF CHEMISORBED AMMONIA (TPD)

2.3.8. INFRA-RED SPECTROSCOPY (IR)

2.3.9. CATALYTIC STUDIES

2.1. INTRODUCTION

The aluminosphosphate molecular sieves have been synthesized using reactive sources of alumina, orthopohosphoric acid, templating or structure directing agent and water, and by heating the gel under hydrothermal conditions.

The sources of raw materials and the methods used for their analysis are discussed briefly. The different instrumental techni-ques employed in establishing the structural features and molecular sieve properties of the synthetic products are also described.

The variations of the physicochemical properties of $AlPO_4$-5, SAPO-5 and MeAPO-5 are generally determined by the measurements of sorption, diffusion, thermal and catalytic properties. The nitrogen sorption isotherm for a pure zeolite is quite characteristic and is distinguishable from that of amorphous materials. The sorption of nitrogen gives a measure of the surface accessible to molecules comparable in size with nitrogen (102). From the sorption capacities of water, n-hexane, cyclohexane and o-xylene the modifications in the pore structure have been determined and the total available void volume has been evaluated. Crystal structure is studied by x-ray diffraction and infrared spectroscopy (103, 104).

The thermal stability of zeolite structure is determined from DTA curve. The high temperature exotherm is often used to determine the thermal stability of the samples.

The surface acidity of these molecular sieves has been

studied by various techniques such as infrared spectroscopy and temperature programmed desorption of ammonia.

2.2. MATERIALS

The synthesis of $AlPO_4$-5, SAPO-5 and MeAPO-5 is carried out using the components illustrated in Table 2.1.

2.2.1. Procedure for the preparation of reactive alumina

The pseudoboehmite was prepared by autoclaving freshly precipitated alumina gel under hydrothermal conditions at 423-473 K and the alumina samples were characterized by x-ray diffraction (XRD) thermal analysis (DTA/TG) and infrared spectroscopy.

Aqueous solutions of aluminium nitrate and ammonium hydroxide were prepared by dissolving 200 gms of the A. R. grade $Al(NO_3)_3.9H_2O$ in 1 L. of water and 50 ml of 25% NH_4OH solution in 500 ml of water respectively. The two solutions were mixed dropwise in a beaker containing 900 ml of water while stirring. The pH of the slurry was maintained at 7-8. The alumina gel was stirred at room temperature for half an hour and transferred to a stainless steel autoclave and covered with 100 ml of water. The autoclave was heated for 2-5 hours at 423-473 K and was cooled to room temperature. The pH of the supernatent solution was adjusted in the range of 7-8. The slurry was allowed to stand overnight at room temperature and the pH was recorded. The gel was then centrifuged, washed with distilled water for 3-4 times, filtered, dried at 373 K for 12 hours, powdered and sieved. The product was then analysed for alumina and moisture content.

TABLE 2.1

SPECIFICATIONS OF THE REAGENT USED IN THE SYNTHESIS AND ANALYSIS

Chemical name		Source
Orthophosphoric acid	(H_3PO_4) 88 % soln.	SD's Fine Chem.
Aluminium sulphate	$Al_2(SO_4)_3.16H_2O$ 98 %	B.D.H. G.R
Aluminium nitrate	$Al(NO_3)_3.9H_2O$ 98 %	B.D.H. G.R
Aluminium chloride	$AlCl_3$ (anhydrous) 98 %	B.D.H. G.R
Psuedoboehmite	(1) AlOOH (synthesised) (65.7% Al_2O_3, 34.3% H_2O)	A.C.C Thane.
	(2) (71.23 % Al_2O_3, 28.8% H_2O	
Sodium silicate	Na_2SiO_3 27.2% SiO_2, 8.4 % Na_2O 64.4 % H_2O	C.P. Gr.water, glass
Silicon dioxide	SiO_2 type 5031 95% SiO_2, 5.0% H_2O	Bombay
Tetraethyl orthosilicate	$(C_2H_5O)_4Si$ 98 %	Aldrich Co.Ltd
Triethylamine	Et_3N 99.00 %	Loba Chemie.
Tripropylamine	$(C_3H_7)_3N$ 100 %	Aldrich.
Tetrapropylammonium hydroxide	$(C_3H_7)_4NOH$ 40 %	Fluka.
Ferric chloride	$FeCl_3$ (anhydrous) 96 %	B.D.H. L.R.
Cobaltous nitrate	$Co(NO_3)_2.6H_2O$ 97 %	B.D.H. L.R.
Magnesium chloride	$MgCl_2.6H_2O$ 98 %	B.D.H. L.R.
Zinc chloride	$ZnCl_2$ (anhydrous) 98 %	B.D.H. L.R.
Hydrochloric acid	HCl 35.4 % Soln.	S.D's Fine Chem.
Hydrofluoric acid	HF 40 % (electronic gr.)	Loba Chem.
Sulphuric acid	H_2SO_4 98 % A.R.	B.D.H.

2.2.2. Preparation of aluminium isopropoxide

A simplified procedure for preparing aluminium isopropoxide (102) is described below :

100 gms of aluminium wire or turnings, 1200 ml of dry, isopropyl alcohol (GR) and 5 gms of mercuric chloride are placed in a 2 liter round bottom flask provided with an efficient reflux condenser. The flask is gently warmed in a heating mantle. Within 10-20 minutes a grayish precipitate appeared and subsequently the reaction became so vigorous that heating was interrupted and the flask was externally cooled. After this spell of vigorous reaction is over, heating was resumed and gentle refluxing was maintained for 6-7 hours. The product was purified by distillation in boiling range 418-423 K at 5 mm.pressure. Aluminium isopropoxide was collected and anlysed, Al_2O_3 content after analysis was 24.70% and isopropyl alcohol 75.30% (theoretical values Al_2O_3-24.94% and isopropyl alcohol 75.06%).

2.2.3. Synthesis of $AlPO_4$-5

The aluminium phosphates were synthesized by hydrothermal crystallization of a reaction mixture prepared by combining reactive sources of phosphate, alumina, water and at least one templating agent which includes an organic amine or a quaternary ammonium compound. Broadly, the reaction mixture had the following chemical composition expressed in terms of molar oxide ratios 1-1.5R : Al_2O_3 :1 $\pm$ 0.2P_2O_5 : 7-100 H_2O

The reaction mixture was stirred till it forms a homogeneous slurry and was loaded in a stainless steel reactor lined with

polytetrafluoroethylene shown in Fig. 2.1. The reactor was heated under autogeneous pressure at a temperature between 373-473 K over a period of 2 hours to 2 weeks. The preferred reaction mixture contains per mole of Al_2O_3, 0.8 to 1.2 moles of P_2O_5, 25-75 moles of water and 0.5 to 1.5 moles of templating agent. The reaction products were quenched in cold water to stop the crystallization process. The solid products obtained were isolated by filtration or centrifuging, washed with hot distilled water and dried in oven at 373 K for 12 hours.

The as-synthesised products contain within their internal pore systems the templating agents used during synthesis, which are removed by calcination at temperatures 673-873 K in presence of flowing air in a muffle furnace to obtain the aluminophosphate in active form.

2.3. PHYSICOCHEMICAL CHARACTERIZATION

2.3.1. Chemical Analysis

$AlPO_4$-5, SAPO-5 and MeAPO-5

(i) Estimation of aluminium as 8-hydroxy quinolate $(Al(C_9H_6OH)_3$.

A known quantity of the $AlPO_4$-5 sample was dissolved in a few ml of conc. HCl, diluted and heated to 343-353 K and appropriate amount (about 40 ml) of oxime reagent was mixed and 2 M ammonium acetate solution was then added slowly until a precipitate just appeared. The mixture was heated to boiling and again 25 ml of 2 M ammonium acetate solution was added dropwise and with constant stirring. The precipitate was allowed to cool and

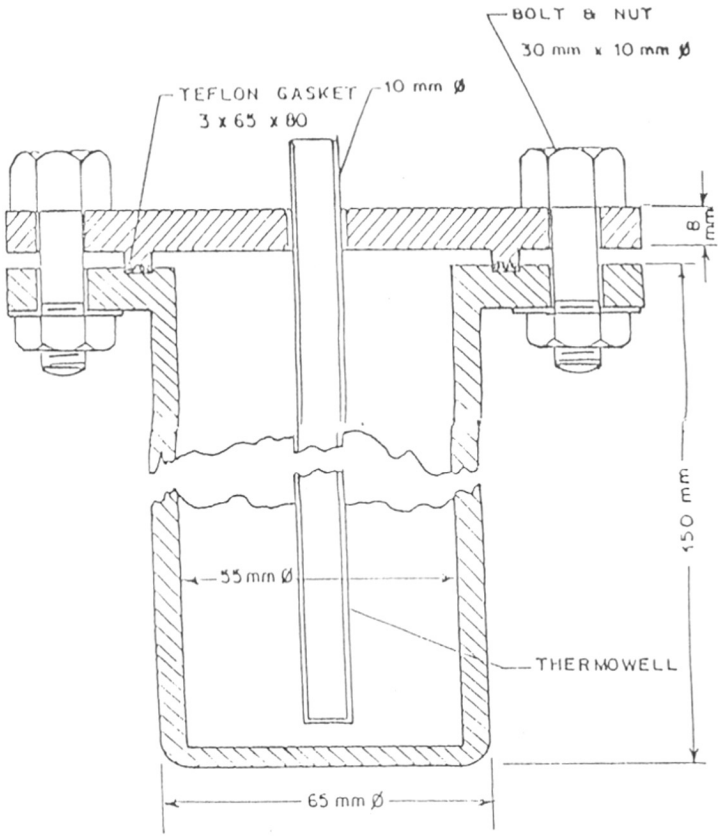

FIG. 2.1 : STAINLESS-STEEL (316) AUTOCLAVE WITH TEFLON-GASKET FOR HYDROTHERMAL SYNTHESIS

filtered through a quantitative filter paper (Whatman No. 41) and washed with ice cold water. The precipitate was transferred into a previously weighed platinum crucible, dried, charred, ignited and weighed as Al_2O_3.

(ii) Estimation of phosphate as magnesium pyrophosphate ($Mg_2P_2O_7$).

A known amount of sample (about 0.5 g) was dissolved in few ml of conc. HCl, diluted and boiled. A few drops of methyl-red indicator was added and about 2 gms of citric acid was added to keep aluminium in solution. Then 25 ml of magnesia mixture was added followed by pure conc. ammonia solution while stirring vigorously until the indicator turned yellow. The solution was allowed to stand at room temperature for 24 hours. The precipitate was then filtered, washed with dilute ammonia solution until the filtrate gave no turbidity with $AgNO_3$ and HNO_3. The precipitate was transferred to a platinum crucible, dried, charred and ignited to a constant weight and weighed as $Mg_2P_2O_7$.

(iii) Loss on ignition

Loss on ignition was found out by igniting about 1 gm of sample in a previously weighed crucible at a high temperature about 1073-1273 K for 1-2 hours.

(iv) Estimation of metal cations

A known amount of (about (250 mg) of sample was dissolved in few ml of conc. HCl or H_2SO_4, mixture was heated and diluted, the volume was made up to 250 ml. This solution was used for estimation of metal cations viz. Fe, Co, Ni, Mg and Zn by atomic absorption spectroscopy (AAS).

(v) Estimation of silica

About 0.5 gm of the sample was ignited in a platinum crucible to a constant weight. After cooling it was moistened with few drops of conc. H_2SO_4, few ml of (5 ml) AR hydrofluoric acid and slowly evaporated to dryness. The HF treatment was repeated twice. From the loss in weight silica was estimated.

(vi) Estimation of alumina in Pseudo Boehmite and aluminium isoproxide :

About 0.25 gm of sample was dissolved in few ml of conc. HCl or H_2SO_4 and diluted. 2-3 gms of NH_4Cl was added and heated to boiling. The addition of NH_4Cl exerts a buffering effect and serves to maintain the desired pH for the precipitation (pH 6.5-7.5) and also helps coagulation of the initially formed colloidal precipitate. To the hot solution was added 1:1 NH_4OH solution till ammonical smell was perceived and it was boiled for 1-2 minutes, filtered, washed, ignited and weighed as Al_2O_3.

(vii) Ion Exchange

About 2 gms of calcined sample was equilibrated with 50 ml of 0.1M NaCl solution at 333 K for 30 minutes. The sample was filtered and washed with hot deionized water till the filtrate is free from Na^+. After drying the sample at 373 K for 12 hrs. about 0.5 gms of the above dried sample was dissolved in few ml of conc. HCl or H_2SO_4 and diluted to 250 ml. The solution was analysed for sodium by flame photometry and aluminium and phosphorous were estimated according to the procedure described earlier.

2.3.2. X-ray diffraction

The samples synthesized at different temperatures and at different period of crystallization were analysed by x-ray powder diffraction method for qualitative and quantitative phase identification. The unit used for analysis was Philips X-ray Diffractometer Model PW 1700 with nickel filtered CuKα radiation (λ = 1.5405). For quantitative phase identification selected reference sample was used and per cent crystallization calculated from the sum of areas of the peaks at 2 θ = 7.5 and 19 to 23. The extent of crystallization is estimated as follows :

$$\%\text{Crystallization} = \frac{\text{Peak area at } 2\theta = 7.5 \text{ and } 19 \text{ to } 23 \text{ of the product}}{\text{Peak area of } 2\theta = 7.5 \text{ and } 19 \text{ to } 23 \text{ of the reference sample}}$$

2.3.3. Thermal analysis

Thermal analysis of the synthesized samples was carried out on an automatic derivatograph (MOM Budapest Type OO-102B) where simultaneous TG/DTG/DTA thermograms are recorded (101). The thermograms of the samples were recorded under the following conditions :

Weight of the sample - 200 mgs

Heating rate - 10 K min^{-1}

Sensitivity : TG : 100

DTA : 1/5

DTG : 1/5

Atmosphere - Flowing air.

Preheated and finely powdered α-alumina was used as the refe-

rence material.

2.3.4. Scanning Electron Microscope

The morphology of pseudoboehmite, $AlPO_4$-5, SAPO-5 and MeAPO-5 were investigated by scanning electron microscope, stereoscan model 150 Cambridge, UK. The sample was dusted on aluminium pegs and coated with an Au-Pd evaporated film to render them conducting.

2.3.5. Nitrogen sorption

Nitrogen sorption was used for the estimation of the surface area and micro pore volume. The sorption was measured on Accusorb Unit (Micromeritics Model 2100E) volumetrically at liquid nitrogen temperature (77 K). The surface occupied by nitrogen molecule was taken to be 16.2 A^{o2}.

2.3.6. Sorption of water and hydrocarbons

The sorption measurements for hydrocarbon vapours and water in the micropores of $AlPO_4$-5 were carried out by using a sensitive gravimetric quartz spring (McBain) balance (Fig. 2.2).

The $AlPO_4$-5 sample (about 100 mgs) was pressed into a pellet and weighed into an aluminium bucket which was attached to the silica spring. The system was evacuated by means of a two stage rotary pump and mercury diffusion pump to a vacuum of about 10^{-6} torr. The sample was activated at 673 K by continuous pumping till a constant weight was obtained. After the sample had attained a constant weight, the temperature of the sample was lowered to the desired value. To study the equilibrium sorption and rate of adsorption, the sorbate was admitted to the sample at

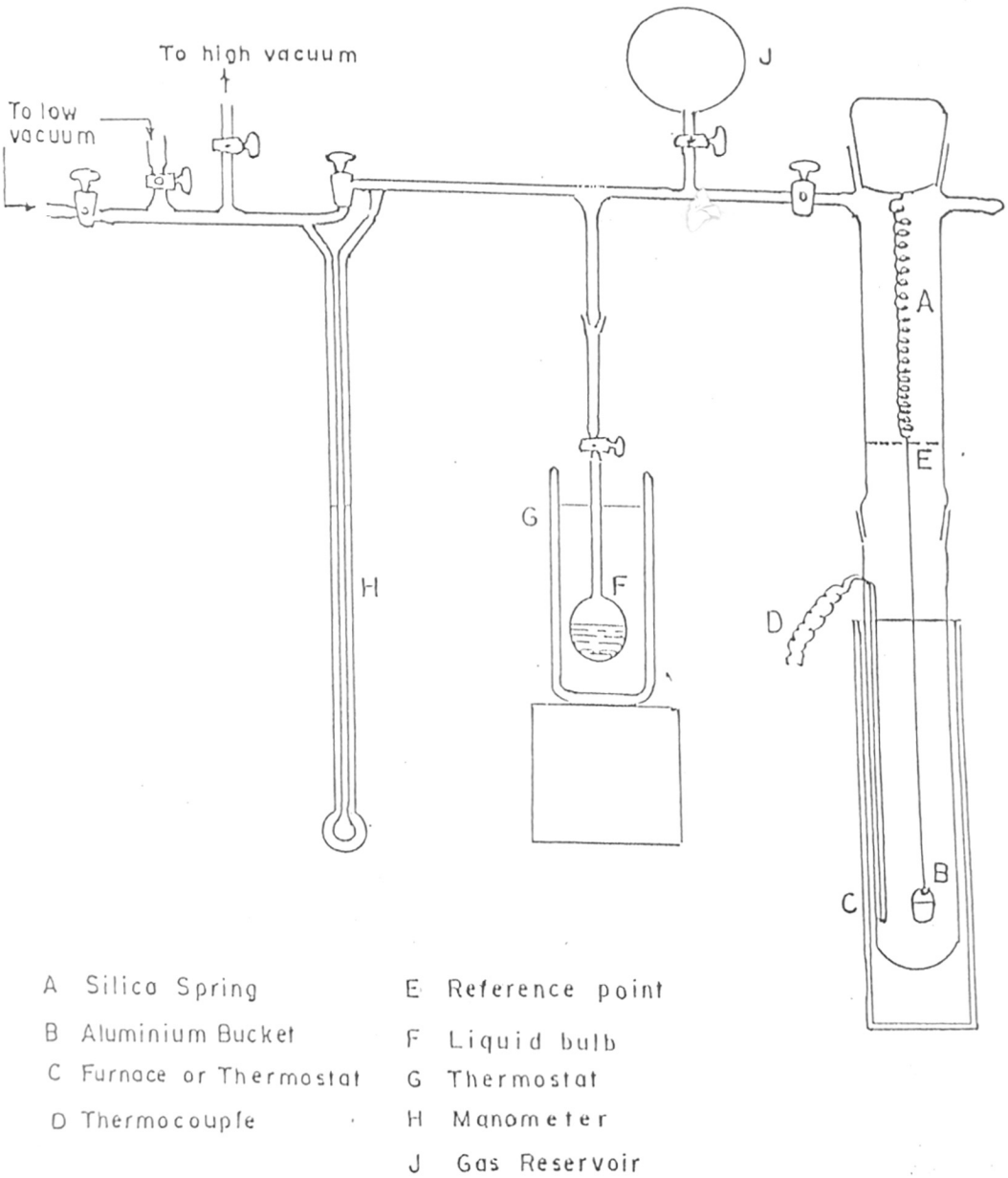

A Silica Spring
B Aluminium Bucket
C Furnace or Thermostat
D Thermocouple
E Reference point
F Liquid bulb
G Thermostat
H Manometer
J Gas Reservoir

FIG. 2·2 : GRAVIMETRIC ADSORPTION UNIT

constant temperature and pressure and the weight gained was recorded on a cathetometer (accuracy ± 0.01 mm) as a function of time. Ater recording the equilibrium sorption, the sample was evacuated and heated at 673 K at about 10^{-6} torr and used for the next sorption measurements.

2.3.7. Temperature programmed desorption of chemisorbed ammonia (TPD of ammonia)

This technique was used to determine the surface acidity and acid strength distribution of the samples. The experimental set up is shown in Fig. 2.3. The catalyst sample (10-20 mesh, 400 mgs) was loaded in the silica reactor which was connected to a sorptometer. After activation at 673 K (10^{-6}torr) the sample was cooled to room temperature and adsorption isotherm of ammonia was determined, physically adsorbed ammonia was removed from the sample by evacuation and ammonia adsorption isotherm was once again determined. The difference in the 1st and 2nd saturation adsorption values gives the total chemisorbed ammonia. The sample was then evacuated at the same temperature and now connected on-line to a conventional gas chromatograph (Shimadzu GC R,A) having thermal conductivity detector and six port valve.

The sample was heated at the rate of 10 k min^{-1} in the flow of (100 ml min^{-1}) ultra pure nitrogen. The concentration of desorbed ammonia as a function of temperature was recorded upto temperature 823 K.

2.3.8. Infrared spectroscopy

Infrared spectroscopic investigations were carried out on Nicolet 60 SXB FTIR Spectrophotometer. For the region of

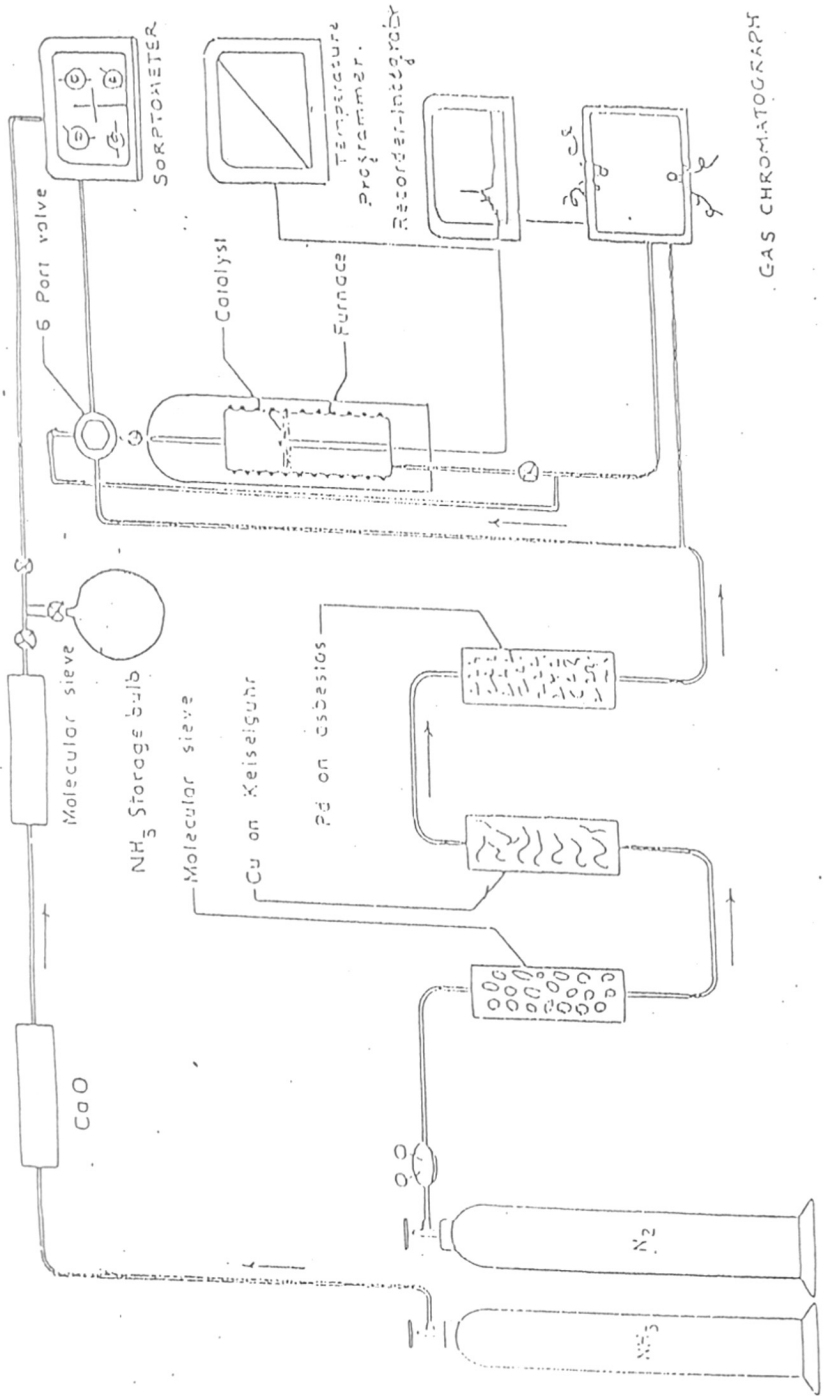

FIG. 2.3: SCHEMATIC DIAGRAM OF TPD. UNIT.

fundamental vibrations of zeolite framework (1300-200 cm^{-1}) Nujol mull technique in the transmittance mode was used.

The nature of surface hydroxyl groups were studied by diffuse reflectance FTIR spectra obtained with the help of Spectra Tech in situ DRFTIRcell. The catalyst sample (250-300 mesh) was evenly spread in the sample cup and placed inside the controlled environment chamber of the cell. It was then slowly heated to 673 K under vacuum (10^{-6} torr) for 6 hours and cooled to room temperature. The IR spectra was recorded in the range 4000-1300 cm^{-1}. The average of 1000 scans was taken at a resolution of 2 cm^{-1}. Then vapours of D_2O, NH_3 and benzene were admitted at 10 torr pressure and allowed 2 hrs for equilibrium. Then physically adsorbed vapours were desorbed at 373 K, sample cooled to 298 K and the spectra were recorded. Spectral substraction techniques were used to analyse the data.

2.3.9. Catalytic reactions

Procedure : Catalytic reactions like n-hexane cracking, o-xylene isomerization etc. were carried out in a fixed bed downflow tubular reactor at atmospheric pressure. The reactor was fabricated from fused silica tube 1.5 cm in diameter and 35 cm in length. The reactor was heated with well defined electrical furnace. The top portion of the reactor serving as a vapouriser-cum-preheater was packed with inert porcelain beads. The reactor assembly is shown in Fig. 2.4.

The catalyst powder was pressed into a 1 cm^2 pellets, crushed sized to 10-20 mesh and was loaded in the reactor column

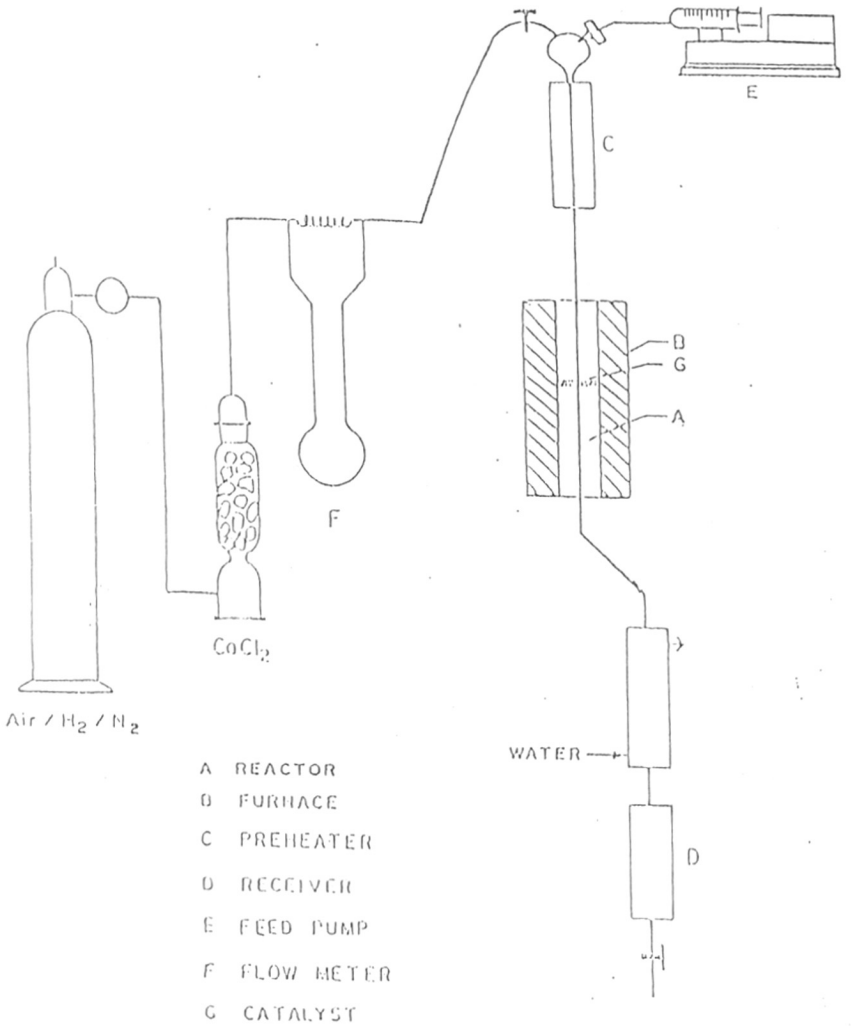

FIG 2·4.: SILICA REACTOR USED FOR CATALYTIC REACTIONS

prior to reacton, the catalyst was activated in a stream of air at 823 K for 5 hours. The catalyst was then flushed with nitrogen and cooled to reaction temperature. The hydrocarbons were fed by a syringe pump (Sage Instrument Model 352) at a constant feed rate, vapourized and passed through the catalyst zone. The condensed reaction products were analysed by gas chromatography (Shimadzu GC R1A) having flame ionisation detector (FID) using 5% di-isodecylphthalate and 5% Bentone-34 on chemisorb W column, (2 m). For analysis of gaseous products, Poropak Q column was used.

CHAPTER - III

SYNTHESIS

3.1. INTRODUCTION

In this chapter the hydrothermal synthesis of aluminophosphate molecular sieves using different sources of reactive alumina and different types of organic templating agents are discussed.

A typical synthesis involves the combination of equimolar amounts of reactive hydrated alumina and orthophosphoric acid in water. To this aluminophosphate gel an organic template was added and this reaction mixture was heated in an autoclave in the temperature range of 373-473 K to effect the crystallization. The general gel composition used for the preparation of $AlPO_4$-5 was 0.5-1.5R : $1.0Al_2O_3$: $1.0P_2O_5$: 40-60 H_2O. The chemical ingredients used were orthophosphoric acid containing 88 % H_3PO_4 (S.D's Fine chem), pseudoboehmite (commercial sample from ACC, containing 71.23 % Al_2O_3 and 28.77 % H_2O), aluminium isopropoxide (synthesised in this laboratory containing 24.70 % Al_2O_3), triethylamine (Loba Chemie, 99.00 %), tripropylamine (Aldrich, 100% pure) and tetrapropyl ammonium hydroxide (Fluka 40% solution). Some of the synthesis variables which influence the reaction are crystallization temperature and time, template concentration and Al/P ratio. Influence of different types of templates on $AlPO_4$-5 were initially studied by using three different templates eg. tripropylamine (Pr_3N), tetrapropylammonium hydroxide (TPAOH) and triethylamine (Et_3N). Later, only tri-ethylamine (Et_3N) template was generally used.

3.2. SYNTHESIS OF ALUMINOPHOPHATE MOLECULAR SIEVES ($AlPO_4$-5)

A reaction mixture was prepared by combining 22.30 gms of orthophosphoric acid (H_3PO_4), 120 gms of water and 14.32 gms of hydrated aluminium oxide (ACC - a peudoboehmite phase) and stirred until homogeneous. To this aluminophosphate gel 18.04 gms of triethylamine was added and the mixture was stirred until homogeneous. The composition of the final reaction mixture in molar oxide ratio was $1.5Et_3N:1.0Al_2O_3:1.0P_2O_5:60H_2O$. The reaction mixture was sealed in a stainless steel reactor and heated in an oven at 473 K at autogeneous pressure for 24 hours. At the end of the crystallization, the autoclave was quenched under cold water. The white crystalline solid product was recovered by centrifugation and repeatedly washed with hot distilled water and dried at 373 K for 12 hours.

The structural features of synthesized aluminophosphates were characterized by various techniques. The x-ray powder diffraction patterns of the products were obtained on a Phillips x-ray diffractometer Model 1700. In reporting the results the interplanar spacings d were calculated from 2θ the Bragg angle and λ were expressed in terms of Angstrom units (A^o). The relative intensities I/I_o were evaluated from the peak heights, I and I_o being the peak height showing maximum intensity of the sample and the reference sample respectively. The XRD data are illustrated in Table 3.1 and the XRD spectra in Fig. 3.1. The product was calcined at 823 K for 12 hours in the flow of air to remove the

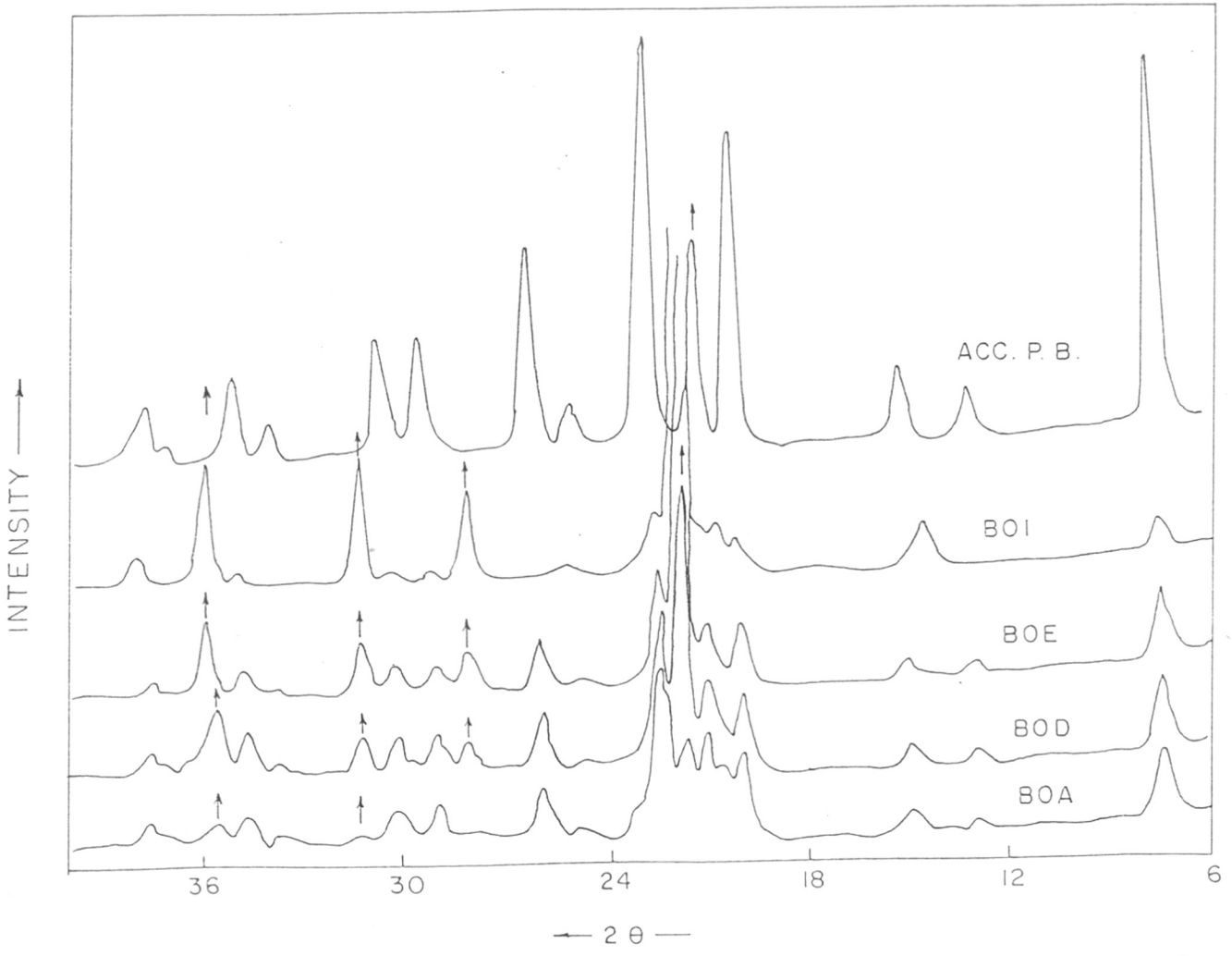

FIG. 3·1 — INFLUENCE OF CRYSTALLITE SIZE OF BOEHMITE ON $AlPO_4$-5 CRYSTALLIZATION (↑: IMPURITY PEAKS)

entrapped organic template. The x-ray diffraction pattern of the calcined product was found essentially identical to that of precalcined sample as shown in Fig. 3.1. However, the peak intensities slightly decreased.

The chemical analysis of the calcined product revealed the molar oxide ratio as $1.0Al_2O_3 : 0.97P_2O_5 : 2.16H_2O$.

Table 3.1 :

X-ray Diffraction data for $AlPO_4$-5 molecular sieve

OBSERVED			REPORTED*		
2	dA^o	$I/I_o \times 100$	2	dA^o	$I/I_o \times 100$
7.6	11.62	68.20	7 .4	11.936	100
13.1	6.75	11.50	12.9	6.856	9.0
15.1	5.86	20.60	14.85	5.96	13.0
19.9	4.45	62.60	19.70	4.50	39..0
21.10	4.22	59.80	20.80	4.267	37.0
22.5	3.98	100.00	22.3	3.983	62.0
24.8	3.58	5.70	24.55	3.623	4.0
26.2	3.39	37.40	25.85	3.44	22.0
29.1	3.06	19.00	28.90	3.087	11.0
30.3	2.94	21.80	30.00	2.976	12.0
33.9	2.64	8.50	33.50	2.67	4.0
34.6	2.59	20.30	34.55	2.593	11.00
37.2	2.41	5.90	36.90	2.434	3.0
37.9	2.37	12.70	37.80	2.378	7.0

Ref.(8.)

3.3. FACTORS INFLUENCING CRYSTALLIZATION OF $AlPO_4$-5 MOLECULAR SIEVES

3.3.1. Influence of crystallaization temperature and crystallization period

In a typical gel composition as described in 3.2, crystallization of $AlPO_4$-5 occurs very rapidly in the temperature range 375-473 K, below 373 K i.e. at 350 K, crystallization of $AlPO_4$-5 was not effected even though the gel was autoclaved for more than one week. Temperature and time play a major role in the crystallization of $AlPO_4$-5 molecular sieves. The starting low pH of the gel (pH 2.7-3.5) reflects the presence of some unreacted ortho -phosphoric acid (H_3PO_4); during synthesis of $AlPO_4$-5, Al and P are consumed in equimolar amounts causing rise in pH (pH 7 to 11) at higher temperature during digestion. Final values of pH 7 to 10 are typical for this gel composition. $AlPO_4$-5 phase is quite stable in the temperature range 373-473 K in the reaction media. However, a small temperature rise of 5 K above 473 K resulted in the formation of a dense aluminophosphate with tridymite and crystobalite structures(21) along with $AlPO_4$-5 phase. The instability of $AlPO_4$-5 above 473 K has been attributed to the unfavourably low equilibrium concentration of template in the pore system leading to subsequent structural collapse. Although $AlPO_4$-5 molecular sieves can be synthesized at 373 K its crystallinity is very poor even after a prolonged crystallaization period. The most favourable temperatures and crystallization periods for obtaining pure $AlPO_4$-5 phase are in the range of 423-473 K and 12-48 hours respectively.

The influence of different templating agents as well as the reaction temperature and period of crystallization are illustrated in Table 3.2. It was observed that at lower crystallization temperature and period, known hydrates of aluminophosphate were formed and at higher temperatures and on prolonged periods $AlPO_4$-5 phase with impurity phases was formed.

3.3.2. Influence of template concentration

Templating or structure directing agents play an important role in the synthesis of microporous structures; in the absence of the template aluminiumphosphate hydrates and dense phases are formed. This was well illustrated by preparing a gel mixture containing equimolar Al and P and varying only the template concentration while maintaining the other variables constant. For the composition containing Et_3N/Al_2O_3 = 0.50, $AlPO_4$-5 phase was formed but the crystallinity was very low. In the absence of Et_3N, known $AlPO_4$-hydrates are formed (21). It is observed in Table 3.3 that the value Et_3N/Al_2O_3 ranging from 1.00-1.5 is optimum for the formation of pure $AlPO_4$-5 microporous phase. At higher ratios of Et_3N/Al_2O_3 > 2.0, $AlPO_4$-5 is not formed as the initial pH of the gel mixture exceeds 7. The initial pH of the gel increases with increased Et_3N concentration. The final pH is insensitive to Et_3N concentration due to the lower solubility of Et_3N in the reaction mixture leading to phase separation of an essentially pure Et_3N layer and a relatively invariant aqueous layer.

Table 3.2

Influence of crystallization period, temperature and template on $AlPO_4$-5.

Gel composition: $1.5RAl_2O_3:P_2O_5:60H_2O$

Template	Reaction		Products*	% Crystallinity of $AlPO_4$-5
	Temp. K	Time (hrs)		
Triethylamine(Et_3N)	353	312	H,MV,V	0.0
	373	24	5, B	36.20
	398	24	5	44.11
	423	24	5	54.30
	453	24	5	88.50
	473	24	5	100.00
	475	24	T,C,5	78.50
Tripropylamine(Pr3N)	373	192	H, MV,V	0.0
	398	24	5,H,MV,B	20.50
	423	24	5, B	32.40
	453	24	5	45.50
	473	24	5,T,C	65.00
Tetrapropylammonium hydroxide (TPAOH)	423	24	5	60.40
	453	24	5	90.50
	473	24	5	100.00

* P.B. = Pseudoboehmite, H = $AlPO_4.1.67H_2O$

MV = $AlPO_4$, $2H_2O$ (Metavariscite)

V = $AlPO_4$, $2H_2O$ (Variscite)

T = $AlPO_4$ (Tridymite)

C = $AlPO_4$ (Crystobalite)

5 = $AlPO_4$-5

3.3.3. Influence of pH on the purity of $AlPO_4$-5 phase

The dominant role played by the pH of the reaction mixture on the formation of pure $AlPO_4$-5 phase has been examined by adding different quantity of HCl to a typical gel composition during synthesis. The gel composition for the synthesis mixture was $xHCl:1.0Et_3N:1.0Al_2O_3:1.0P_2O_5:60H_2O$

Though the total concentration of Et_3N and H_3PO_4 is kept constant the addition of the HCl will produce a mixture of Et_3N and Et_3NH^+Cl- in the new reaction gel. Under these very limited conditions the HCl appears to have distructive effect on crystallization of $AlPO_4$-5 possibly due to the considerable higher acidity produced in the gel. These data are presented in the Table 3.4. In more acidic media dense phases of known hydrated aluminophosphaates are formed. It is concluded that most favourable initial pH of the reaction media is above 2.60 for the formation of pure $AlPO_4$-5 phase.

3.3.4. Influence of Al/P ratio

Generally aluminophosphate molecular sieves are prepared by using equimolar amounts of Al and P. If the gel compoosition is varied slightly from this preferred mole ratio, different phases are formed. This behaviour can be illustrated by changing the mole ratios of Al and P as shown in Table 3.5. For a typical gel composition, $1.5Et_3N:xAl_2O_3:yP_2O_5:60H_2O$ crystallization period and temperature were maintained at 24 hours and 423 K respectively. The products observed in above synthesis (Table 3.5) are

consistent with the consumption of equimolar amounts of Al and P until the limiting species are consumed. When moles of Al in the gel exceeds 'P' substantially, excess boehmite is present in the final product. This apparently does not interfere with the crystallization of $AlPO_4$-5. However, when moles of 'P' in the gel substantially exceeds Al the excess p remains unreacted in the mother liquor. Excess phosphate typically added as H_3PO_4 has distructive effect on $AlPO_4$-5 formation due to low pH of the gel and only hydrates of aluminophosphates are formed.

Table 3.3

Influence of template concentration.

Gel composition $mEt_3N:Al_2O_3:P_2O_5:60H_2O$

Crystallization time = 24 hrs, Temp. 453 K

Moles of Et_3N m	pH Initial	pH Final	Products*
0.0	1.5	3.40	H.T.C.
0.5	2.70	7.25	5, B
1.0	3.10	7.80	5
1.25	3.30	8.00	5
1.50	3.70	8.20	5
2.0	7.20	10.20	U

* U = Unidentified impurity phases

Table 3.4

Influence of pH

Gel composition xHCl:1.25R : Al_2O_3:P_2O_5 : 60H_2O

Crystallization time = 24 hrs, Temp. 453 K

Modes of HCl(x)	pH		Products
	Initial	Final	
0.0	3.25	8.10	S
0.5	2.60	5.90	S, H, T
1.0	1.20	2.50	H, T

Table 3.5 : Influence of Al/P ratio

Gel composition : 1.25Et_3N:xAl_2O_3:yP_2O_5:60H_2O

Crystallization time = 24 hours, Temp. = 453 K.

Moles of Al_2O_3(x)	Moles of P_2O_5(y)	pH		Products
		Initial	Final	
1.1	0.9	5.5	8.5	S
1.2	0.8	6.10	9.10	S,B
0.9	1.1	2.90	6.90	S,B
0.8	1.2	1.60	4.80	H,MV

3.3.5. Influence of sources of alumina

Aluminophosphate molecular sieves were synthesized by using different sources of alumina. It was observed that $AlPO_4$-5 synthesis is only effective when reactive alumina is used as alumina source. Several batches for $AlPO_4$-5 synthesis were prepared by using aluminium salts like $Al(NO_3)_3.9H_2O$; anhydrous $AlCl_3$, $Al_2(SO_4)_3.6H_2O$ and sodium aluminate for alumina source. Freshly precipitated aluminium phosphate was also used, but $AlPO_4$-5 molecular sieve was not formed in the above systems. As illustrated in the previous section alumina in pseudoboehmite phase with proper crystallite size was very reactive and formed microporous $AlPO_4$-5 with good crystallinity.

The hydrothermal treatment of freshly prepared aluminium hydroxide gel yields a number of crystalline aluminas depending on the pH of the gel, the temperature and the period of treatment. The physico-chemical properties of such alumina obtained are found to vary with preparation conditions.For example, the course of their thermal decomposition depends upon the nature of aluminium hydroxide used as a starting material (72,73). The alumina prepared by hydrothermal treatment at 423 K for 2 hours shows broad peaks of low intensity typical of pseudoboehmite phase (74). As the time (2-50 hrs) and the temperature (423-473 K) for the hydrothermal treatment increases the XRD pattern shows sharper peaks.

The crystallite size of various alumina samples (75) used was estimated by Debye Scherrer equation

$$D = \frac{K\alpha}{\beta \cos\theta}$$

where α is the wave length of x-ray radiation (1.54A^{o}), θ is the Bragg angle, β is the breadth of the x-ray peak in radians and K is the shape factor which is approximately equal to unity. This leads to the conclusion that the crystallite size increases with increase in reaction time and temperature.

The crystallite size of the synthetic and commercial alumina is given in Table 3.6. The pseudoboehmite samples were further characterized by infrared spectroscopy (Fig. 3.2). IR spectra of all samples are similar except a marked variation in the absorption band at 1350-1450 cm^{-1} (1380-1350 cm^{-1} - NO^{-}_{3} and 1450-1410 cm^{-1}-NH_4^{+}) attributed to NO_3^{-} and NH_4^{+} ions. Impurity ions strongly adsorbed on the surface of aluminium hydroxide are apparently present in the reaction mixture. The chemical analysis of the samples shows the presence of NH_4^{+} ions ranging from .02-0.12% and NO_3^{-} ions ranging from 0.05-0.3%. IR bands in the region of fundamental vibrations of -OH groups (3800-3650 cm^{-1} not shown) indicated complex nature of these spectra. Nevertheless it is clearly seen that as the aging of the gel in the preparation of pseudoboehmite increases, the intensity of absorption bands in the region 3800-3700 cm^{-1} which are known to be relatively more basic decreases. Simultaneously the intensity of the bands in the lower frequency region (3700-3550 cm^{-1}) increases. This indicates that the pseudoboehmite surface becomes more acidic as the aging time increases. It can also be noted

Table 3.6 : Influence of the nature of pseudoboehmite on the synthesis of $AlPO_4$-5.

Sample	Aging temp.& time k/hrs.	Crystal -lite size A°	Concentration of impurity in Pseudoboehmite % NH_4^+	% NO_3^-	*I/I_o of (1450-1350 cm-1 band)	% Crystal -linity of $AlPO_4$-5
BoM	423/2	48.5	.02	.05	9.80	93.14
BoA	473/2	65.0	.04	0.08	6.82	65.34
BoD	473/15	88.8	.06	0.15	4.10	45.40
BeE	473/50	95.6	.09	0.20	3.21	34.70
BoI	Commercial	199.3	0.12	0.30	2.16	22.40
ACC P.B.	-do-	35.0	.01	0.02	1.0	100.00

* I = Intensity of IR bands of NH_4^+ and NO_3^- groups at (1450-1350 cm^{-1} in poseudoboehmite prepared.

I_o = That of pseudoboehmite obtained from A.C.C. Bombay.(A.C.C. P.B.

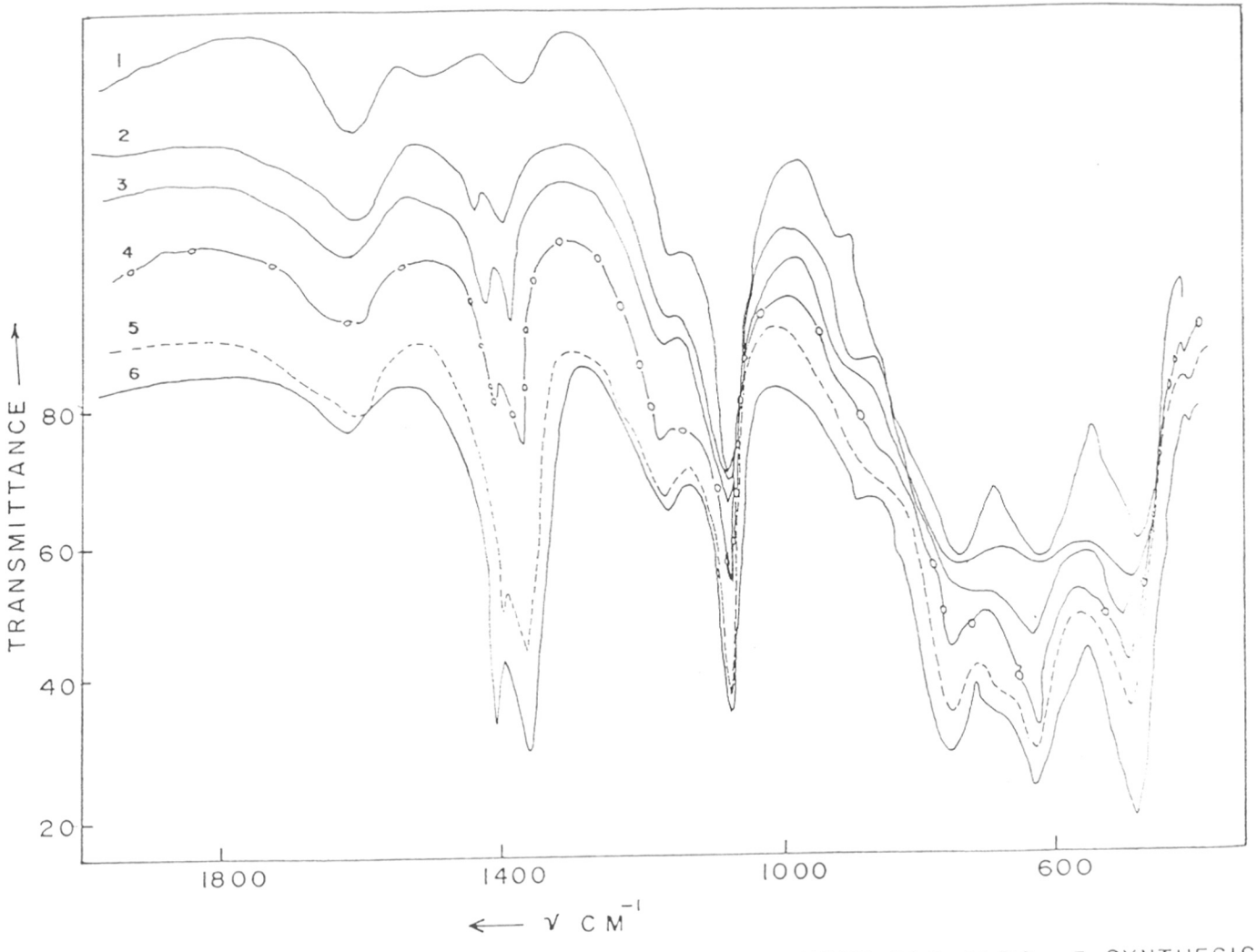

FIG 3.2 : IR SPECTRA OF PSEUDOBOEHMITE USED FOR $AlPO_4$-5 SYNTHESIS
1) ACC-P.B. 2) BoM 3) BoA 4) BoD 5) BoE 6) BoI

that the crystallite size increases as the aging time increases.

Active aluminium oxide is one of the most frequently studied catalyst material (77, 78). The relative abundance of acidic and basic centers on alumina is found to depend strongly on the nature and amount of impurity by which it is contaminated during the preparation (79, 80). It is reasonable to presume that as the crystallite size increasesmore and more NH_4^+ and NO_3^- ions from the mother liquor are occluded into the particle voids and/or anchored on the surface during aging (peptization) period. Hence the reactivity of such pseudoboehmite samples with orthophosphoric acid apparently depends on its acid base proprties. These features are exemplified by the nature of the $AlPO_4$-5 products obtained by using these samples as shown in the Table 3.6 and the XRD spectra as shown in Fig.3.1. It is observed that as the crystallite size of the boehmite sample increases, in addition to $AlPO_4$-5 phase, some other impurity phases with additional peaks at 2θ = 21.6, 28.3, 31.2 and 35.8 are formed.

$AlPO_4$-5 prepared by using aluminium isopropoxide as the alumina source has maximum crystallinity and is free from other impurity phases . The XRD pattern did not show any unreacted alumina in the form of boehmite phase.

3.4. KINETICS OF CRYSTALLIZATION OF $AlPO_4$-5

Kinetic study for the crystallization of $AlPO_4$-5 was carried out for selected batch compositions to determine the kinetic parameters namely the apparent activation energy for nucleation and crystallization. The XRD spectra and the SEM of $AlPO_4$-5

molecular sieves crystallized for different periods are shown in Fig. 3.3 and Fig. 3.4 respectively. It is observed that at 473 K and 2 hours crystallization period the crystallization of $AlPO_4$-5 has just started while samples heated for less than 2 hours are almost amorphous. At crystallization period greater than 4 hrs. the formation of hexagonal and plate like crystals were observed. The x-ray intensity increases with the crystallization period. After 24 hours almost 100% crystalline $AlPO_4$-5 with well defined hexagonal rod shaped crytstals are formed, while after 48 hours the product was found to contain dense phase aluminophosphates along with $AlPO_4$-5 phase.

The crystallization curves of aluminophosphate molecular sieve ($AlPO_4$-5) synthesized by using pseudoboehmite and aluminium -isopropoxide in the temperature range 373-473 K and crystallization period 0-72 hours are illustrated in Figs. 3.5A and 3.5B. The reaction gel composition used for the synthesis of $AlPO_4$-5 was 1.5 Et_3N : 1.0 Al_2O_3 : 1.0 P_2O_5 : 60 H_2O.

The crystallization curves in Figs.3.5 A and B show that the rate of crystallization significantly depends on the reaction temperature. As the reaction temperature of the gel is increased the solubility of the reacting components is also increased and hence the composition of the liquid phase in such heterogeneous system exerts beneficial effect on crystallization process.

The sigmoid nature of the crystallization curves exhibits two characteristic distinct stages (102) involved in the crystallization process namely

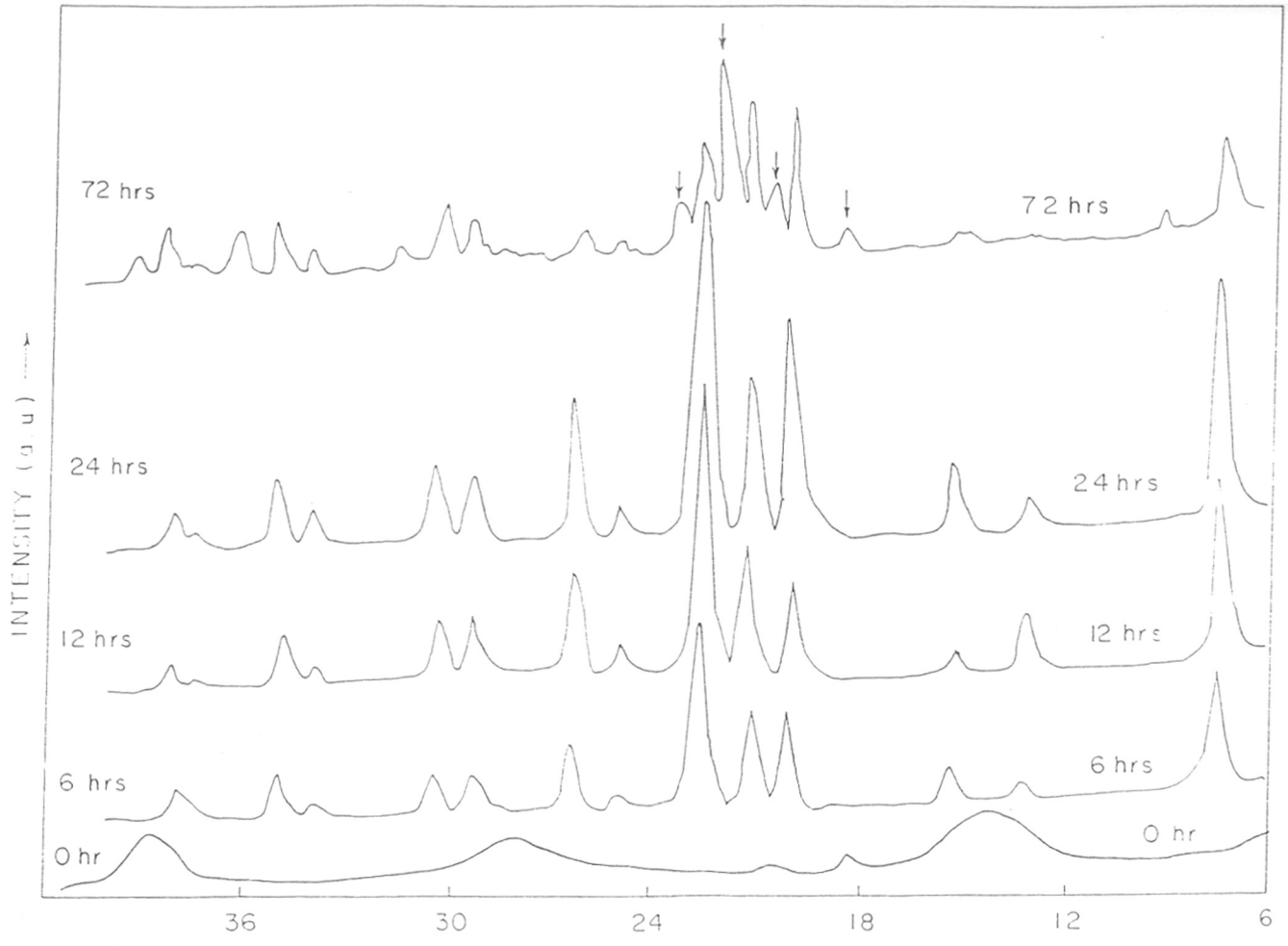

FIG. 3.3 – INFLUENCE OF CRYSTALLIZATION PERIOD ON XRD CRYSTALLINITY OF $AlPO_4$-5 (↓: IMPURITY PEAKS)

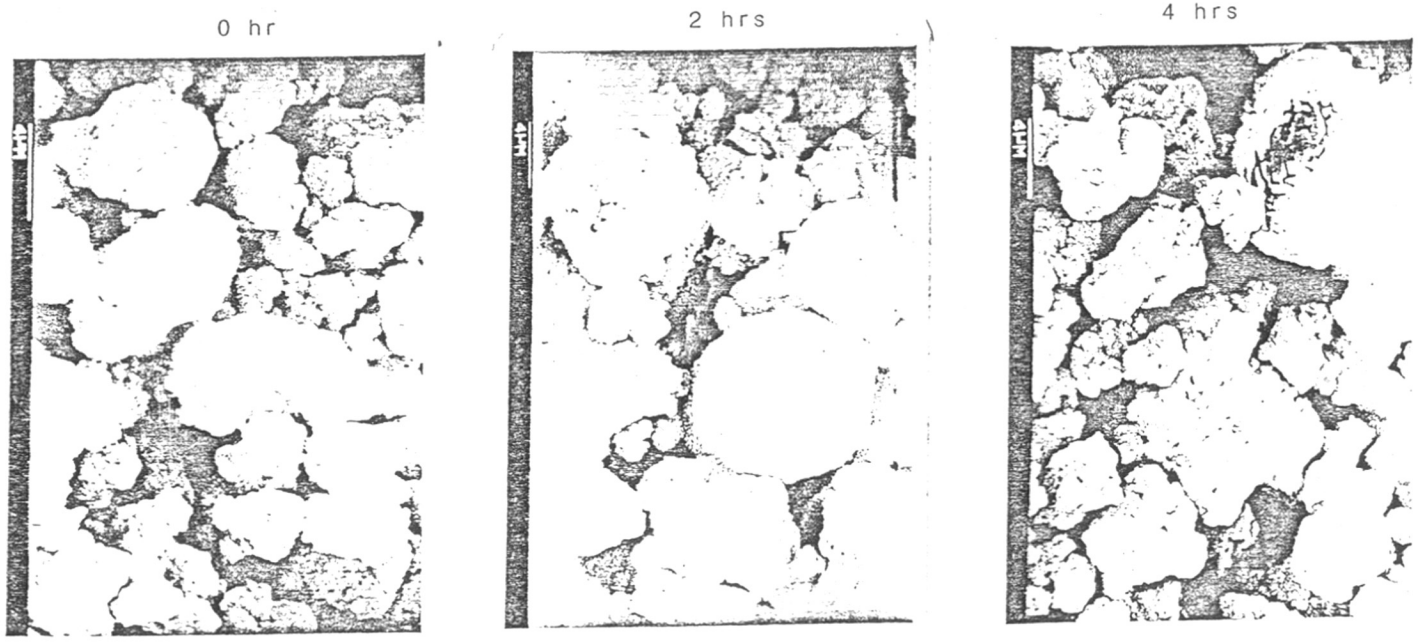

Fig. 3.4. SEM PHOTOGRAPHS OF $AlPO_4$-5 CRYSTALLISED AT DIFFERENT PERIODS.

Contd ...

Fig. 3.4

(6 hrs)

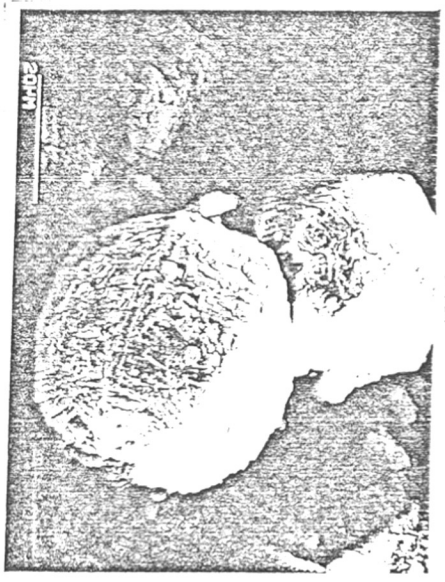

(25 hrs)

(72 hrs)

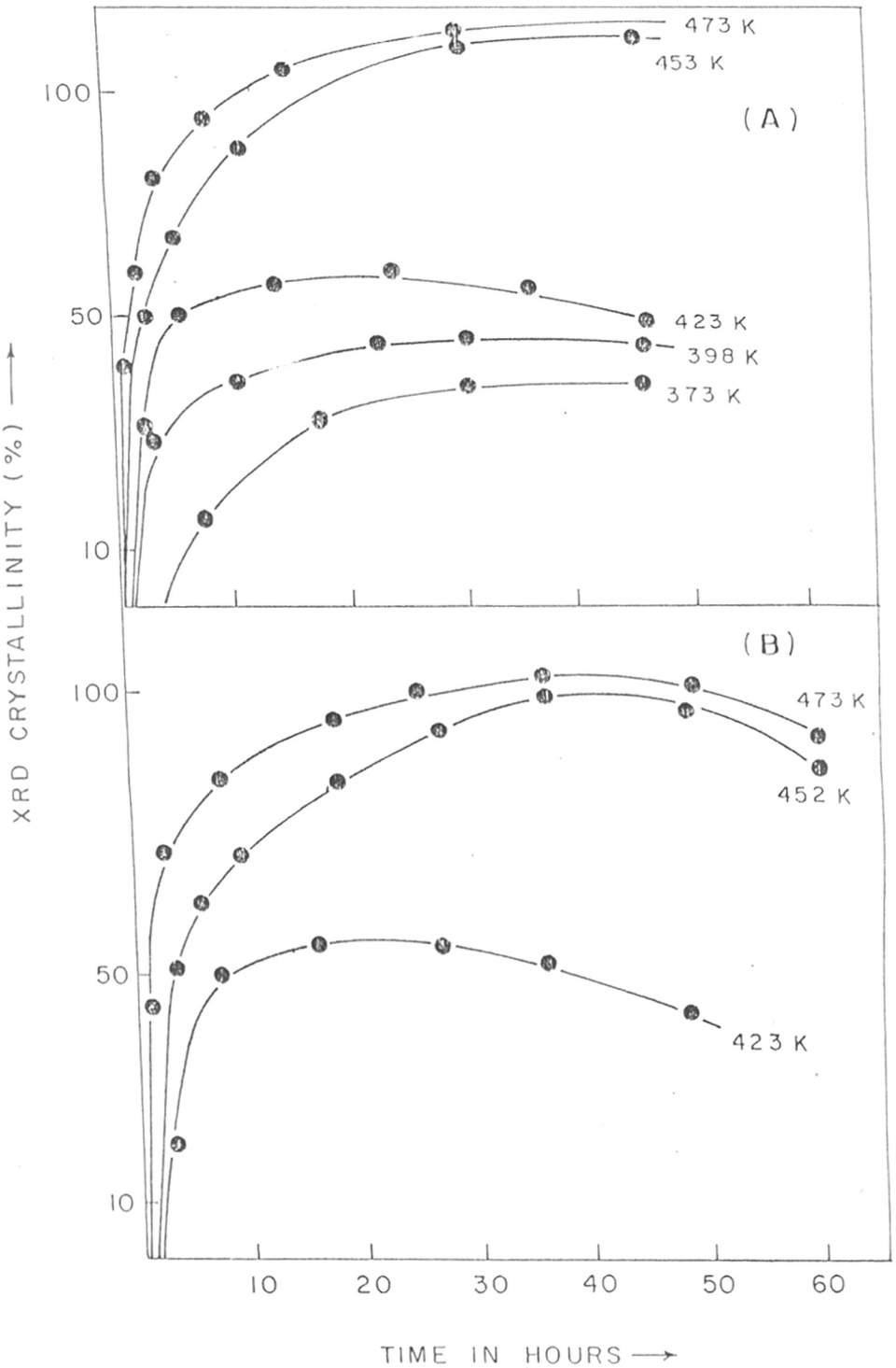

FIG. 3·5 – KINETICS OF CRYSTALLIZATION OF $AlPO_4$-5 USING (A) PSEUDOBOEHMITE, (B) ALUMINIUM ISOPROPOXIDE

(1) an induction period when nuclei are formed, and

(2) a crystal growth period when nuclei grow into crystals. The induction period is defined as the time required for providing the suitable condition for the nuclei formation rather than the time which is necessary for the growth of the nuclei to a critical size (102).

The observed acceleration of crystallaization evidently must be connected with the increase in the rate of nuclei formation. The rate of any cryustallization process is determined by the rate of nuclei formation and the rate of crystal gowth. The crystallization rate is defined as the rate of conversion at 50% conversion level per hour. The decrease in the rate of crystallization observed above certain per cent conversion may be due to the decrease in the reactant concentration in the solution.

Assuming that the formation of nuclei during the induction period is an energetically activated process and since nucleation is the rate determining step during the induction period, the apparent energy for the process of nucleation (En) was calculated from the temperature dependance of the rate of nucleation. The rate of nucleation has been assumed to be inversely proportional to the induction period. The temperature dependance of the rate of nucleation was expressed by Arrhenius Equation and apparent activation energy for nucleation E_n was calculated from the

expression

$$\frac{d\ln(1/n)}{d(1/T)} = \frac{En}{R} \qquad \ldots 1$$

where 'n' is induction period, that is the point on the crystallization curve where conversion to the crystalline phase is just started, T is the absolute temperature and R is the gas constant.

Similarly E_c, the apparent activation energy for crystal growth was calculated from the temperature dependance of the rate of crystallization and was obtained from the point on the crystal-lization curves where crystallization is 50%. The rate equation may be represented as

$$\frac{d(\ln 1/\theta)}{d(1/T)} = \frac{-E_c}{R} \qquad \ldots (2)$$

where θ represents time in hours for 50% crystallization, T the absolute temperature and R is the gas constant. Figs. 3.6A and B illustrate the temperature dependance of the rate of nucleation and crystallization. The calculated values of E_n and E_c are listed in Table 3.7.

Table 3.7

The apparent activation energy for nucleation and crystallization of $AlPO_4$-5

Sample	E_n, kJ mole-1	E_c, kJ mole-1
$AlPO_4$-5 (pseudoboehmite)	40.40	66.12
$AlPO_4$-5 (aluminium isopropoxide)	45.44	83.70

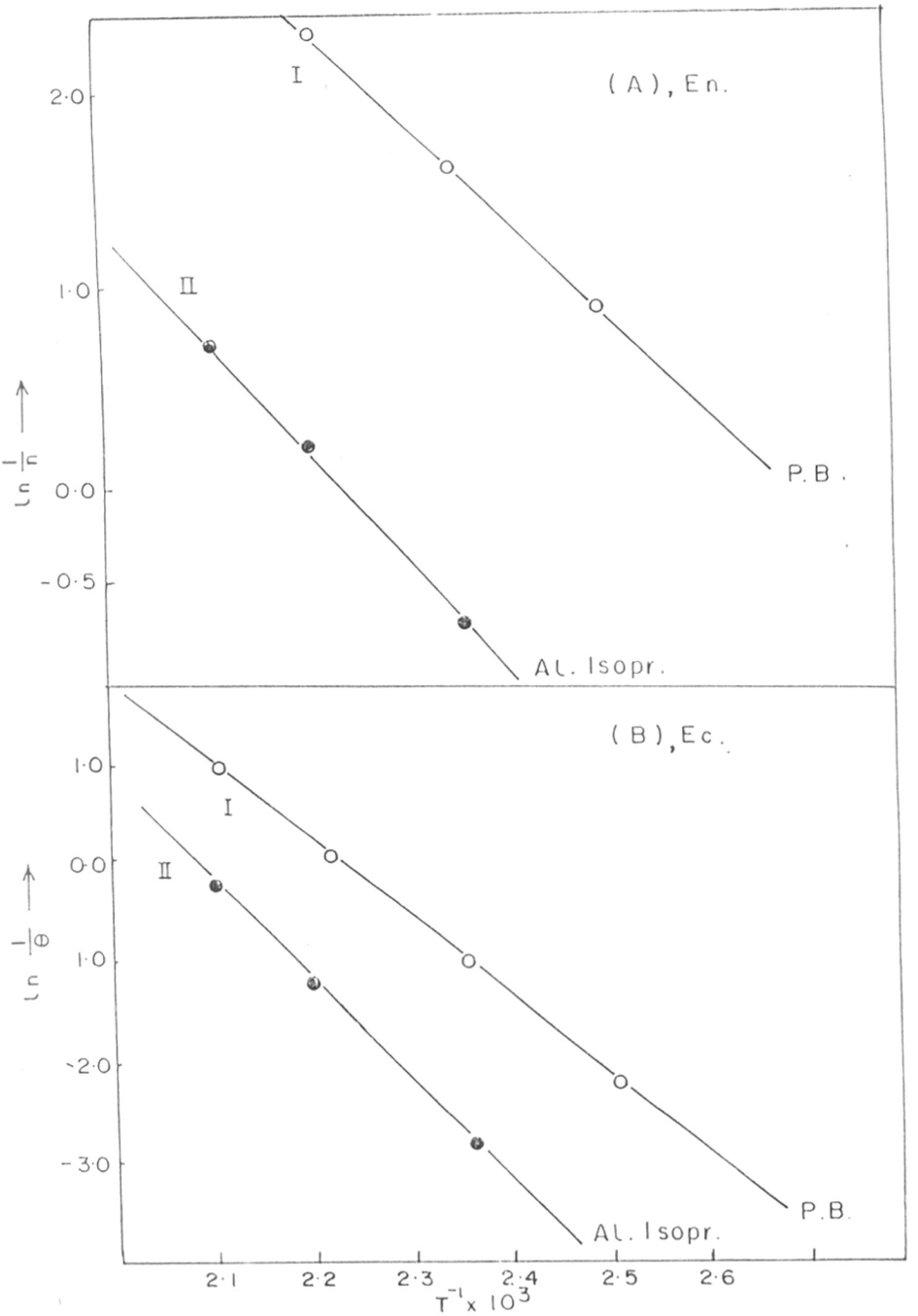

FIG. 3·6 : ARRHENIUS PLOTS FOR (A) NUCLEATION AND B) CRYSTALLIZATION OF $AlPO_4$-5 USING (I) PSEUDOBOEHMITE (II) Al. ISOPROPOXIDE.

Tapp et al. (103) have shown that in the reaction mixture of $AlPO_4$-5 synthesis, it is the meta variscite and variscite which are formed in situ which further lead to nucleation and crystal growth of $AlPO_4$-5. The effect of alcohol produced as a result of hydrolysis of starting materials like aluminium isopropoxide and tetraethyl orthosilicate has been already recognised in zeolite synthesis (104) and attributed to the low solubility of silica in solution in presence of alcohol. We have also observed that (Table 3.7) activation energy for nucleation and crystal-lization for $AlPO_4$-5 preapared by using aluminium isopropoxide is higher than that when pseudoboehmite is used. This may be attributed to the influence of alcohol originated from hydrolysis of isopropoxide on the dissolution of matavariscite and variscite to give free nuclei of $AlPO_4$-5 precursors.

The crystallization curves shown in Figs. 3.6 A and B can be described mathematically by Avarami-Erofeev equation as (106a,b)

$$\ln[1/1-\alpha] = kt^m \qquad \ldots (3)$$

where α and t are fractional conversion and reaction time respectively while k and m are constants. To check that the zeolite formation in our case confirms the above general picture, the data were fitted to the above equation and the results illustrated in Fig. 3.7. show a good fit. The values of k and m obtained from the linear plot are given in Table 3.8. A good fit of the

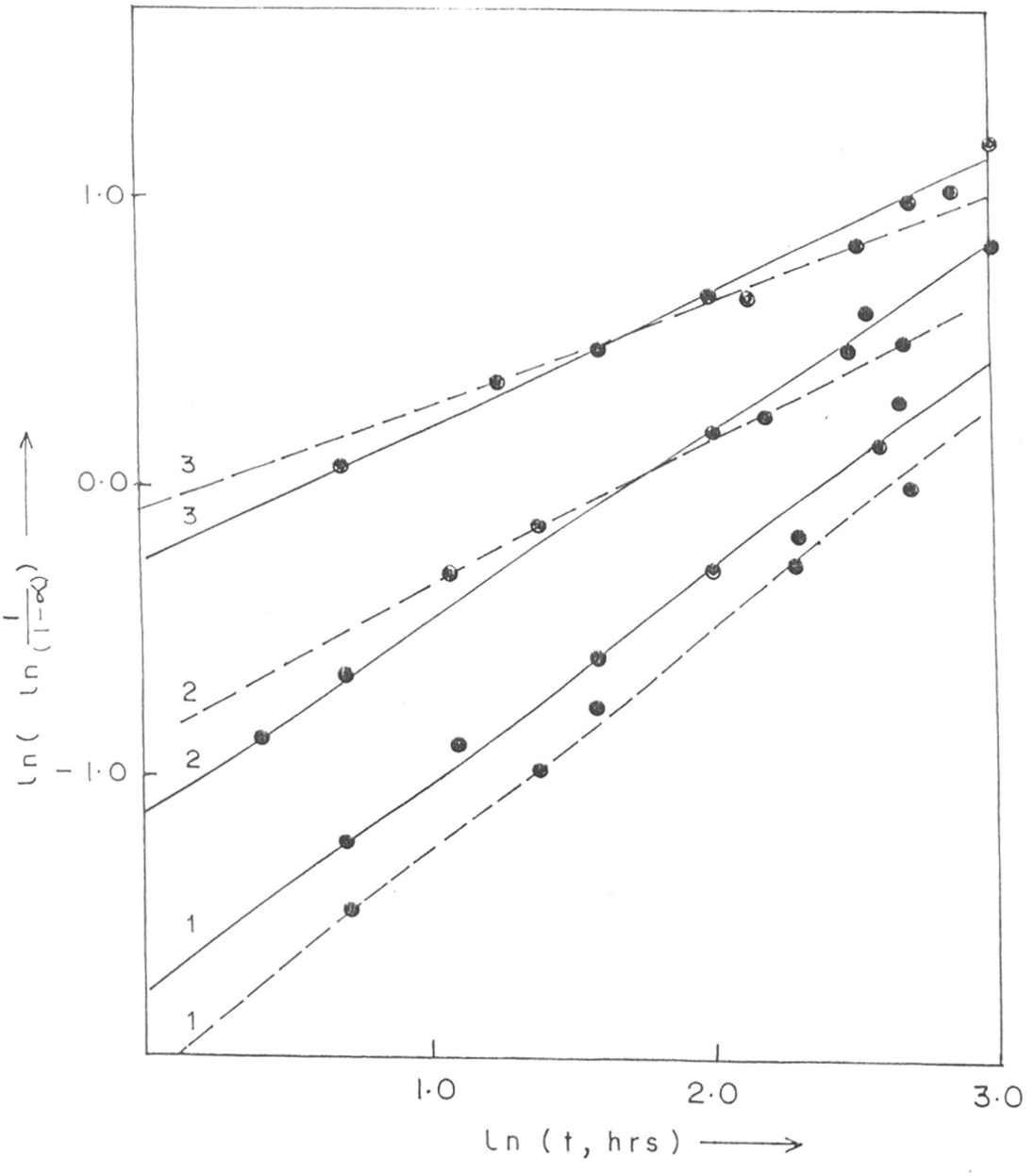

FIG·3·7 : FIT OF EXPERIMENTAL DATA TO AVARAMI-EROFEEV eqn. AT 1) 423, 2) 453, 3) 473 K USING (—) PSEUDO BOEHMITE, (---) Al. ISOPROPOXIDE.

Table 3.8

Avarami-Erofeev parameters for $AlPO_4$-5 synthesis

Synthesis Temp.K	Using Psuedoboehmite		Using Al isopropoxide	
	$k \times 10^2$	m	$k \times 10^2$	m
423	8.33	0.71	7.25	0.80
453	18.25	0.67	17.40	0.52
473	57.20	0.47	72.00	0.38

data (correlation coefficient $\approx$1) imply that the crystallization of $AlPO_4$-5 can be successfully described at least mathematically by Avarami-Erofeev equation. The values of k and m with variation in temperature indicate that the rate of nucleation and crystallization of $AlPO_4$-5 changes in a complex manner with temperature. Figs. 3.6 A and B show that the rate of nucleation is very fast during $AlPO_4$-5 synthesis as compared to ZSM-5 type zeolites; crystal growth gradually increases as the temperature and time is increased. It has been observed that at lower temperature (< 373 K) amorphous material is formed and at higher temperatures > 473 K and on prolonged crystallization periods dense phases of $AlPO_4$-xH_2O with crystalline impurities along with $AlPO_4$-5 phase are formed. The presence of dense phase i.e. tridymite and crystobalite $AlPO_4$-xH_2O structures in the products were mainly confirmed by XRD (by comparing the XRD patterns of known physical mixtures of $AlPO_4$-5 and tridymite). It appears that at higher reaction temperature the mobility of templating organic species increases so that they can come out of pores of

the framework structures easily. This may result into the unstable state of host structure as evidenced by the appearance of dense phase impurities at high temperatures.

3.5. SYNTHESIS OF SUBSTITUTED MOLECULAR SIEVES-SAPO-5

3.5.1. Synthesis of SAPO-5

As has been described earlier, SAPO-5 is considered as a silicon substitution in $AlPO_4$-5 framework. By certain modifications in physical and chemical conditions in $AlPO_4$-5 synthesis, SAPO-5 can be obtained. The basic difference in the two is that we need a reactive source of silica in addition to reactive source of aluminium and phosphorous and a suitable organic templating agent. The composition of the final gel precursor can be represented in terms of molar oxide ratio as

$$1.5\ R : x SiO_2 : 1.0\ Al_2O_3 : 1.0\ P_2O_5 : 60\ H_2O$$

where x was varied from 0.2 to 2 (0.2, 0.5, 1.0 and 2.0).

In general several batches of the homogenized hydrogels were transferred to different stainless steel autoclaves and placed in the oven at required preset temperature. The reactors were removed at regular intervals of time, quenched to room temperature, filtered, washed and dried at 393 K for further characterization

The x-ray diffraction pattern of the product is similar to that of $AlPO_4$-5 and is compared with that of standard SAPO-5 sample (Table 3.9).

Table 3.9 : XRD data of SAPO-5

SAPO-5 (synthesized)			SAPO-5 (reported)*		
2θ	dA°	I/I x 100	2θ	dA°	I/I x 100
7.5	11.80	44.00	7.5	11.80	100
12.8	6.91	8.43	12.9	6.86	12
15.0	5.90	15.10	15.0	5.90	26
19.8	4.48	47.00	19.9	4.46	61
21.0	4.23	57.23	21.1	4.21	53
22.40	3.96	100.00	22.45	3.96	77
24.80	3.96	6.00	24.80	3.59	5
25.80	3.45	39.20	26.00	3.43	30
29.00	3.08	22.90	29.10	3.07	17
30.00	2.98	22.30	30.15	2.96	19
33.60	2.67	6.00	33.65	2.66	5
34.40	2.60	19.30	34.65	2.59	16
37.0	2.43	4.80	37.10	2.42	2
37.7	2.38	15.10	37.7	2.38	7

* US Pat. 4,440,871 (1984)

The percentage crystallinity is calculated from the XRD intensities as follows :

$$\% \text{ Crystallinity} \quad \frac{\sum 2\theta, 7.6 \text{ to } 37.9 \text{ (observed)}}{\sum 2\theta, 7.6 \text{ to } 37.9 \text{ (standard)}}$$

3.5.2. Influence of source of silica and alumina

In view of the profound influnece of the source of alumina observed in the preparation of $AlPO_4$-5, similar studies were also done to investigate the influence of source of silica and alumina for SAPO-5 preparation. Gel composition was kept as 1.5 Et_3N : 1.0Al_2O_3 : 1.0SiO_2 : 1.0P_2O_5 : 60H_2O. Organic template was Et_3N.

The orthophosphoric acid supplied P_2O_5. Pseudoboehmite and aluminium isopropoxide were the sources of Al_2O_3 and precipitated silicon dioxide or tetraethyl orthosilicate were the sources of SiO_2. The observations were summarized in Table 3.10. The salient features which can be noted are :

(i) Aluminium isopropoxide gives purer products with microsil silica or tetraethyl orthosilicate.

(ii) The time for 50% crystallization is in the order microsil + pseudoboehmite < ethyl orthosilicate + pseudoboehmite < microsil + aluminium isopropoxide < ethyl orthosilicate + aluminium isopropoxide.

Hydrolysis of aluminium isopropoxide to give aluminium hydroxide and isopropyl alcohol, and depolymerization and peptization of tetraethyl orthosilicate to give silica gel and ethyl alcohol are fairly fast reactions. It is a known (104) fact that the presence of alcohol hinders the condensation of AlO_4 and SiO_4 tetrahedral units to form the precursor species for framework nucleation probably by shielding, by coordinating to those tetrahedral units hindering them to become bare ions for condensation (104) .In addition it is also to be noted that these alcohols form azeotropic mixtures which have comparatively higher boiling points.

3.5.3. Influence of the template

The template structure relationship is very flexible in the case of SAPO-5 synthesis, similar to $AlPO_4$-5. Protonated amines are as efficient as tetrafunctional hydroxides. For example,the effect of template on the purity and crystallinity was evaluated

Table 3.10 : Influence of source of silica and alumina on the purity of SAPO-5

Gel composition : $1.5Et_3N:Al_2O_3:SiO_2:P_2O_5:60H_2O$

Sample	Source		Reaction Temperature in hours for Xn			
	Silica	Alumina	Temp.K	50% Xn	100% Xn	Product purity
A	SiO_2 microsil	P.B.	423	35	-	P.B.+SAPO-5
			453	5	32	SAPO-5
			473	1.5	24	SAPO-5
B	Tetra-ethyl orthosilicate	P.B.	423	38	-	P.B+SAPO-5 + trace impurity
			453	5.5	36	SAPO-5
			473	2.0	26	
C	SiO_2 microsil	Al. isopr.	423	37	-	SAPO-5
			453	6.0	36	SAPO-5
			473	2.5	28	SAPO-5
D	Tetra-ethyl orthosilicate	Al. isopr.	423	40	-	SAPO-5
			453	8.0	40	SAPO-5
			473	4.0	48	SAPO-5

P.B. - Pseudoboechmite

Al.isopr - Aluminium isopropoxide

Xn - Crystallization

with three different templates. The experimental data as summarized in Table 3.11 show that while triethylamine is as effective a template as tetrapropyl ammonium hydroxide in that 100% SAPO-5 phase is obtained within the reaction period of 24-48 hrs. Tripropylamine gave a product of lower crystallinity with some impurity phases as can be seen from the XRD pattern shown in Fig. 3.8.

Table 3.11 : Influence of template on the purity of SAPO-5

Gel composition : $1.5R:Al_2O_3:P_2O_5:SiO_2:60H_2O$

Template R	Temp. K	Xyln period hrs.	% Crystallinity of SAPO-5 phase
Triethyl-amine (Et_3N)	473	24-48	100.00
Tetrapropyl ammonium hydroxide (TPAoH)	473	24-48	100.00
Tripropyl amine	473	24	85.00
(Pr_3N)	473	48	70.00

3. 5.4. Influence of SiO_2 concentration

Even though incorporation of Si in the framework of $AlPO_4$-5 is energetically demanding process, the substitution is found to be possible in the whole range of concentration. They were obtained according to procedure described earlier at 473 K within 24 hours. The chemical composition of the precursor gel and products obtained are summarized in Table 3.12. All the samples show similar XRD pattern without any impurity phases (Fig. 3.9).

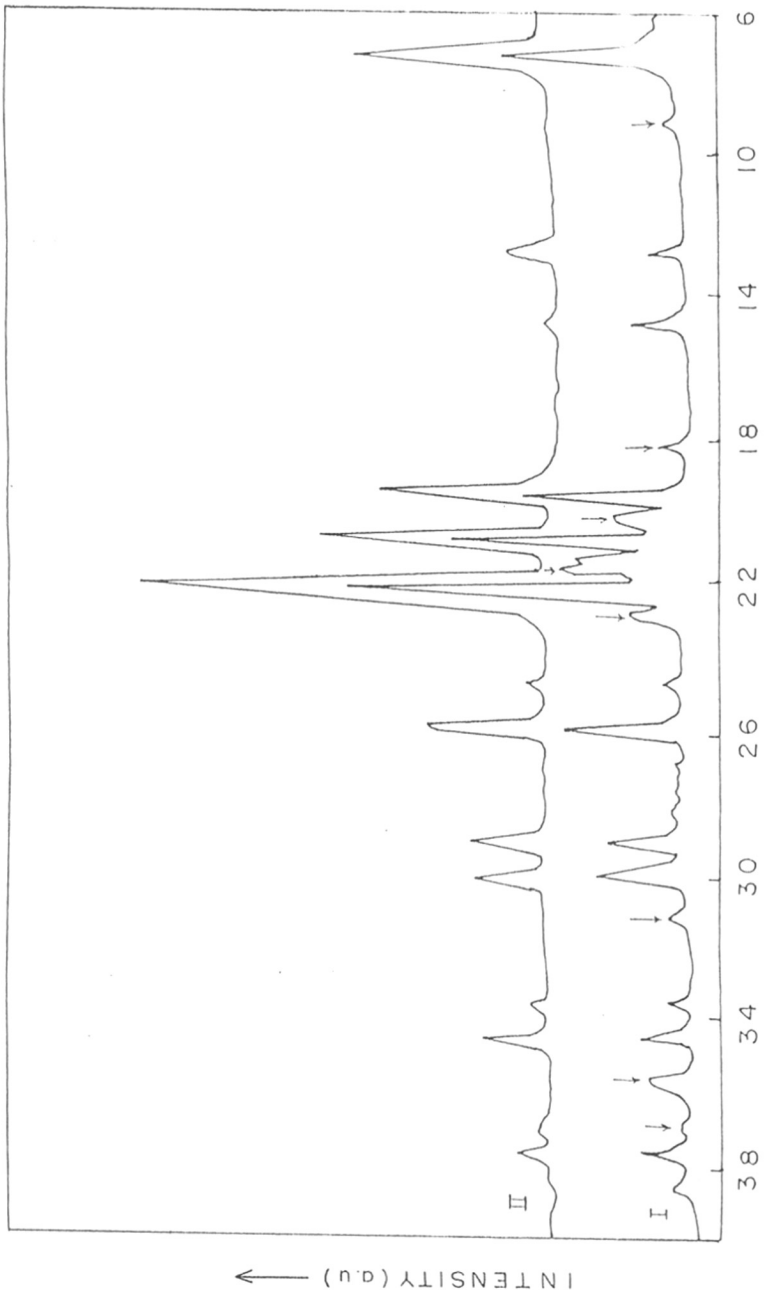

FIG.3.8 INFLUENCE OF TEMPLATE ON SAPO-5 SYNTHESIS I) Pr_3N AND II) TPAOH. (↓ – IMPURITY PHASE)

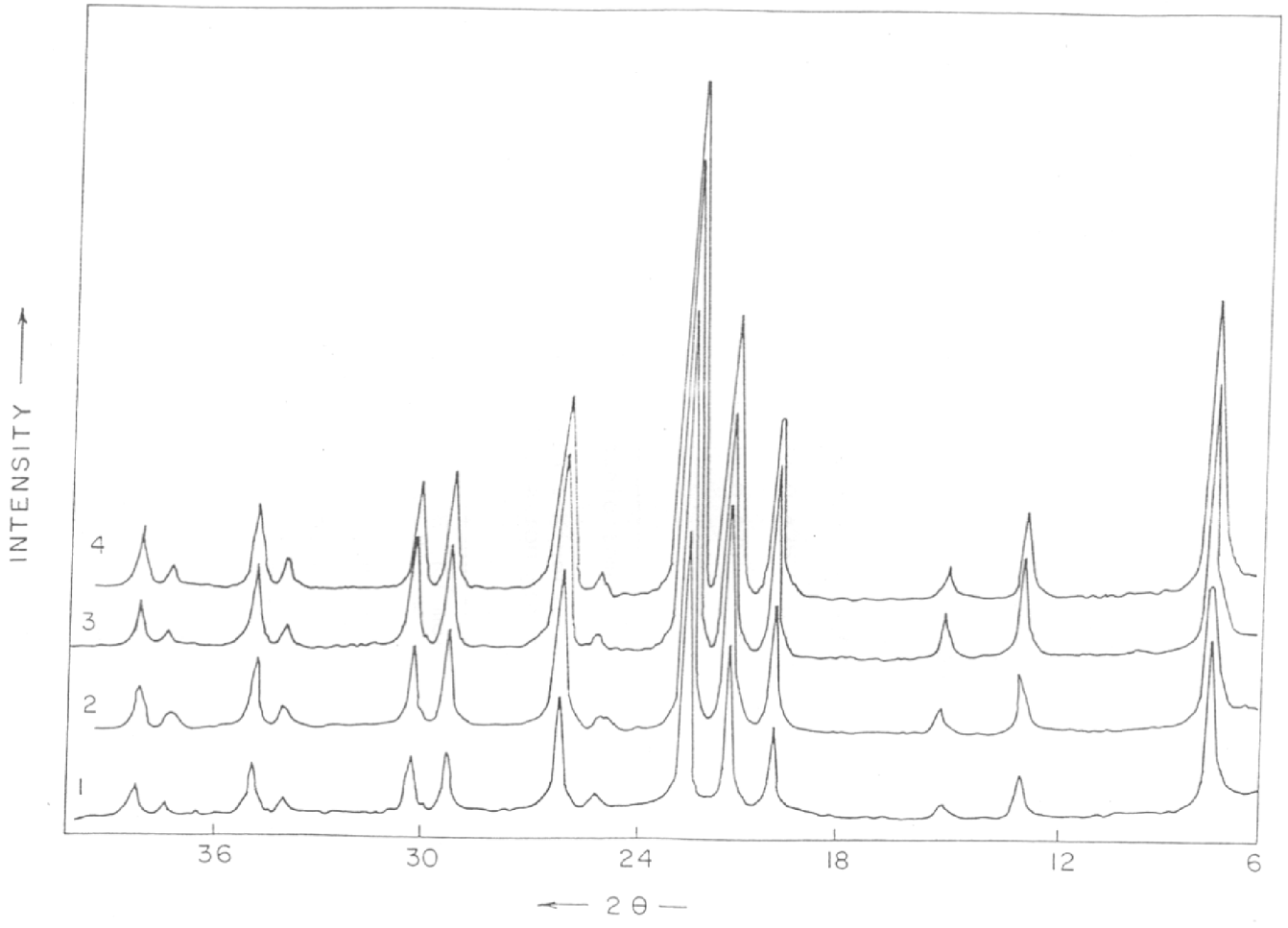

FIG 3·9 - INFLUENCE OF SiO_2 CONCENTRATION IN THE SYNTHESIS OF SAPO-5

(1) (2) (3) (4)

SAPO-5 (I), SAPO-5 (II), SAPO-5 (III), SAPO-5 (IV)

Table 3.12 - Chemical composition of metal phosphate molecular sieves

Sample	Precurser gel (m.f.)				Crystalline product (m.f.)			
	R*	Me	Al	P	R*	Me	Al	P
AlPO-5	0.75	-	0.5	0.5	0.039	-	0.51	0.49
SAPO-5I	0.75	0.024	0.49	0.49	0.038	0.09	0.48	0.43
SAPO-5II	0.75	0.06	0.47	0.47	0.040	0.21	0.45	0.34
SAPO-5III	0.75	0.11	0.44	0.44	0.041	0.29	0.42	0.28
SAPO-5IV	0.75	0.20	0.40	0.40	0.039	0.39	0.37	0.24
MgAlPO-5	0.75	0.05	0.475	0.475	0.037	0.055	0.445	0.50
ZnAlPO-5	0.75	0.05	0.475	0.074	0.037	0.025	0.465	0.50
CoAlPO-5	0.75	0.05	0.475	0.475	0.033	0.035	0.46	0.50
FeAlPO-5	0.75	0.05	0.475	0.475	0.031	0.035	0.455	0.50

m.f. = mole fraction, R* = organic template.

Table 3.13 : Kinetic parameters of crystallization for SAPO-5

Sample	E_n KJ mole^{-1}	E_e KJ mole^{-1}
AlPO-5 (P.B.)	40.40	66.12
SAPO-5 PB + SiO_2	67.20	100.44
SAPO-5 Al.isopropoxide + SiO_2	71.94	106.53
SAPO-5 PB + ortho-Et.silicate	73.52	110.13

It is interesting to note that there is no appreciable change in unit cell size on increasing concentration of Si from 0.09-0.39 mole fraction as contradictory to zeolites where unit cell contraction takes place on increasing Si concentration. This can be attributed to the fact that Si-O (1.62 A^{O}) bond length is almost equal to the mean of the bond lengths of Al-O (1.75 A^{O}) and P-O (1.52 A^{O}).

3.5.5. Kinetics of crystallaization

Kinetic study was done for a selected batch composition to determine kinetic parameters. General procedure has been already described. For example, reactant gel mixture was prepared by adding 14.4 gm pseudoboehmite, 22.30 gm orthophosphoric acid, 120 gm of water, 6.31 gm of SiO_2 and 18.02 gm of Et_3N according to the procedure described earlier, and autoclaved hydrothermally for different duration at 423, 453 and 473 K respectively. Percen-tage crystallinity was also determined from XRD spectra (Fig. 3.10) as mentioned earlier. The crystallization curves are depicted in Fig. 3.11 A and B. The reaction temperature strongly influences the kinetics of the process because when the temperature of the crystallization is increased, the solubility of the reactant also increases. Higher temperature also helps in stripping off of the hydration shell of aluminium hydroxide and silicic acid to form bare AlO_4, SiO_4 and PO_4 tetrahedra to enable them to combine to form framework structures. The crystallization curves are typically sigmoid,characteristic of process involving two different stages (i) an induction period when nuclei are formed, and (ii) a crystal growth period when nuclei grow into

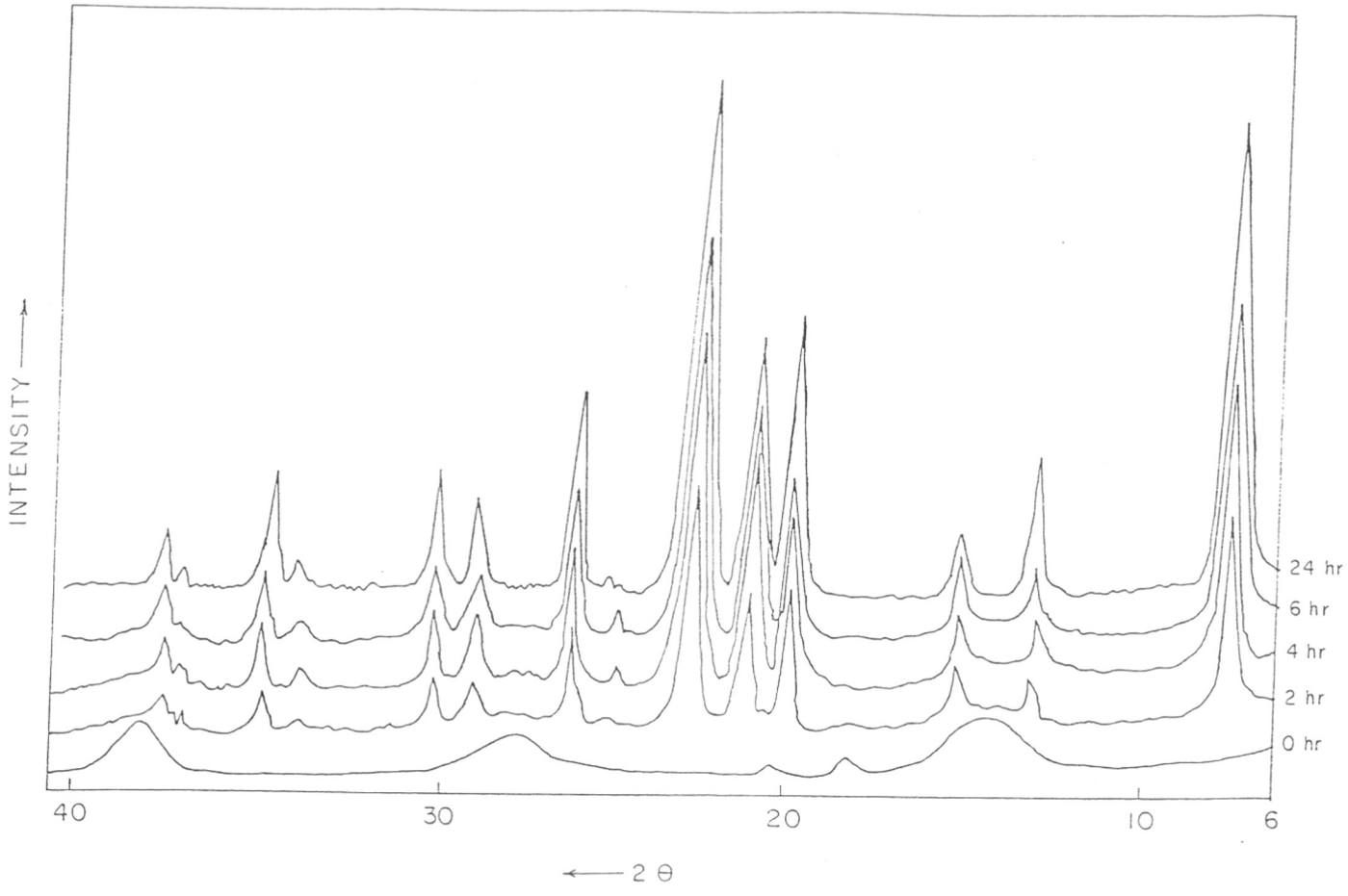

FIG 3·10 - INFLUENCE OF CRYSTALLIZATION PERIOD ON XRD CRYSTALLINITY OF SAPO - 5

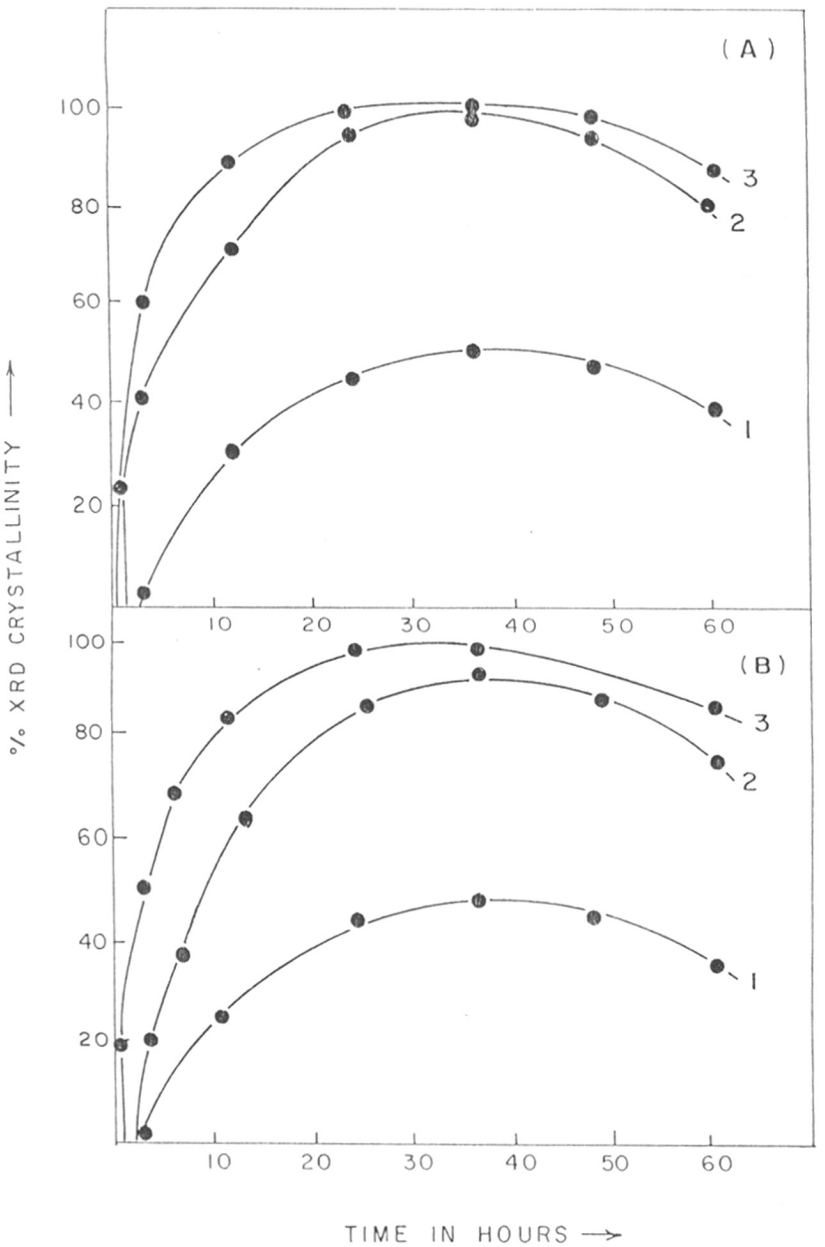

FIG. 3·11 - KINETICS OF CRYSTALLIZATION OF SAPO-5 AT 1) 423, 2) 453, 3) 473 K USING (A) P.B.+ SiO_2 (B) P.B.+ ORTHOETHYL SILICATE.

crystals. The apparent activation energy for nucleation and crystal-lization for SAPO-5 are graphically determined (Fig.3.12) applying Arrhenius equation. The calculated values of E_n and E_c are listed in Table 3.13. The experimental fit of the data to Avrami-Erofeev equation is illustrated in Fig.3.13 and the parameters calculated are given in Table 3.14. From the values of E_n and E_c for $AlPO_4$-5 and SAPO-5 materials, which are significantly lower than corresponding values for zeolites, it seems that the isomorphous substitution of Si in the $AlPO_4$ system can be achieved more readily than of Al in SiO_2 system like in zeolite (76). Zeolites cannot be prepared in acidic medium whereas crystallization of $AlPO_4$-5 can occur over a wider range of pH conditions. During the crystallization the medium of $AlPO_4$-5 synthesis changes from acidic to alkaline which reduces the tendency of substituting species to have octahedral coordination and favours to assume ionic forms suitable for incorporation into the growing precursor species. This seems to be the plausible reason why aluminophosphate molecular sieves have lower E_n and E_c than the zeolitic molecular sieves.

From these results following conclusions can be drawn :

(1) The apparent activation energy for nucleation (E_n) and crystallization (E_c) for SAPO-5 is considerably higher (e.g. 67.2 and 100.44 KJ $mole^{-1}$) than for $AlPO_4$-5 (40.4 and 66.2 KJ $mole^{-1}$). The substitution of Si in $AlPO_4$-5 framework is supposed to be preformed by substituted amorphous phase metavariscite and variscite . In addition , this process involves the formation of

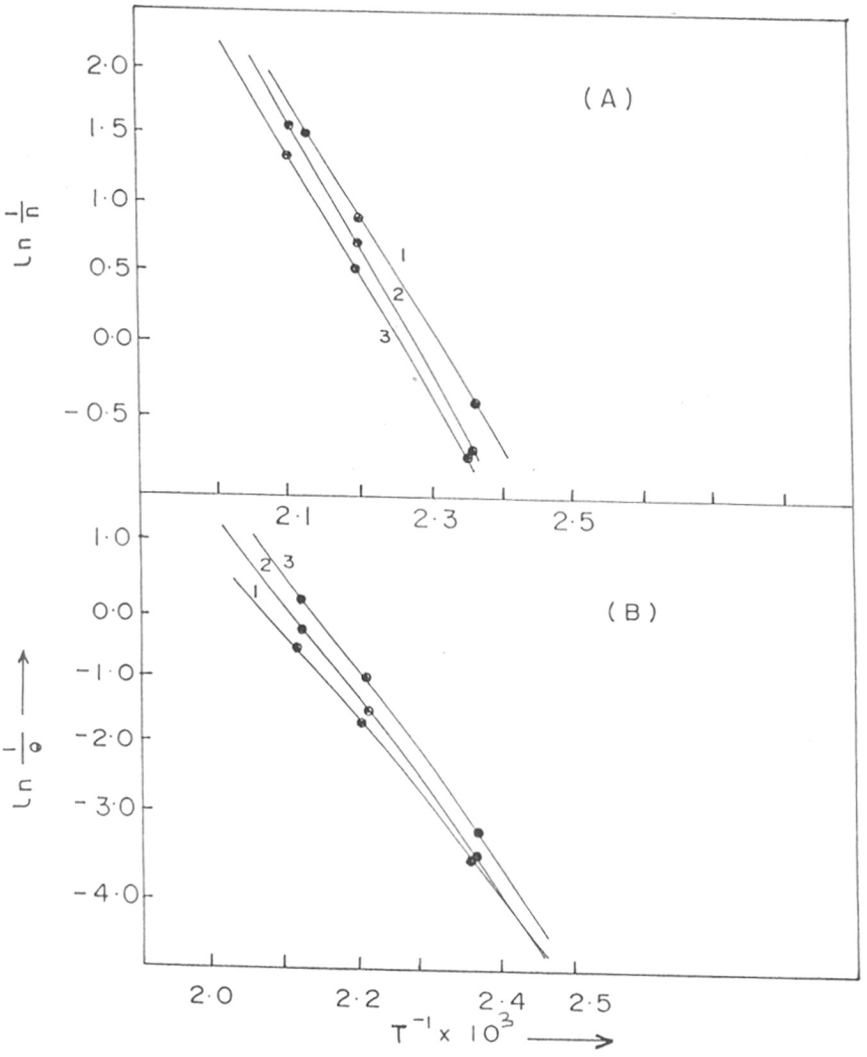

FIG. 3.12 : ARRHENIOUS PLOTS FOR NUCLEATION(A), CRYSTALLIZATION (B) FOR SAPO-5 USING PB (1), AL.ISOPROPOXIDE (2), AND ORTHO ETHYL SILICATE (3).

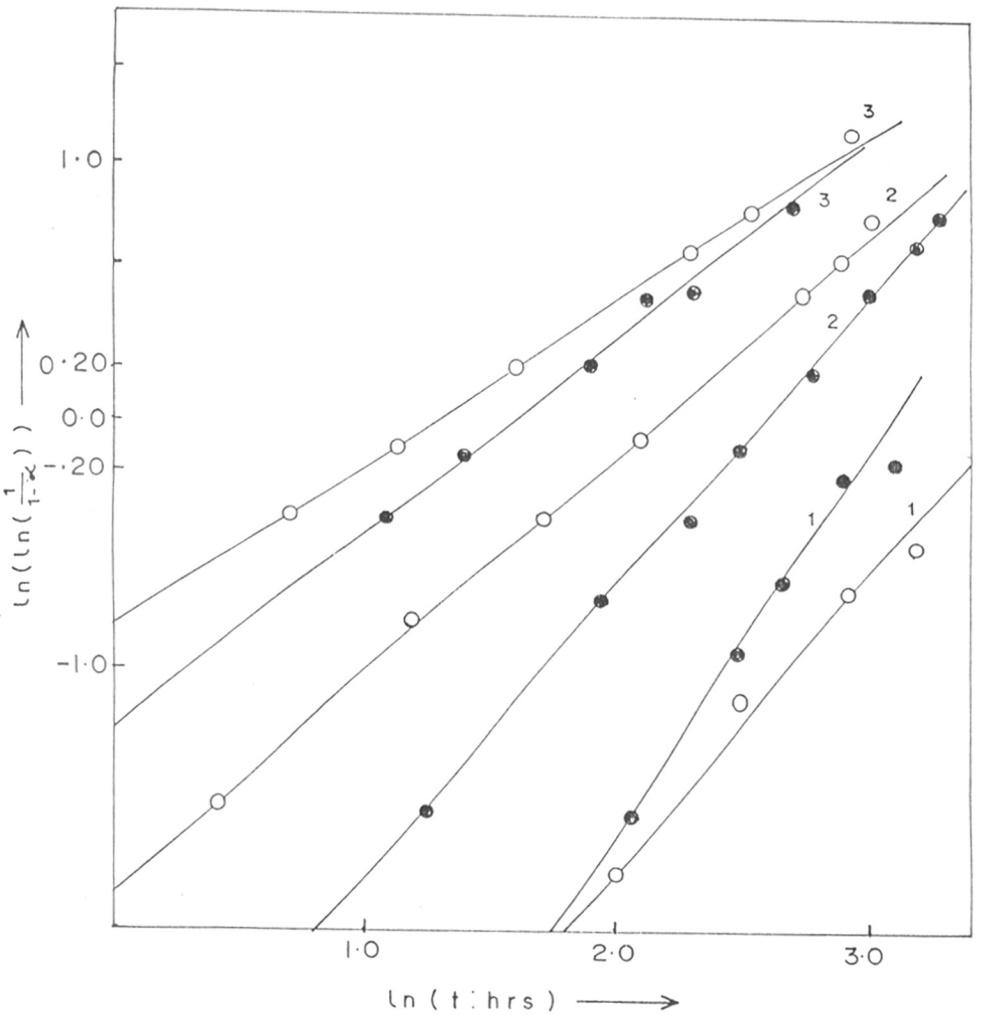

FIG. 3.13

FIT OF EXPERIMENTAL DATA TO AVARAMI-EROFEEV EQUATION, at 1) 423, 2) 453, and 3) 473 K FOR SAPO-5 USING P.B. + SiO_2 (●) AND P.B. + Et. SILICATE (○)

Table 3.14 : Avarami-Erofeev parameters for SAPO-5

Synthesis Temp. K	SAPO-5 (P.B.)		SAPO-5 (Al.isopr)		SAPO-5 (Et.Si)	
	$K \times 10^2$	m	$K \times 10^2$	m	$K \times 10^2$	m
423	2.94	1.16	2.90	1.25	4.16	1.44
453	11.80	0.86	16.30	0.73	7.70	1.13
473	28.00	0.65	24.30	0.60	20.25	0.77

P.B. - Pseudoboehmite.

Al.isopr. - Aluminium isopropoxide.

Et.Si. - Tetra ethyl ortho silicate

precurser species by proper condensation of yet another species (i.e. SiO_4) in addition to AlO_2^- and PO_2^+. Hence higher E_n and E_c for SAPO-5 than for $AlPO_4$-5 can be attributed to this effect.

(2) E_n and E_c are found to increase systematically as the amount of alcohol produced by hydrolysis of aluminium isopropoxide and/or tetraethyl orthosilicate increases in the reaction mixture. Such influence in zeolite preparation is well recognised (104). The dilution of the gel is also one of the contributing factor in this regard because dilution is a crucial factor in hydrothermal synthesis.

(3) E_n and E_c for SAPO-5 are considerably lower than those for zeolite crystallization because they are crystallized in acidic to slightly alkaline medium where stability of ionic species for forming precurser for framework formation is favourable.

(4) Nevertheless the crystallization of SAPO-5 follows the kinetic features similar to that for zeolite crystallization.The most preferred crystallization period and temperature are 24-48 hours and 453-473 K respectively.

3.6. METAL SUBSTITUTED ALUMINOPHOSPHATES (MeAPO-5)

Incorporation of catalytically active metals in aluminophosphate ($AlPO_4$) molecular sieves to improve catalytic activity and selectivity is a well known technique (13). Metals in such systems may be present as a part of framework or as extra framework species. If present in the framework they produce anionic sites with negative charge coupled with exchangeable cations and Brönsted acid sites and if present outside the framework they can

act as charge balancing cationic, polyhydroxy or oxide species.

The present study was undertaken to prepare Fe, Co, Mg and Zn incorporated $AlPO_4$-5 molecular sieves and to study their physicochemical and catalytic properties.

3.6.1. Synthesis of MeAPO-5

The hydrothermal synthesis of crystalline metal aluminophosphates was carried out by crystallization of a reaction mixture containing a source of alumina and orthophosphoric acid in 40-60 moles of water and 0.1 mole of any one metal salt from the group (Mg, Zn, Co, Fe,). To the above gel mixture 1.5 moles triethylamine was added slowly while stirring till the gel becomes homogeneous. The gel was loaded in a stainless steel reactor lined with teflon and autoclaved at 473 K for 24 hours. The optimum crystallization period and temperature as observed in the synthesis of $AlPO_4$-5 and SAPO-5 was in the range of 24-48 hours and 453-473 K respectively. Therefore, the crystallization of MeAPO-5 was carried out at 473 K for 24 hours to get the product with the maximum crystallinity . The gel composition of MeAPO-5 used for the synthesis is

$$1.5\ Et_3N{:}0.9\ Al_2O_3{:}1.0\ P_2O_5{:}0.1\ MeO_n{:}40\text{-}60\ H_2O$$

MeAPOs exhibit (29) a wide range of compositions within the general formula $(Me_xAl_yP_z)O_2$ with x varying between 0.01 to 0.3 the actual data available for MeAPOs indicate that in the as-synthesized materials only relatively small quantities of metals are incorporated. The highest degree of substitution in the large pore variant is reported (12) to be 0.08. The general substitu-

tion mechanism of di- and trivalent Me ions in AlPO-n structures seems to be an exclusive replacement of Al atoms.(23).

The crystallized products were characterized by XRD, SEM, DTA/TG, sorption of probe molecules like water, n-hexane, cyclohexane and o-xylene. Temperature programmed desorption and diffuse reflectance F.T.I.R. was used to characterize the acid site distribution and surface hydroxyl groups.

Characterization

The XRD data of the as-synthesized MeAPO-5 listed in Table 3.15 indicates that the XRD patterns of the microporous crystalline metal aluminophosphates were similar to that of $AlPO_4$-5 molecular sieves (8). However, the intensity pattern for ZnAlPO-5, MgAlPO-5, CoAlPO-5 and FeAlPO-5 differed from that of $AlPO_4$-5.

The morphology of MeAPO-5 examined by SEM (Fig. 3.14) indicates that incorporation of metals in $AlPO_4$-5 to prepare MeAPO-5 was accompanied by a marked change in crystal growth. $AlPO_4$-5 exhibits a mixture of spheroidal aggregates and hexagonal barrel shaped crystals, whereas the metal substituted $AlPO_4$-5 consists of a mixture of well defined hexagonal barrels (20-40 μ) hexagonal plates and small ill-defined clusters. The electron microprobe analysis of large single crystals indicated relatively low concentration of substituted metal in the large barel shaped crystals.

Results of chemical analysis in terms of mole fractions are listed in Table 3.12. MeAPOs molecular sieves are in general hydrophilic and adsorb water preferentially over common hydrocar-

Table 3.15 : XRD data of MeAPO-5

2 θ	dA°	$AlPO_4$-5	ZnAlPO-5	MgAlPO-5	CoAlPO-5	FeAlPO-5
7.6	11.62	63.22	100	86.05	54.11	48.80
13.1	6.75	11.50	21.11	13.95	11.76	12.20
15.1	5.86	20.61	23.60	25.58	17.65	15.85
19.9	4.45	62.64	52.63	70.54	52.94	44.60
21.1	4.22	59.77	38.42	41.08	57.65	57.32
22.5	3.98	100.00	75.26	100.00	100.00	100.00
24.8	3.58	5.75	3.68	6.20	7.06	4.90
26.2	3.40	37.40	30.00	47.30	37.65	35.40
29.1	3.06	18.97	14.74	20.95	21.20	23.20
30.3	2.94	21.84	19.47	31.00	31.76	21.95
33.9	2.64	8.47	4.21	7.75	8.23	5.10
34.6	2.59	20.34	16.87	24.03	21.20	14.50
37.20	2.41	5.93	3.16	5.42	5.88	4.78
37.9	2.37	12.71	12.10	15.50	18.82	13.45

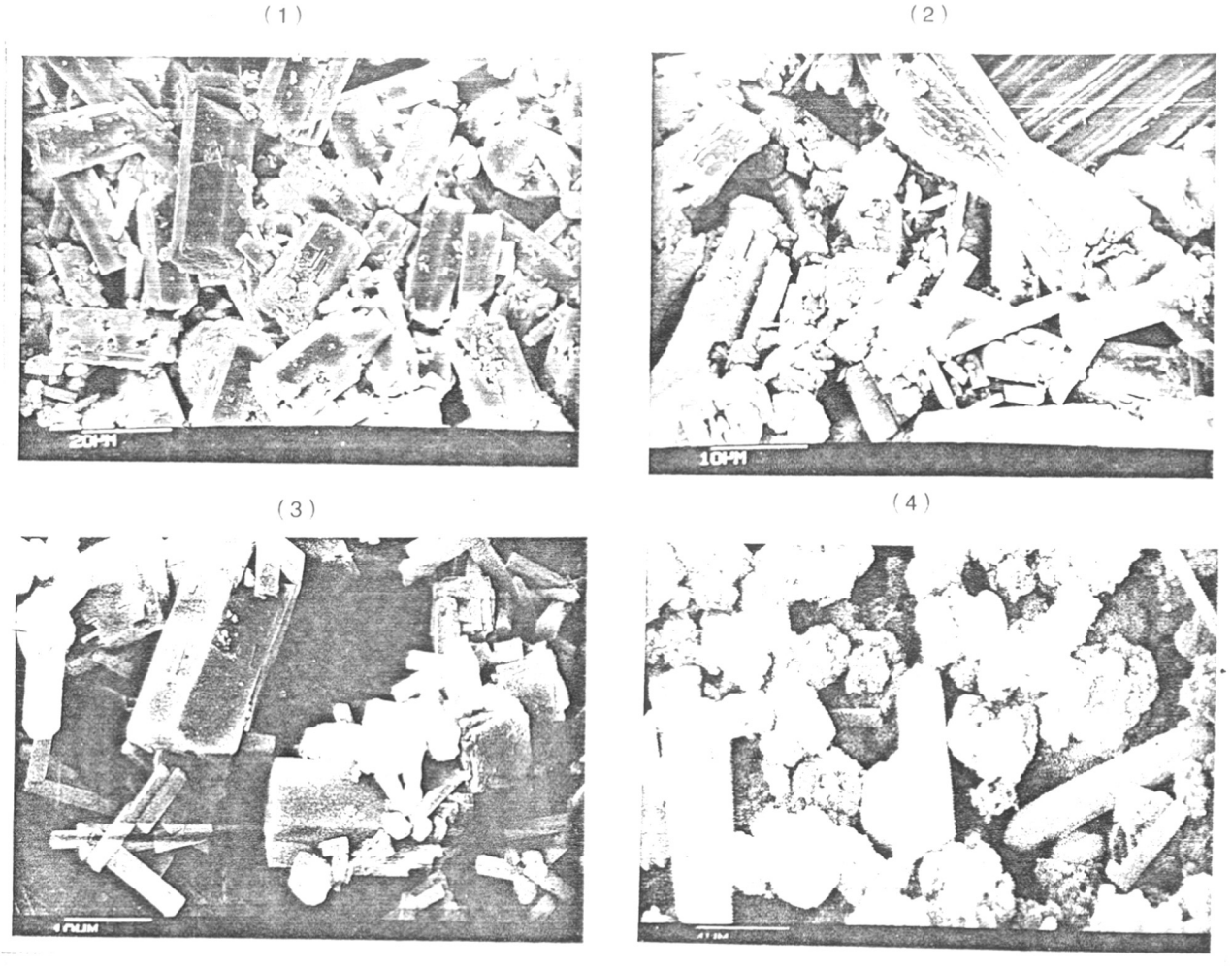

Fig. 3.14. SEM PHOTOGRAPHS OF (1) ZnAlPO-5, (2) MgAlPO-5, (3) CoAlPO-5 and (4) FeAlPO-5.

bon molecules and also exhibit considerable ion exchange capacity. The adsorption properties of the present MeAPOs appear to be quite similar to those of the low silica aluminosilicate zeolites.

CHAPTER - IV

PHYSICOCHEMICAL - CHARACTERIZATION

4.1. THERMAL ANALYSIS

4.1.1. Aluminophosphates ($AlPO_4$-5)

Thermal analysis has been applied for characterizing $AlPO_4$-5 and modified $AlPO_4$-5 molecular sieves (MeAPO-5). It is possible to determine the nature of templating species, kinetics of crystallization, energetics of sorbent desorption and thermal stability of framework structure from thermal analysis. The typical TG/DTA curves for highly crystalline $AlPO_4$-5 as-synthesised and calcined samples are illustrated in Fig. 4.1. The TG/DTG curves for Et_3N-$AlPO_4$-5 show that the removal of triethylamine and water occluded in the channels of aluminophosphates occurs in discrete stages. The data on the temperature ranges and the weight losses in different stages are presented in Table 4.1. Water from the external surface and the channels is desorbed in the first stage having peak temperature at 373 K. It is about 8.5% for the highly crystalline product. The removal of triethylamine and additional water takes place. in the following stages at the peak temperature of 673 K. The triethylamine starts desorbing with simultaneous cracking to smaller molecules by successive elimination reactions (31)

$$(C_2H_5)_3N \longrightarrow C_2H_4 + NH(C_2H_5)_2$$
$$(C_2H_5)_2NH \longrightarrow C_2H_4 + NH_2C_2H_5$$
$$C_2H_5NH_2 \longrightarrow C_2H_4 + NH_3$$

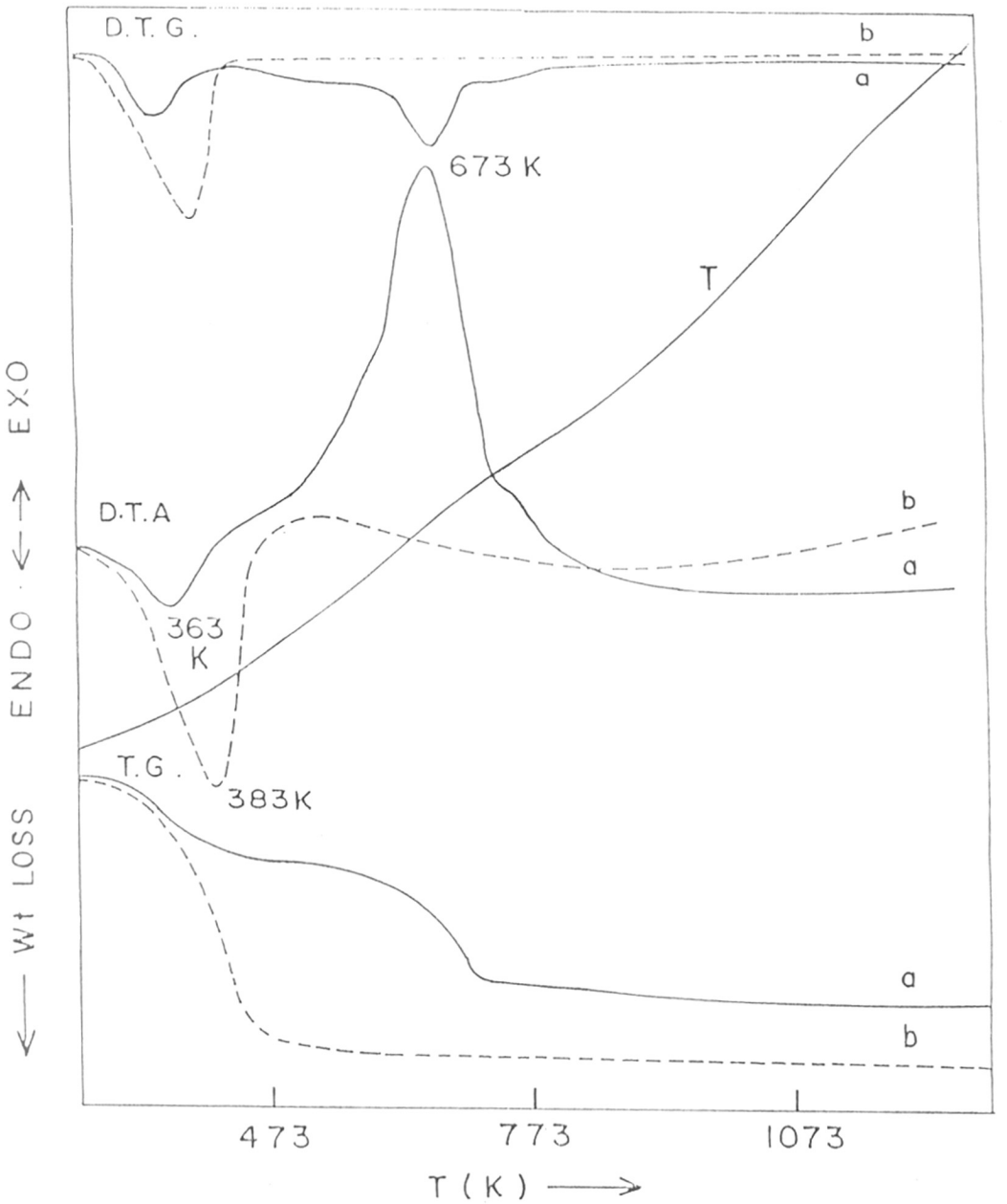

FIG.4·1: THERMOGRAMS OF $Et_3N-AlPO_4-5$ (—,a) $AlPO_4-5$ (---,b)

Table 4.1 : Characteristics of thermograms of Et_3N-$AlPO_4$-5 Et_3N-SAPO-5 and Et_3N-MeAPO-5 molecular sieves

Sample	% Crystal-linity phase-5	Dehydration Peak Temp.K	% wt loss	Decomposition Peak Temp.K	%wt. loss	Org.temp -late wt% loss	Total % wt. loss	Temp-late cc/g.
$AlPO_4$-5	50.20	353	4.5	553	8.5	3.50	13.00	0.096
	72.30	353	6.3	563	10.00	5.00	16.30	0.095
	88.40	358	7.2	568	11.50	6.20	18.70	0.096
	100.00	363	8.5	587	12.00	7.10	10.50	0.097
SAPO-5	53.10	358	4.00	683	9.34	3.70	13.34	0.096
	70.00	363	5.00	698	10.67	4.90	15.67	0.096
	90.00	363	6.00	708	11.90	6.20	17.90	0.095
	100.00	368	6.60	713	12.80	6.55	19.40	0.090
MgAlPO-5	93.00	373	8.50	723	9.00	6.50	17.50	0.096
ZnAlPO-5	94.00	353	8.00	793	10.00	6.70	18.00	0.098
CoAlPO-5	85.00	373	7.00	693	10.00	5.90	17.00	0.095
FeAlPO-5	60.00	378	8.50	743	9.50	5.90	18.00	0.094

and their oxidation products. Since the kinetic diameters of triethylamine(7.8A^{o}), ethylene (3.9A^{o}) and ammonia (2.6A^{o}) are smaller than the pore opening of $AlPO_4$-5 (8.0A^{o}), they can diffuse out of the channels easily under these conditions. The channels of $AlPO_4$-5 are polar (16), therefore, the triethylamine molecules can be strongly held in the channels — at lower temperatures but at higher temperatures they are desorbed although some cracking can also occur. A small weight loss (0.5%) in the last stage beyond 825 K may be attributd to desorption of ammonia and/or triethylamine and oxidation of residual coke produced during cracking reactions.

The thermogram of pure $AlPO_4$-5 shows single step desorption of water (383 K) from the micropores of $AlPO_4$-5. $AlPO_4$-5 is found to be stable at least upto 1273 K because no exothermic peak of structural collapse is observed.

In Fig. 4.2, the TG weight loss in endo-and exothermic desorption temperature ranges are plotted against per cent crystallinity for a number of samples of different crystallinity. As the crystallinity increases, the weight loss due to endothermic desorption of water, the weight loss in the region of exothermic decomposition and notably that due to loss of organic template increases linearly. From organic loss it has been found that about one triethylamine molecule per unit cell is occluded in the framework and about 0.095 ml/g pore volume is occupied by triethyamine which is a measure of the volume of the voids large enough to accommodate the template molecule. The additional weight loss in the exothermic region can therefore be accounted for the water trapped inside the pores unoccupied by triethyl-

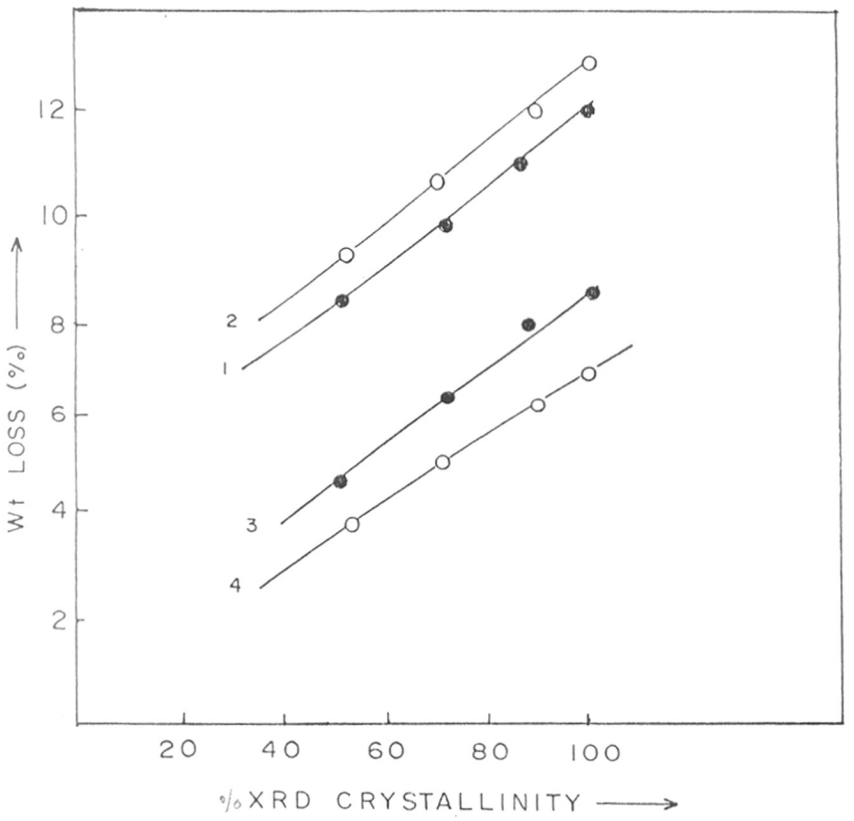

FIG. 4.2 : VARIATION OF Wt. LOSS ON DESORPTION OF WATER (3,4) AND DECOMPOSITION OF TEMPLATE (1,2) WITH % XRD CRYSTALLINITY OF $Et_3N-AlPO_4-5$ (●) AND $Et_3N-SAPO-5$(II) (○)

amine.

4.1.2. Kinetics of dehydration

In order to study the physical significance of the desorption of water from microporous aluminophosphate molecular sieves, it can be assumed that the numerical value of the order of reaction (n) is proportional to the number of monomolecular layers that constitute the film of water adsorbed on the surface of the molecular sieves. The activation energy E_d for the desorption of zeolitic water has been calculated from the TG curves using the Coats-Redfern equation (I) (116) and the Piloyan-Novikova (117) equation (II). Similarly, E_d was also evaluated from the relation (III) described by Piloyan-Novikova for the DTA curves. The order of reaction, (n), was independently calculated from the DTA endotherm using Kissinger's emperical formula (118) (IV) which are summarized below

$$\log \frac{(\log (1-\alpha)}{T^2} = \log \frac{AR}{E_b}\left(1 - \frac{2\,RT}{E}\right) - \frac{E_{TG}}{2.303\,RT} \quad \ldots\ldots \quad (1)$$

$$\log \left(\frac{m}{T^2}\right) = A' - \frac{E_{TG}}{2.303\,RT} \quad \ldots\ldots\ldots\ldots\ldots \quad (II)$$

$$\log (\Delta T) = C' = \frac{E_{DTA}}{2.303\,RT} \quad \ldots\ldots\ldots\ldots\ldots \quad (III)$$

$$n = 1.26\,(S)^{1/2} \quad \ldots\ldots\ldots\ldots\ldots \quad (IV)$$

where m is the mass loss at time t, α is the relative mass loss, n is the order of reaction, T is the temperature (K), b is the rate of heating of the sample, ΔT is the deviation of the DTA curve from the base line and 's' is the shape index factor which is equal to the ratio of the segments formed by the intersection of tangents to the points of inflextions of the thermal effects with the base line. The value of n was found to be nearly one.

The typical plots of log $[-\ln(1-\alpha)/T^2]$ vs 1/T for $AlPO_4$-5 and modified $AlPO_4$-5 are shown in Fig. 4.3. The characteristics of DTA curves along with corresponding E values are given in Table 4.2. The activation energy for dehydration for $AlPO_4$-5 is found to be 42.8 KJ $mole^{-1}$ which is comparable to that for ZSM-5 zeolite (86). The surface nature of $AlPO_4$-5 molecular sieve is reported to be weakly to mildly hydrophilic. According to recent literature (115), the adsorbed water in $AlPO_4$-5 is known to form crystal hydrates. The relatively high activation energy for desorp-tion can be attributed to this property of $AlPO_4$-5 molecular sieves.

4.1.3. Silico aluminophosphates (SAPO-5)

Typical thermal decomposition patterns of SAPO-5 molecular sieve precursers having 0.09 and 0.39 mole fractions of silicon (Et_3 N-SAPO-5(I) and Et_3N-SAPO-5(IV) respectively are given in Fig.4.4. In the first stage, at a peak temperature of 423 K, a wt. loss of about 6.6 % is observed which is due to dehydration of physically adsorbed water on the pore opening and on the external surface of the sample. The DTA shows two exothermic peaks at 653 and 713 K which correspond to the wt.loss of 12.8% in TG and have been attributed to the oxidative decomposition of triethylamine. The fact tha this decomposition occurs in two stages (at 653 and 713 K) implies ...

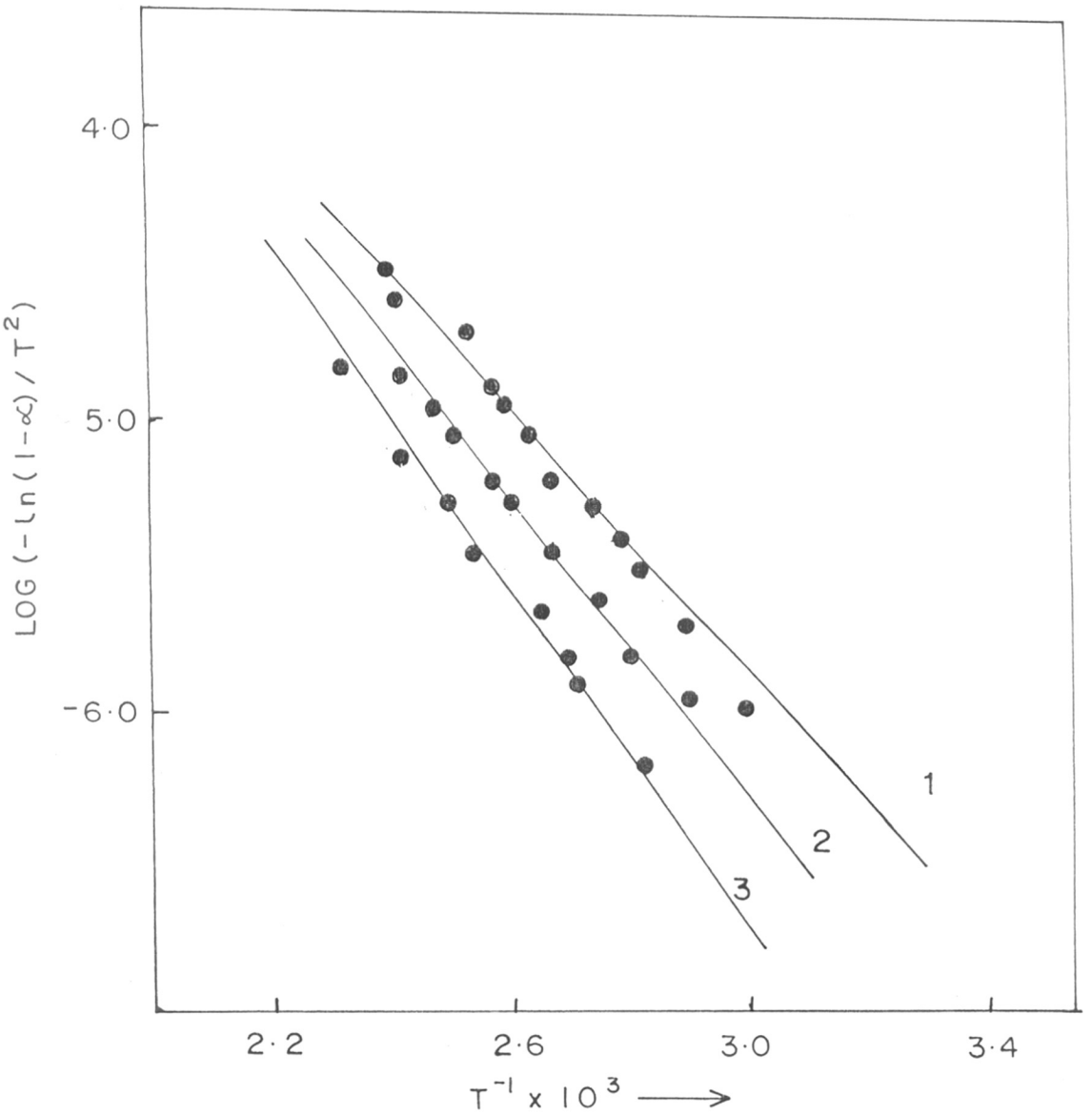

FIG. 4.3 : PILOYAN - NOVIKOVA PLOTS FOR
1) $AlPO_4$-5, 2) SAPO-5, 3) ZnAlPO-5

Table 4.2 : Kinetic parameters for dehydration of $AlPO_4$-5 and MeAPO-5 molecular sieves

Sample	% wt. loss	DTA Endo.Tmax K	Activation energy for dehydration E_d KJ mole-1
$AlPO_4$-5	20.00	378	42.80
SAPO-5(I)	18.60	383	49.00
SAPO-5(II)	18.00	413	50.40
SAPO-5(III)	17.33	418	54.20
SAPO-5(IV)	16.00	423	56.90
MgAlPO-5	17.70	393	55.40
ZnAlPO-5	19.30	388	49.70
CoAlPO-5	17.00	373	48.50
FeAlPO-5	16.00	368	46.00

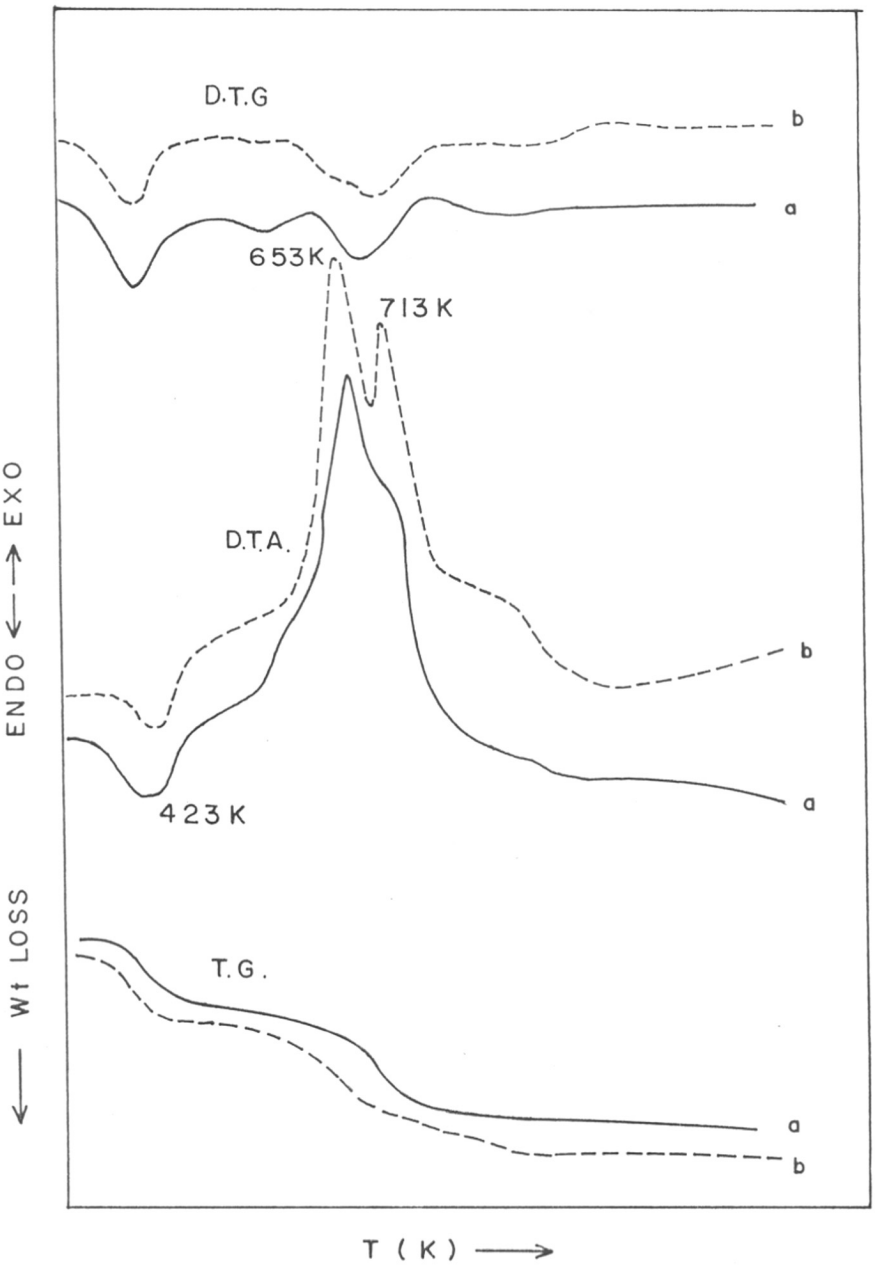

FIG 4.4 : THERMOGRAMS OF Et_3N – SAPO-5 (I) (a), AND Et_3N - SAPO-5 (IV) (b).

that triethylamine molecules in SAPO-5 occupy two energetically non-equivalent positions in the framework or interact differently with neighbouring moities distributed in the structure. As the mole fraction of Si in SAPO-5 is increased from 0.09 to 0.39 (compare curve a and b in Fig. 4.4) the intensity of the exothermic peak at 673 K is relatively lower than that for high temperature exothermic peak at 713 K. For Et_3N-$AlPO_4$-5, no high temperature exothermic peak is observed. Hence, these peaks can be assigned to the decomposition of occluded neutral triethylamine and protonated triethylamine interacting with the negative charge on the framework, due to isomorphous substitution of Si in SAPO-5. There are many papers reporting such observations for high silica zeoalites (111), FeAPO-5 (112) and CoAlPO-5 (113) molecular sieves for example.

The relative parameter of oxidative decomposition of triethylamine occluded in SAPO-5 and the total carbon + nitrogen content in the sample is related to the percentage of XRD crystallinity. This is illustrated in Fig. 4.2. The weight loss in the region of oxidative decomposition and organic loss is found to be linearly proportional to the amount of crystalline SAPO-5. The pore volume accessible to triethylamine is around 0.1 ml/g which suggests that in addition to this, SAPO-5 contains some internal pores accessible to only smaller molecules like H_2O. From the amount of organic loss, it can be concluded that in Et_3N-SAPO-5 molecular sieve there is one triethylamine molecule per unit cell occluded in the channels.

A small weight loss of about 0.6% in the last stage of oxida-tive decomposition can be attributed to the burning of carbona-ceous deposits produced by cracking products of triethylamine.

4.1.4. Kinetics of dehydration of SAPO -5(I-IV)

Isomorphous substitution of Si into $AlPO_4$-5 framework probably occurs by a mechanism involving replacement of P by Si. Increasing amount of Si substitution in this mode should result in increasing anionic framework, consequently icnreasing hydrophilicity. Kinetic analysis of dehydration of SAPO-5 samples with different moles of Si (SAPO-5, I to IV with Si moles 0.09 to 0.39) was carried out by applying Piloyan-Novikova's equation as explained for $AlPO_4$-5. The order of reaction 'n' which was obtained by shape index method was found to be 1. The typical plot of log $[-\ln(1-\alpha)/T^2]$ vs T^{-1} for SAPO-5 (IV) is illustrated in Fig. 4.3. Values of the apparent activation energy for dehydration for all the samples are tabulated in Table 4.2. The peak temperature for dehydration increases from 383 K for SAPO-5(I) to 423 K for SAPO-5(IV), and is higher than that for $AlPO_4$-5 (373 K). The corresponding apparent activation energies for dehydration E_d were found to be 49.0, 50.4, 54.2 and 56.9 KJ $mole^{-1}$ whereas for $AlPO_4$-5, E_d is only 42.8 KJ $mole^{-1}$. It may be concluded that SAPO-5 is more hydrophylic than $AlPO_4$-5 which increases with increase in Si content.

4.1.5. Metal alumino phosphates (MeAPO-5)

Thermogravimetric analysis has been applied to $AlPO_4$-5 molecular sieves modified by Co, Zn,Fe and Mg cations. The characte-

ristics of TG/DTG/DTA curves for these materials are summarized in Table 4.1. The nature of thermograms is comparable to that of SAPO-5. Endothermic desorption of water, two step oxidative decom-position of triethylamine and the burning of residual carbonaceous material in the last stage are broadly similar to SAPO-5. It can be noted that in all cases the oxidative decomposition of triethylamine is complete at around 830 K. Hence we have calcined all these materials at 823 K in the flow of air to obtain active catalysts.

From the Table 4.1 it is clear that in all forms of $AlPO_4$-5 triethylamine fills all the accessible volume in the channels irrespective of charge on the framework. The number of template molecules per unit cell for all these materials is also found to be about 1.0 per unit cell.

Order of reaction 'n' calculated by shape index method is about 1.0. Activation energy for dehydration E_d, was calculated by Piloyan-Novikova's method. The values are tabulated in Table 4.2. It varies from 46 to 55 KJ mole^{-1}. The exact correlation between E_d and nature of cation cannot be noticed because some amorphous impurity is found in all these samples. Nevertheless, they are thermally stable upto 1273 K. This has been confirmed by XRD patterns of the residues obtained after thermal analysis upto 1273 K.

4.2. ADSORPTION PROPERTIES

The pore structure of molecular sieves containing solids is usually characterized by physical adsorption of N_2 at liquid nitrogen temperature. The analysis of such adsorption isotherms is useful in determining the micropore volume and pore size distribution of composite materials containing molecular sieves (119-121)

The typical adsorption isotherms for N_2 on $AlPO_4$-5 molecular sieves obtained for samples of different crystallinity are given in Fig. 4.5. As the XRD crystallinity of $AlPO_4$-5 increases, the type of isotherm tends to change from Langmuir type II to type I isotherm and indicate increased adsorption at low relative vapour pressure. This can be attributed to the increase of micropores due to increased amount of $AlPO_4$-5 crystalline phase associated with decrease in mesopore and macropores due to decrease in amorphous material. Several methods are available for the analysis of adsorption isotherms.

4.2.1. Methods of data analysis

The B.E.T. and Langmuir equations have been employed to estimate the equivalent specific surface areas of the adsorbent materials. Gregg and Sing (122) have questioned the applicability of BET equation to microporous adsorbents. Dubinin et al (123) have proposed a new theory which is based on volume filling. Inspite of various objections, the BET equation is still universally used for the estimation of surface areas of microporous adsorbents including zeolites (124, 125). Langmuir equation was

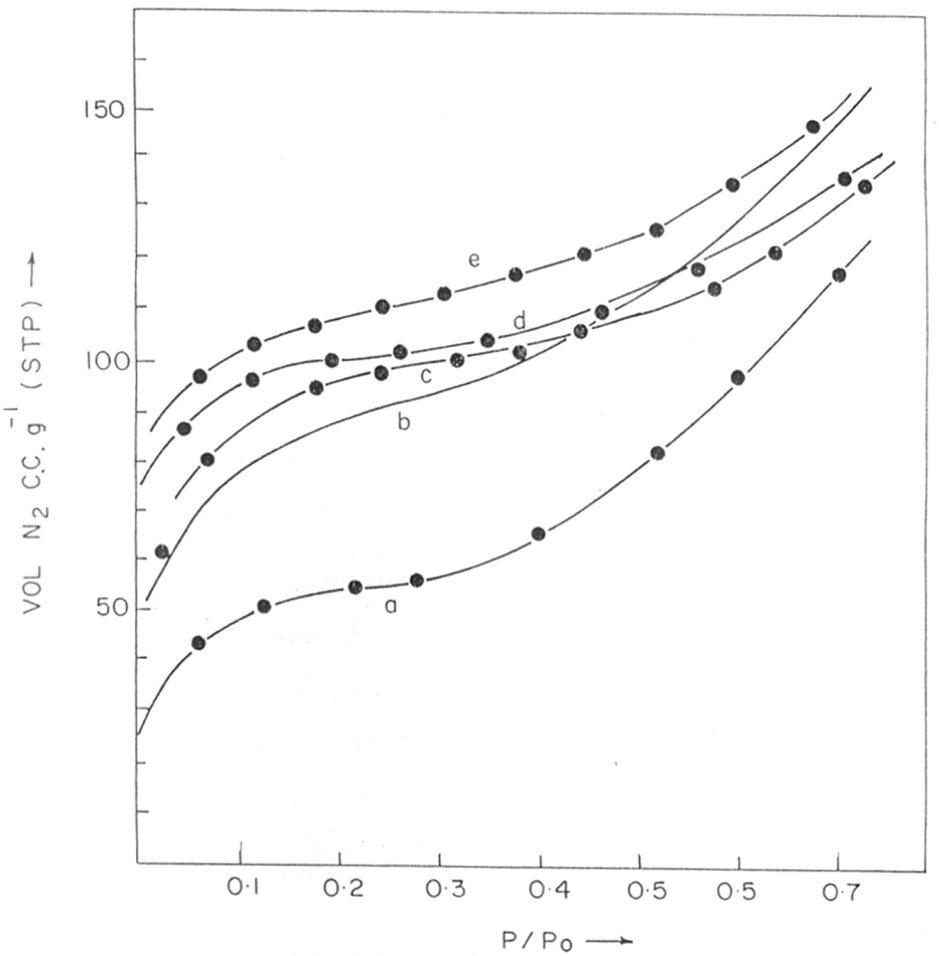

FIG. 4·5 - ADSORPTION ISOTHERMS OF N_2 (77 K) ON $AlPO_4$-5 SAMPLES OF a) 50 %, b) 78 %, c) 91 %, d) 96 %, e) 98 % XRD CRYSTALLINITY.

recently used to explain the adsorption of nitrogen in zeolites and to estimate their surface areas on the assumption that the point of inflection in the isotherm corresponds to the filling of micropores and not to the completion of the monolayer.

The BET equation is represented as

$$V = \frac{V_m C P}{(P_o - P)\left[1 + (C-1)\frac{P}{P_o}\right]} \quad \ldots\ldots\ldots \quad (1)$$

It may be transformed to :

$$\frac{P}{V\,(P_o - P)} = \frac{1}{V_m C} + \frac{C-1}{V_m C} \times \frac{P}{P_o} \quad \ldots\ldots\ldots\ldots \quad (2)$$

where $C = e^{(E_1 - E_2)/RT}$

V = the volume (at STP) of gas adsorbed at pressure P.

Vm = the monolayer capacity.

Po = the saturation vapour pressure of the adsorbate at atemperature T (K)

E_1 and E_2 are the average values of the heat of adsorption and liquifaction respectively.

The Langmuir model assumes that the adsorption surface is homogeneous. In the simplified form, the equation is represented as $\frac{V}{Vm} = \frac{K_1 P}{1 + K_1 P}$ or $K_1 = \frac{P\,(1-\theta)}{\theta}$ ..... (3)

where θ is surface coverage, V is the amount adsorbed at pressure P and Vm is the monolayer capcaity, and in the case of zeolites

the point corresponding to void filling.

If the heat of evaportion in the second and higher layer is

slightly higher than that of liquifaction,then the adsorption isotherm will asymptotically becomes verical at P/Po = 0.9. On the other hand, if the heat of evaporation of the higher layer is lower than that of liquifaction, then the isotherm will not become vertical until at P/Po > 1.0. The BET equation then reduces to Langmuir equation

$$V = \frac{VmCPP_o}{P_o(P_o+CP)} = \frac{VmCP}{P_o+CP} \quad \ldots\ldots\ldots\ldots \quad (4)$$

$$= \frac{VmKP}{1+KP} \quad \ldots\ldots\ldots\ldots \quad (5)$$

where K = P/Po. The above simplification shows that the Langmuir equation is a special case of BET equation.

Typical Langmuir and BET plots for nitrogen adsorption at 77 K on $AlPO_4$-5 are shown in Fig. 4.6. The Langmuir plot shows a linear relation over a wider range of relative pressure as compared to that of the BET equation.

The Langmuir equation has been derived for localized adsorption on the assumption that heat of adsorption and change in entropy (ΔH and ΔS) are independent of surface coverage and therefore the adsorption of different gases and vapours in molecular sieve zeolites (126) can be explained on this basis.

Dubinin Equation

The pore dimensions of zeolites are nearly equal to those of the adsorbent molecules. Due to adsorption forces the adsorption in micropore leads to volume filling in the entire volume of

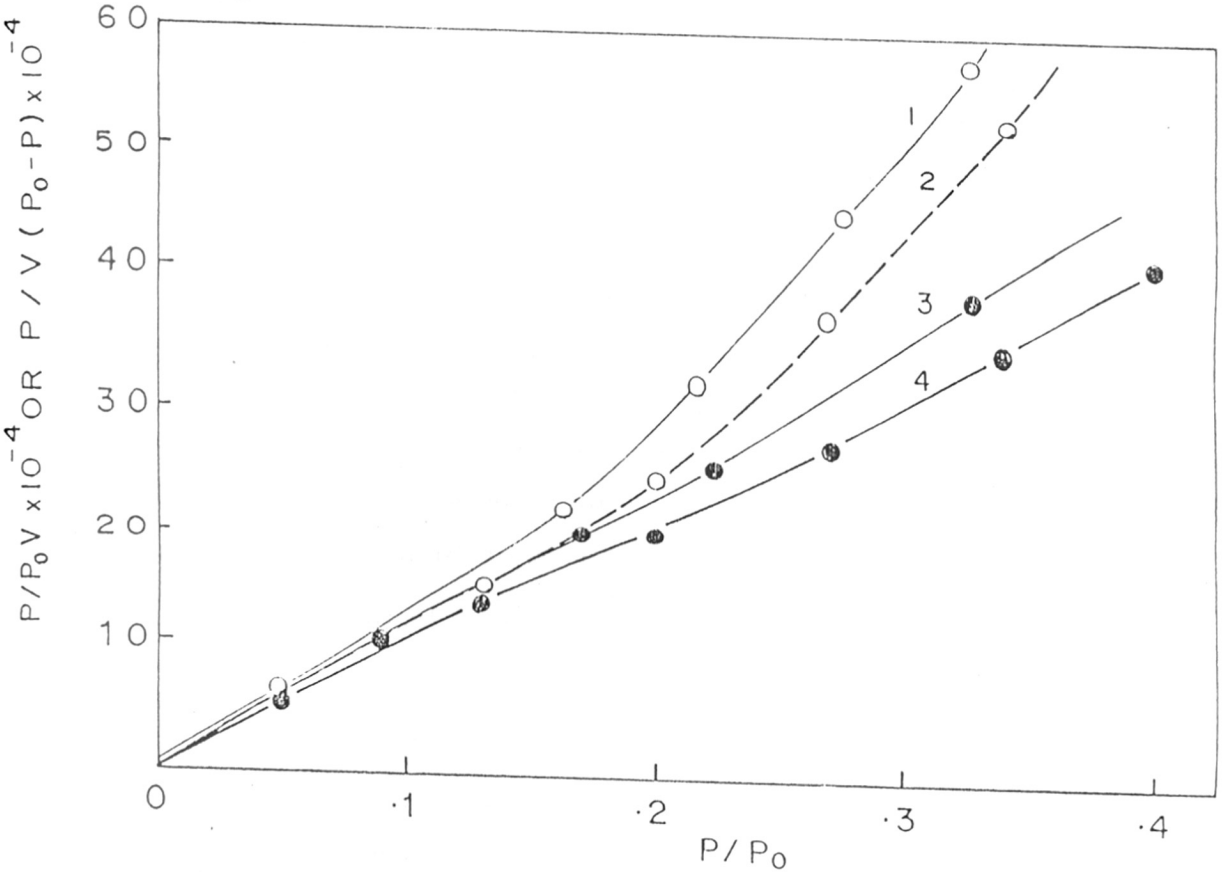

FIG. 4·6 BET (1,2), AND LANGMUIR (3,4) PLOTS FOR SAPO-5 AND $AlPO_4$-5 RESPECTIVELY.

micropores. This concept was further developed by modifying the Polanayi's theory fo adsorption (127). Two major functions were associated with the parameters of adsorption equilibrium, the adsorption value at temperature T (K) and equilibrium pressure P, are expressed as

$$A = RT \ln \frac{P_o}{P} \qquad .. 6$$

and

$$W = aV^* \qquad .. 7$$

where A is the change in free adsorption energy or difference in the chemical potential of liquid state and adsorbed state, Po the standard pressure, P the equilibrium pressure and W is the adsorption volume, V is the molar volume of the adsorbate. The theory is based on the principle concept that

$$(\delta A/\delta T)aV^* = 0 \qquad .. 8$$

and

$$(A/A_o)aV^* = \beta \qquad .. 9$$

The equations (8) and (9) imply that the characteristic curve, A = f (aV^*) is temperature invariant and at equal filled volume of the adsorption space, a V^*, the ratio of the differential molar work of adsorption of a given vapour to that of a standard vapour is a constant and is called affinity coefficient β.

The Polanayi's adsorption equation has been modified by Dubinin and Raduskevich (127). The following equation has been extensively applied to microporous adsorbents like carbon and zeolites

$$W = W_o \exp\left(\frac{KA^2}{2}\right) \qquad \ldots\ldots\ldots\ldots \qquad (10)$$

From equations 6, 7 and 10, we obtained the following equations (11 and 12) for the adsorption isotherm

$$a = \frac{W_o}{V^*} \exp\left(-\frac{BT2}{\beta^2}\right) \left(\log \frac{P_o}{P}\right)^2 \quad \ldots\ldots\ldots \quad (11)$$

for vapour which $T \leq To$,

$$W = W_o \exp\left(-\frac{BT2}{\beta^2}\right) \left(\log \frac{P_o}{P}\right)^2 \quad \ldots\ldots\ldots \quad (12)$$

where W and Wo are the volumes of filled space at pressure P and temperature T (K) and limiting volume of the adsorption space or pore respectively. B is a temperature independent constant. Below the boiling point of adsorbate liquid, V is taken as the molar volume of the liquid. The equation (12) is used in the following simplified forms

$$\log W = \log W_o - \frac{BT^2}{2.303 \cdot \beta^2} \left(\log \frac{P_o}{P}\right)^2 \quad \ldots\ldots\ldots \quad (13)$$

$$\text{or } \log a = C - D \left(\log P_o/P\right)^2 \quad \ldots\ldots\ldots\ldots\ldots \quad (14)$$

Therefore the plot of log a against $(\log P_o/P)^2$ should give a straight line with intercept

$$C = \log \frac{Wo}{V^*} = \log a_0 \quad \ldots\ldots\ldots\ldots\ldots\ldots \quad (15)$$

and slope

$$D = 0.434\ BT^2/\beta^2 \quad \ldots\ldots 16$$

From the limiting volume of adsorption space a_o, the total void volume V_p at the zeolite cavity is evaluated from equation (17).

$$V_p = a_o/dt \quad \ldots\ldots 17$$

where dt is the density of the adsorbate at T K.

We have used the Dubinin-Radusk̆ovich (DR) equation (127) to evaluate the micropore volume of $AlPO_4$-5 molecular sieves. Typical Dubinin plots log a against $(\log P_0/P)^2$ for nitrogen adsorption on $AlPO_4$-5 is shown in Fig. 4.7. The values of a_o and B obtained from the intercept and slope of the lines are given in Table 4.3. The BET surface areas obtained for differnt $AlPO_4$-5 materials are also included for comparison.

The Dubinin plots (Fig.4.7) indicate that D-R equation can be applied to N_2 adsorption on $AlPO_4$-5 molecular sieves. The micropore volume thus calculated is proportional to the x-ray cry stallinity of $AlPO_4$-5 samples as can be seen from the Fig.4.8. The deviation in the higher pressure region could be attributed to the presence of transition pores due to amorphous part in the sample.

Adsorption of water in zeolites has been extensively studied (128). It was found that (129) H_2O sorption was dependent on the type of cations present. The sorption of water is specific in nature and results from dipole-dipole interaction, hydrogen bonding (129) with surface hydroxyl groups and cations associated with tetrahedrally coordinated Al atoms which are also hydrophilic centers. The capacity for water depends upon structural OH groups and exchangeable cations. Water is also associated with alumino phosphate molecular sieve since it is synthesized in hydrothermal conditions. It has tetrahedrally coordinated Al atoms and has a polar channel system but there are no exchangeable cations as the overall framework is electrically

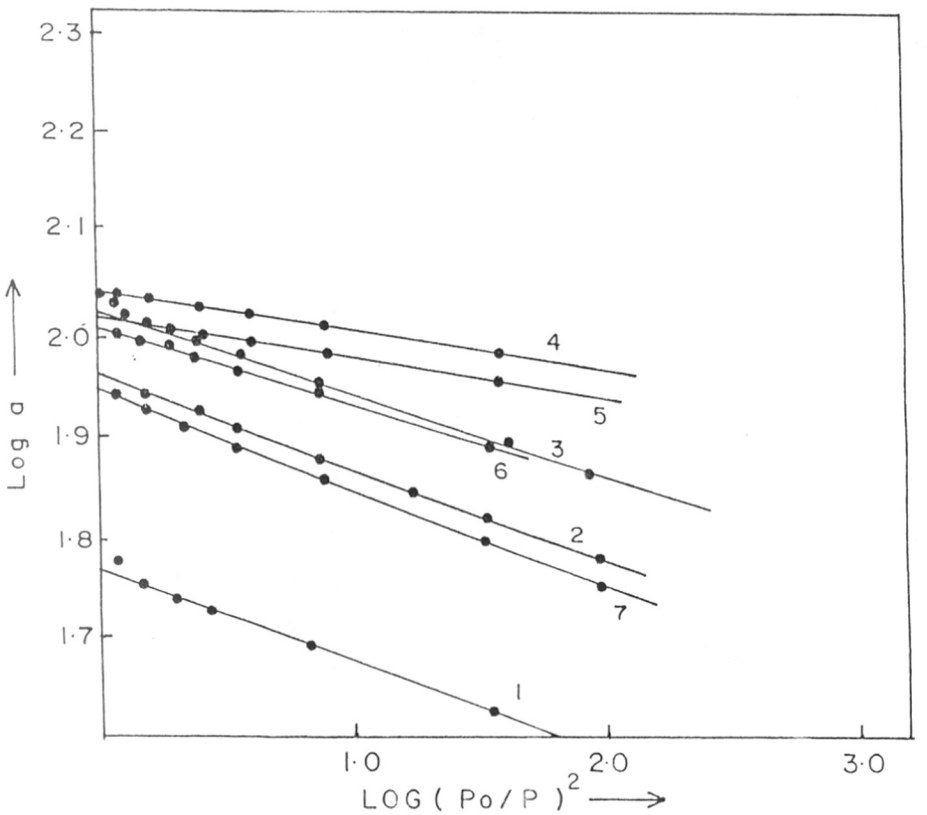

FIG.4.7 : DUBININ PLOTS OF N_2 ADSORPTION (77K) ON $AlPO_4$-5 SAMPLES OF 1) 50%, 2) 78%, 3) 91%, 4) 96%, 5) 98%, 6) 88%, 7) 75% XRD CRYSTALLINITY.

Table 4.3 : Adsorption of nitrogen at (77 K) on aluminophosphate molecular sieves

Sample	% Crystallinity	Pore vol. a_o cc/g	Parameter B X 10^5	BET surface area m^2/g
$AlPO_4$-5(5)	50.00	0.09	3.67	261.30
$AlPO_4$-5(12)	78.00	0.14	4.16	356.20
$AlPO_4$-5(24)	95.00	0.16	3.16	396.90
$AlPO_4$-5(36)	98.00	0.17	1.46	401.60
$AlPO_4$-5(48)	100.00	0.176	1.50	408.00
$AlPO_4$-5(64)	88.00	0.158	3.11	375.50
$AlPO_4$-(76)	75.00	0.136	3.73	340.00
SAPO-5(2)	53.1	0.08	3.55	195.00
SAPO-5(12)	70.00	0.13	3.90	266.00
SAPO-5(24)	90.00	0.14	4.16	361.10
SAPO-5(36)	95.00	0.155	3.00	372.50
SAPO-5(48)	100.00	0.17	1.46	380.00
SAPO-5(72)	88.00	0.15	3.0	335.00
MgAlPO-5	93.00	0.11	1.94	353.00
ZnAlPO-5	95.00	0.12	3.90	365.00
CoAlPO-5	85.00	0.092	4.44	323 .70
FeAlPO-5	80.00	0.080	1.30	253.40

Figs. in the bracket refer to crystallization time in hours.

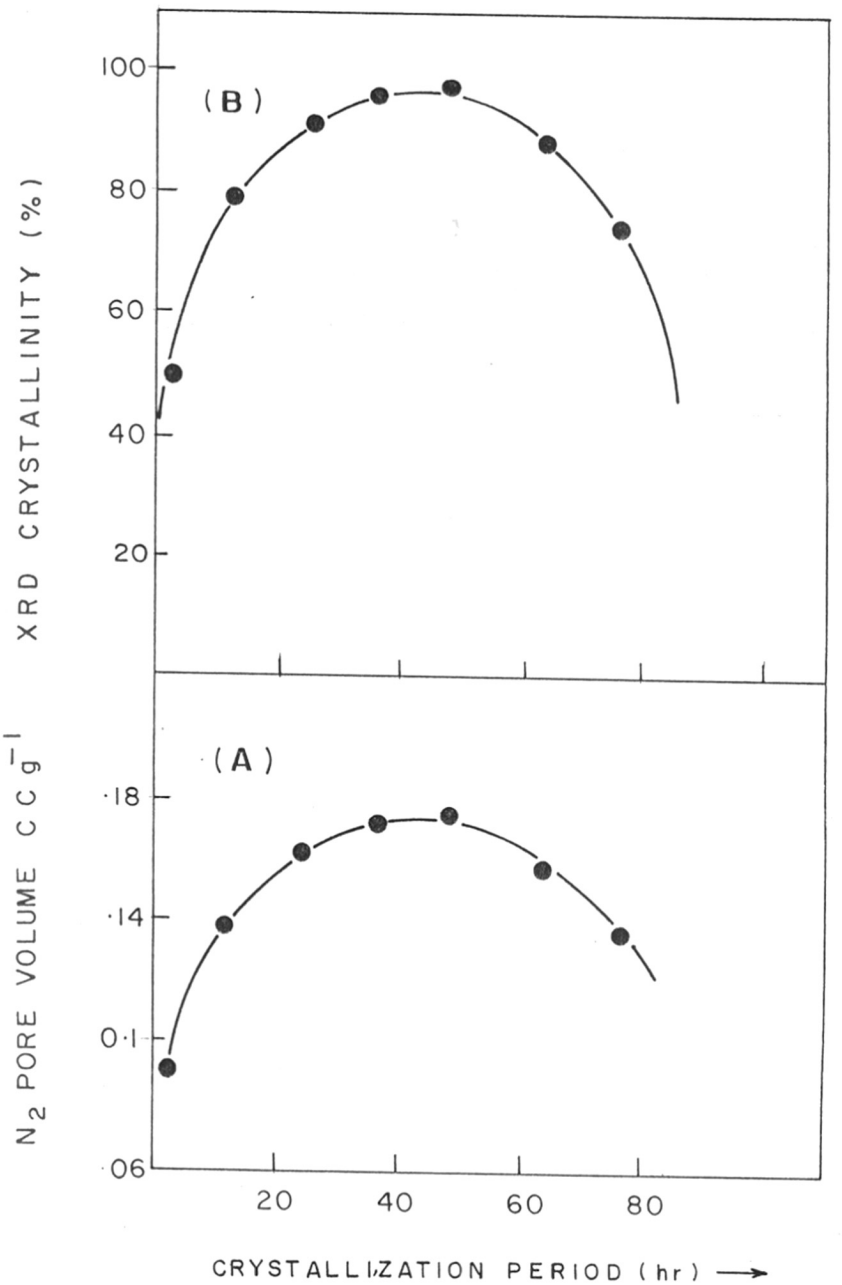

FIG. 4·8 – VARIATION OF N_2 POREVOLUME (A) AND XRD CRYSTALLINITY (B) WITH CRYSTALLIZATION PERIOD.

neutral. Yet water is found to be accessible to smallest voids in the structure giving rise to expected pore volume as per framework structure (128).

Adsorption isotherm of H_2O at 298 K on $AlPO_4$-5 is plotted in the Fig. 4.9. The saturation capacity for H_2O was obtained by extrapolation of isotherms to relative vapour pressure (P/P_o) = 1.0. The value (0.29 cc/g) is in agreement with the values reported by Wilson et al (115).

4.2.2. Adsorption properties of SAPO-5

Physical adsorption of N_2 at 77 K was employed to study the pore structure of SAPO-5 materials as well. Nature of adsorption isotherms is similar to those for $AlPO_4$-5. Langmuir equation is applicable more satisfactorily than BET equation (Fig.4.6). Pore volume determined by Dubinin-Radhuskavich equation (Fig.4.7, Table 4.3) is linearly proportional to the XRD crystallinity of the sample and the value for pure SAPO-5 is comparable to the literature value.

Isomorphous substitution of Si for P or Al or both in $AlPO_4$-5 framework can give rise to negative, positive or neutral framework, creating bridging hydroxyls (Si-O(H)-T), silanol (Si-OH) and siloxane (Si-O-Si) groups. Water adsorption becomes specific on bridging OH groups, in the electorstatic potential within the micropore. As the silicon content in the framework zeolite molecular sieve increases, heat of adsorption of water decreases for Na-mordenite (132) and HZSM-5 (83) as a result of decrease in anionic charge in the framework. For SAPO-5 molecular sieves,

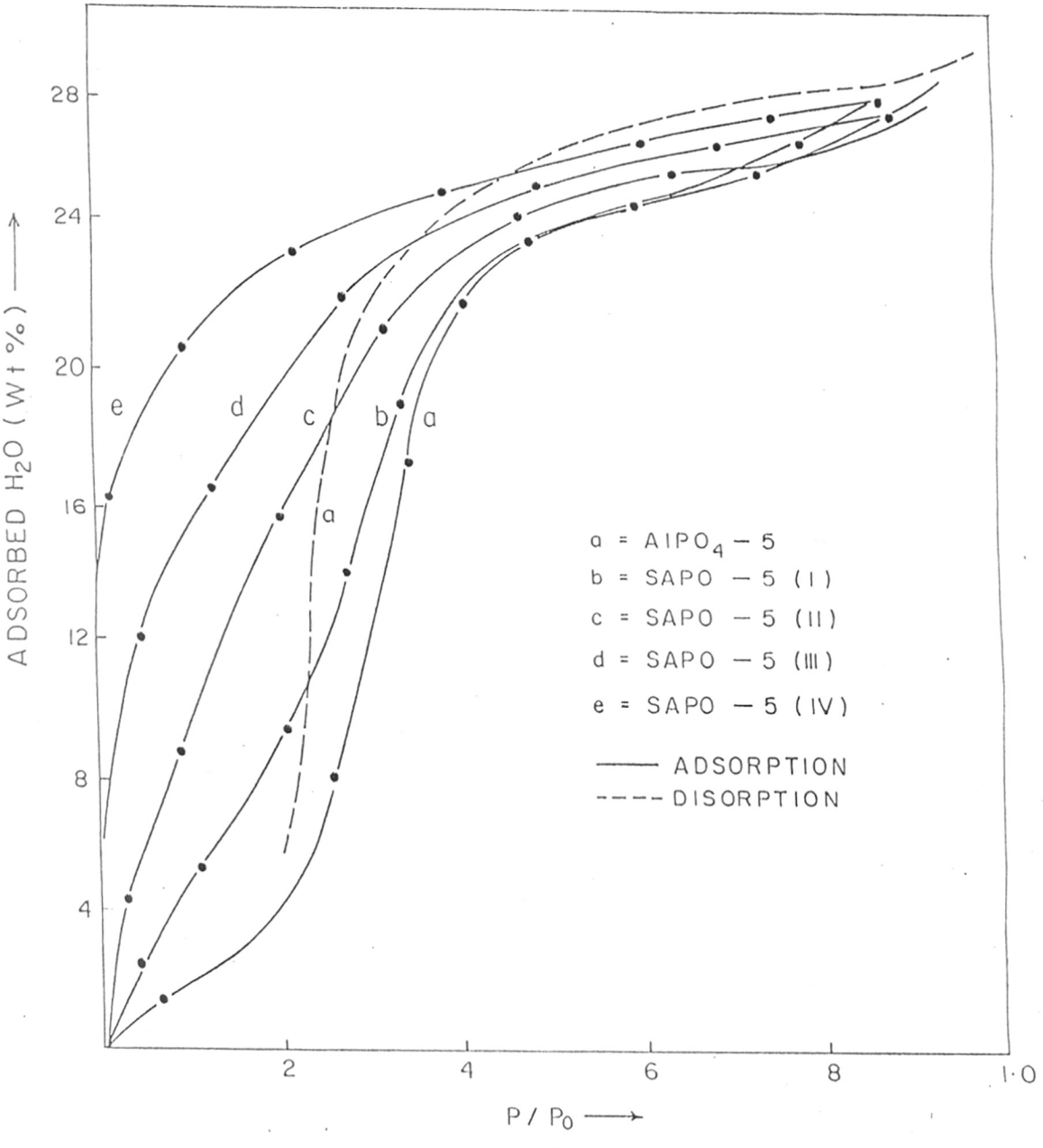

FIG. 4·9 ADSORPTION ISOTHERMS OF H_2O AT 298 K

anionic charge density increases with increase in SiO_4 tetrahedra. Therefore, to investigate the influence of this change, we determined H_2O adsorption isotherms on SAPO-5 samples with different Si content (0.09, 0.2, 0.29, 0.39 moles) which are given in Fig. 4.9. As can be seen from the Fig.4.9, the nature of isotherms change from type V to type I as Si incorporation increases in $AlPO_4$-5. The isotherm for SAPo-5(IV) is nearly identical to high silica zeolite molecular sieves. The adsorbed volume of H_2O at relative pressure (P/Po) less than 0.20, significantly increases on increase in Si in SAPO-5. But the saturation capacity obtained by extrapolation of isotherms to relative pressure P/Po = 1.0 is about 0.29 for all samples. This shows that the surface becomes more hydrophilic as a result of replacement of AlO_4 and PO_4 tetrahedra by SiO_4 tetrahedra thereby increasing anionic potential field in the SAPO-5 micropores. It can be noted that the apparent activation energy for thermal desorption of H_2O (Table 4.2) also increases with increase in Si content. It may be due to the increasing contribution of dipole-dipole interaction of SAPO-5 faramework-water pair rather than coordinatively bound H_2O forming crystal hydrate similar to $AlPO_4$-5 molecular sieves. The silanol groups Si-OH and siloxane groups Si-O-Si on the framework, if present, may not contribute to the adsorption of H_2O as they are reported to be hydrophobic (133).

Adsorption capacities for H_2O, n-hexane, cyclo-hexane and o-xylene on four SAPo-5 molecular sieves are included in the Table

Table 4.4 : Sorption capacities of pure and modified $AlPO_4$-5

Sample	% Sorption			
	Water	n-hexane	c-hexane	o-xylene
$AlPO_4$-5	29.3	9.1	9.5	10.1
SAPO-5(I)	29.0	9.0	9.3	9.7
SAPO-5(II)	28.6	8.9	9.1	9.4
SAPO-5(III)	28.7	8.5	8.4	9.0
SAPO-5(IV)	27.3	8.0	8.1	8.7
MgAlPO-5	25.40	7.80	9.40	8.20
ZnAlPO-5	26.10	7.33	8.53	7.70
CoAlPO-5	24.41	8.0	8.1	9.5
NiAlPO-5	19.9	6.2	6.3	7.11
FeAlPO-5	16.30	5.1	5.3	6.50

4.4. The values are comparable to that reported by Union Carbide (15).

It is to be noted that sorption volume decreases slightly on increasing Si in SAPO-5 which may be due to some amorphous material present in the sample.

4.2.4. Adsorption properties of MeAPO-5

Pore volume calculations applying D.R. equation show that MeAPO-5s have values less than expected as per XRD crystallinity (Table 4.3). The nature of isotherms are indicative of micropore, mesopores and macropores; XRD crystallinity was also not 100% compared to standard $AlPO_4$-5 material. Hence it can be assumed that the pores of MeAPO-5 are blocked and occluded by amorphous material to some extent.

Adsorption of H_2O on MeAPO-5 for all samples is less than that expected for pure sample and XRD crystallinity is also found to be low for some of these MeAPO-5 samples. Adsorption volume for n-hexane, c-hexane and o-xylene tabulated in Table 4.4 also show decrease in crystallinity.

4.3. INFRARED SPECTROSCOPY

4.3.1. $AlPO_4$-5 molecular sieves

Due to the microporous framework structure and large mobility of adsorbed water molecules, aluminophosphate molecular sieves are similar to the aluminosilicate molecular sieves. Because the masses (Al + P)/2 and Si are similar, the aluminophosphate molecular sieve and the zeolites show similar characteristic frequencies in the fundamental framework vibrations. Flanigen et al. (37) have assigned the bands in their IR spectra to different

vibrations in the zeolite structures. Vaimakis et al (134) have correlated asymmetric P-O-P vibrations of dense phase phosphates to Sanderson's electronegativity differences and concluded that the relation is qualitatively similar and has the same origin as in zeolites. By studying IR and Raman spectra, Pitz et al (134) have compared the vibrational modes of quartz and berlinite framework and assigned the peaks for $AlPO_4$-5 and SAPO-5 molecular sieves. On the basis of these studies, the following assignments can be made (Table 4.5).

Table 4.5 : I.R. assignments (cm^{-1})

Wave number (cm^{-1})	Assignments
480	T-O-T bending (T = Al, P, Si)
560	Double 6,4 ring
630-750	Al-O-Al stretching
1000-1300	T-O-T asymmetric stretching

IR spectra in this region for $AlPO_4$-5 molecular sieves with vary -ing crystllinity are shown in Fig.4.10. As the XRD crystallinity increases from 20-100 %. the vibrational band intensity of T-O-T groups at 705 and 560 cm^{-1} increases gradualy. Jacobs et al (191) have assigned the band at 550 cm^{-1} to the distorted double-5-ring in ZSM-5 zeolite. The absorption in this region has been correlated to the XRD crystallinity of ZSM-5 zeolite and A type zeolites. Therefore, it was interesting to examine the IR spectra of $AlPO_4$-5 systems also for such correlations if

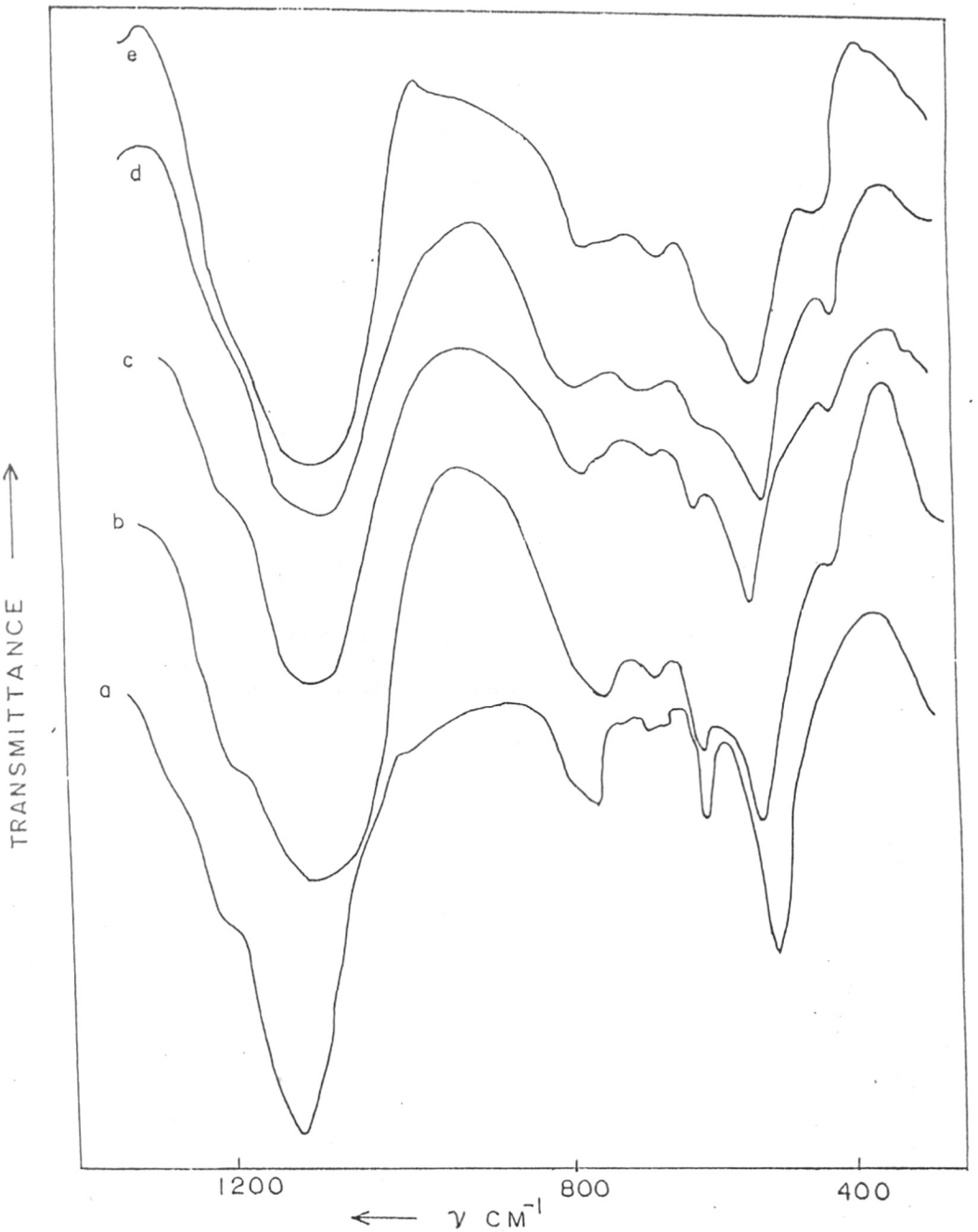

FIG. 4·10 : I.R. SPECTRA OF $AlPO_4$-5 HAVING XRD CRYSTLLINITY a) 100%, b) 79%, c) 50%, d) 20% e) AMORPHOUS.

it exists. In the Fig. 4.11 the relative intensity of the band at 560 cm^{-1} to that at 480 cm^{-1} for Et_3N-$AlPO_4$-5 is plotted against the XRD crystallinity. Indeed, a linear relation was found as can be seen in the figure. It is to be noted that even at 0 % crystallinity as per XRD, IR spectra shows some crystallinity which can be due to the fact that crystallite sizes less than 5 nm cannot be detected by this technique.

In the Fig.4.12, diffuse reflectance ir spectra of Et_3 N-$AlPO_4$-5 samples pretreated in different manners in the controlled environment of DRFTIR cell are shown. The spectra c, d and e were obtained after evacuating the sample cell at 373, 473 and 573 k respectively. Then dry air was flushed through the sample in the cell and it was heated at 773 K for 10 hours, cooled down to 673 K and evacuated before obtaining spectrum 'f'. The curve 'a' is the difference spectrum of 'e' and 'f' whereas curve 'b' is the spectrum of pure triethylamine. The bands at 2980, 2950, 2905 and 2800 cm^{-1} in the spectra 'c', 'd', and 'f' can be assigned to CH_3 and CH_2 stretching vibrations in comparison with those of pure triethyl-amine (Curve b). In the hydroxyl stretching region, weak bands are observed at 3800, 3740 and 3670 cm^{-1}. These bands cannot be due to adsorbed water, because water is removed by evacuation at high temperature. In the curve 'f' as the organic in the sample was oxidatively decomposed before recording the spectrum, no bands due to CH_3 stretching are observed and a slight increase in the intensity of bands at 3800, 3740 and 3670 cm^{-1} are noted. These bands are assigned (41) to terminal hydroxyl group stret-

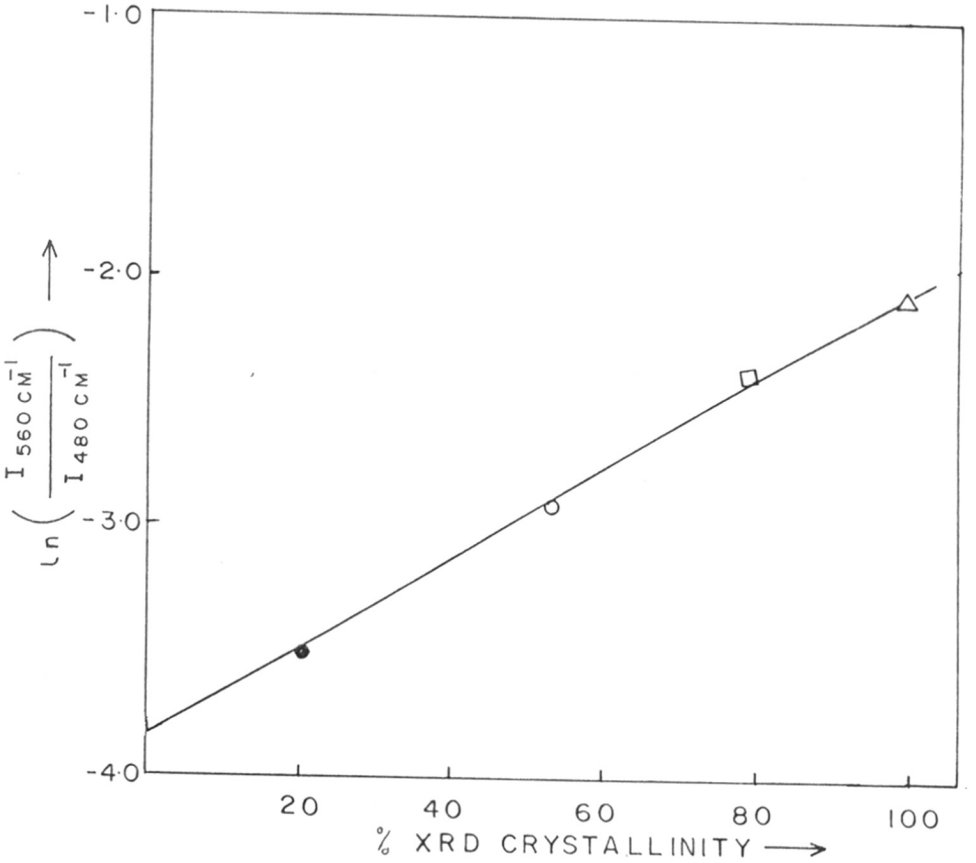

FIG. 4·11 : VARIATION OF I.R. CRYSTALLINITY OF $Et_3N-AlPO_4-5$ WITH XRD-CRYSTALLINITY. (●) 20%, (○) 55%, (□) 79%, AND (△) 100% XRD CRYSTALLINITY.

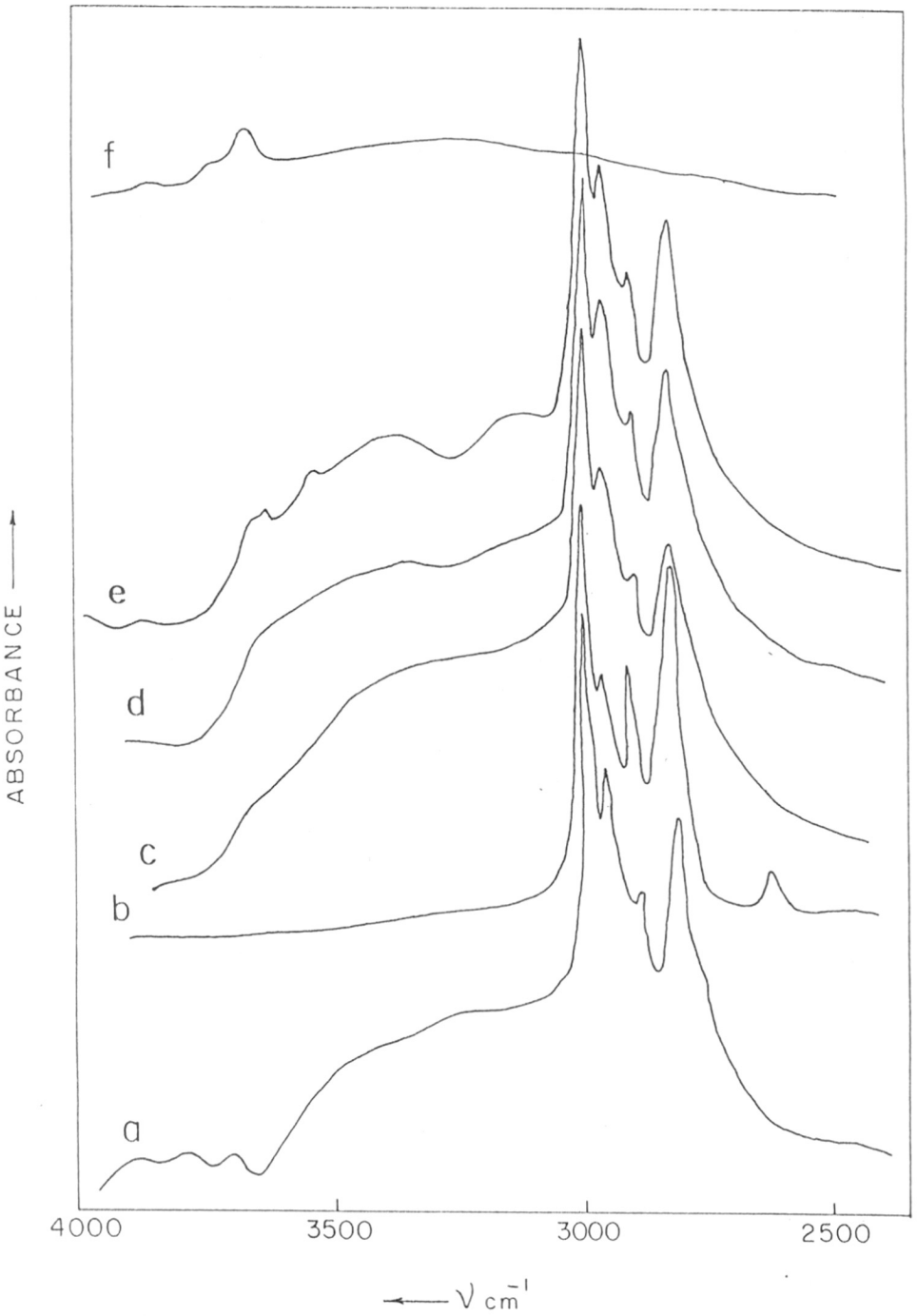

FIG. 4.12 — DIFFUSE REFLECTANCE F.T.I.R SPECTRA OF (f) PURE $AlPO_4$-5, (e) Et_3N — $AlPO_4$-5 (573), (d) Et_3N — $AlPO_4$-5 (473), (c) Et_3N — $AlPO_4$-5 (373) (b) PURE Et_3N (a) DIFFERENCE (e — f)

ching vibrations ν(P-OH) and ν(Al-OH) respectively on the surface of $AlPO_4$-5. The spectrum of triethylamine occluded in Et_3N-$AlPO_4$-5 sample (curve a) obtained as a difference spectrum is identical to that of pure triethylamine except the absence of a weak band at 2600 cm^{-1}. This is attributed to strain on tri-ethylamine molecule occluded in the channel. This organic moiety is stable inside the channel, as it could not be removed at 575 K in vacuum (curve f).

Bennet et al (16) have studied the tetrapropyl ammonium hydroxide-$AlPO_4$-5 system by single crystal x-ray crystallography. They arrived at the conclusion that Al-O-P linkage in $AlPO_4$-5 is alligned in the direction parallel to 12-membered channel system and that tetrapropyl ammonium hydroxide occluded is also polarised. Therefore, we can conclude that triethylamine is also polarised and held strongly in the polar channel of Et_3N-$AlPO_4$-5 molecular sieve.

The nature of these hydroxyl groups having vibrational bands at 3800, 3740 and 3670 cm^{-1} were further characterised by adsorption of D_2O, benzene and pyridine. $AlPO_4$-5 sample (200-250 mesh) was placed in the sample cup of DRFTIR cell and evacuated at 673 K for 6 hours, cooled to 373 K and then D_2O, benzene or pyridine vapours (10 mm pressure) were admitted to the sample, allowed to equillibriate for one hour and then loosely adsorbed sorbate was removed by evacuating at the same temperature, then spectrum was recorded. From this spectrum, that of pure sample was subtracted. The resulting difference spectra for D_2O, benzene and pyri-

dine (curves a, b and c) are presented in Fig. 4.13. From the spectrum of D_2O adsorption (curve a), it can be seen that duetetrium exchange readily took place giving rise to removal of bands due to O-H groups (negative peaks at 3800, 3740 and 3670 cm^{-1}) and new bands due to O-D groups at 2787, 2742 and 2692 cm^{-1} appeared. However, rate of exchange was found to be comparatively slow indicating that these groups may be weakly acidic. On adsorption of benzene, the structural hydroxyl groups at 3800, 3740 and 3670 cm^{-1} were shifted to 3720, 3650 and 3425 cm^{-1}. It is reported (135) that when H-bonded complexes with weakly adsorbed bases are formed, the IR bands of OH groups with acidic properties are shifted towards lower frequencies and the extent of shift is considered as the Brönsted acid strength of that OH group. From the data, we can see that OH groups in $AlPO_4$-5 are not strong as the shift is very much less compared to that for known acidic zeolites like HY.

Infrared spectrum of pyridine adsorbed on $AlPO_4$-5 is shown in Fig. 4.13 (curve c). It indicates that intensity of the bands at 3800, 3740 and 3670 cm^{-1} are affected. The weak bands of adsorbed pyridine in the region of C-C stretching vibration are observed near 1633, 1608, 1548, 1492 and 1447 cm^{-1}. The bands at 1633 and at 1548 cm^{-1} are very weak compared to those at 1608 and 1455 cm^{-1}. These sets of bands are assigned (136) to the C-C stretching vibrations of pyridinium ions adsorbed on Brönsted acid sites and to the coordinatively bonded to Lewis acid sites respectively. The band at 1492 cm^{-1} is common to both types of adsorbed pyridine.

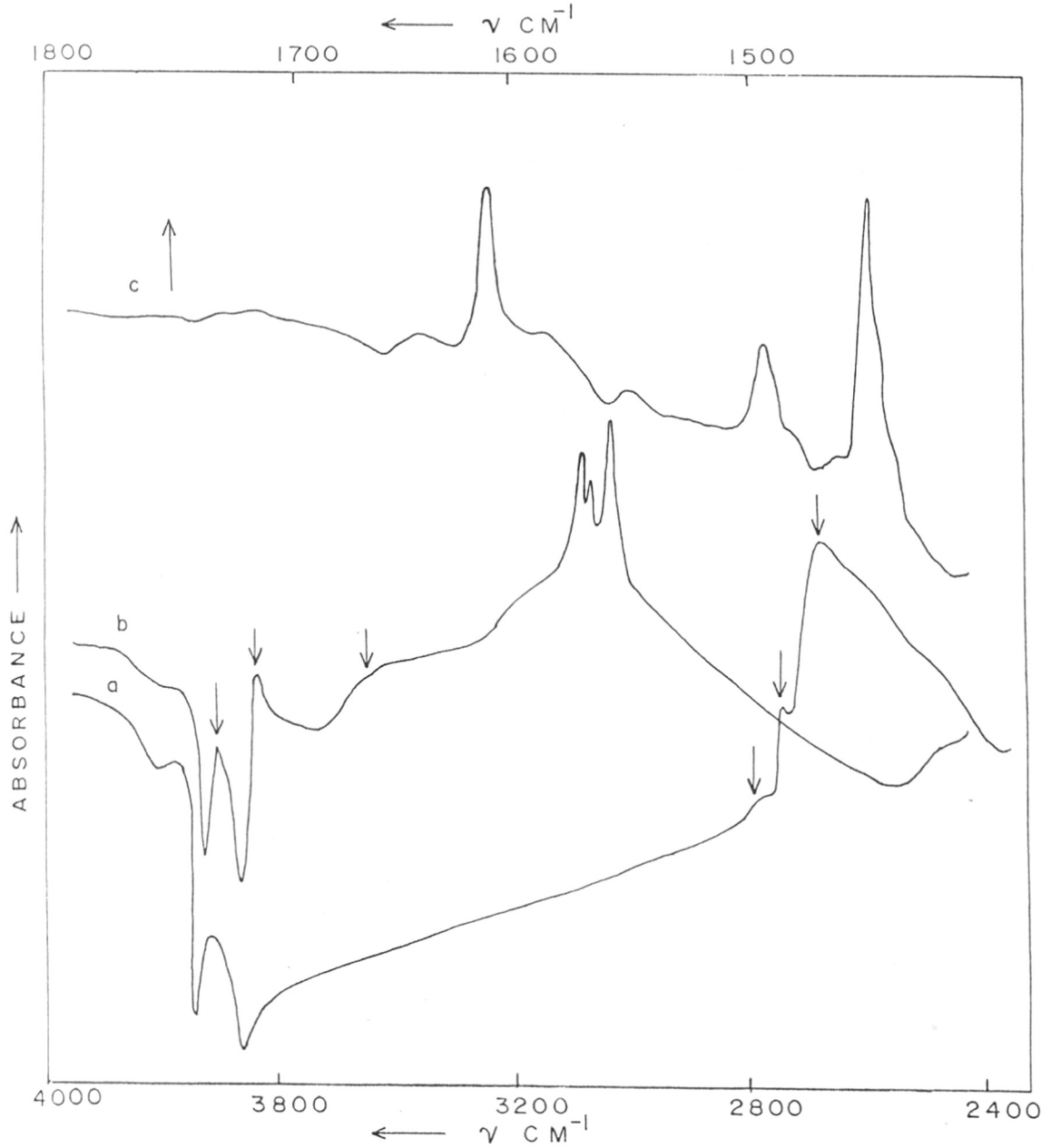

FIG. 4·13 : DIFFERENCE F.T.I.R. SPECTRA OF $ALPO_4$-5 ON ADSORPTION OF a) D_2O, b) BENZENE c) PYRIDINE.

Therefore, from the IR studies on the adsorption of D_2O benzene and pyridine we can conclude that Brönsted acid sites on $AlPO_4$-5 are negligible and there are some Lewis acid sites which can be due to P-OH and Al-OH groups.

4.3.2. SAPO-5 molecular sieve

The FTIR spectra of SAPO-5 samples in the fundamental framework vibration region are shown in Fig. 4.14. The main features of the spectra are similar to that of $AlPO_4$-5. The vibrational frequencies of SAPO-5 (I-IV) in this region are summarised in Table 4.6. It is to be noted that all the bands due to asymmetric and symmetric stretching vibrations of linked tetrahedra shift gradually to higher wave numbers as the Si content in SAPO-5 increases. Flani gen et al. (32) obtained identical results for the zeolites. By considering zeolite framework as consisting of O-T-O harmonic oscillators, they have attributed this shift to difference in bond length of Si-O (1.62) and Al-O (1.75). As the T atom is at the centre, shift due to asymmetric stretching vibrations can only be explained by this consideration. Szostak and Thomas (137) investigated the phenomenon by proposing Si-O-T as the harmonic oscillator. Based on the change in the reduced mass of Si-O-T oscillator, the significant shift in all types of vibrations in the framework are expected. We can extend this principle to Al-O-T oscillator in alumino phophate molecular sieves as well. On replacing T atom from heavier 'P' to lighter Si atom, the bands due to the assymetric and symmetric vibrations of framework should appear at lower wave

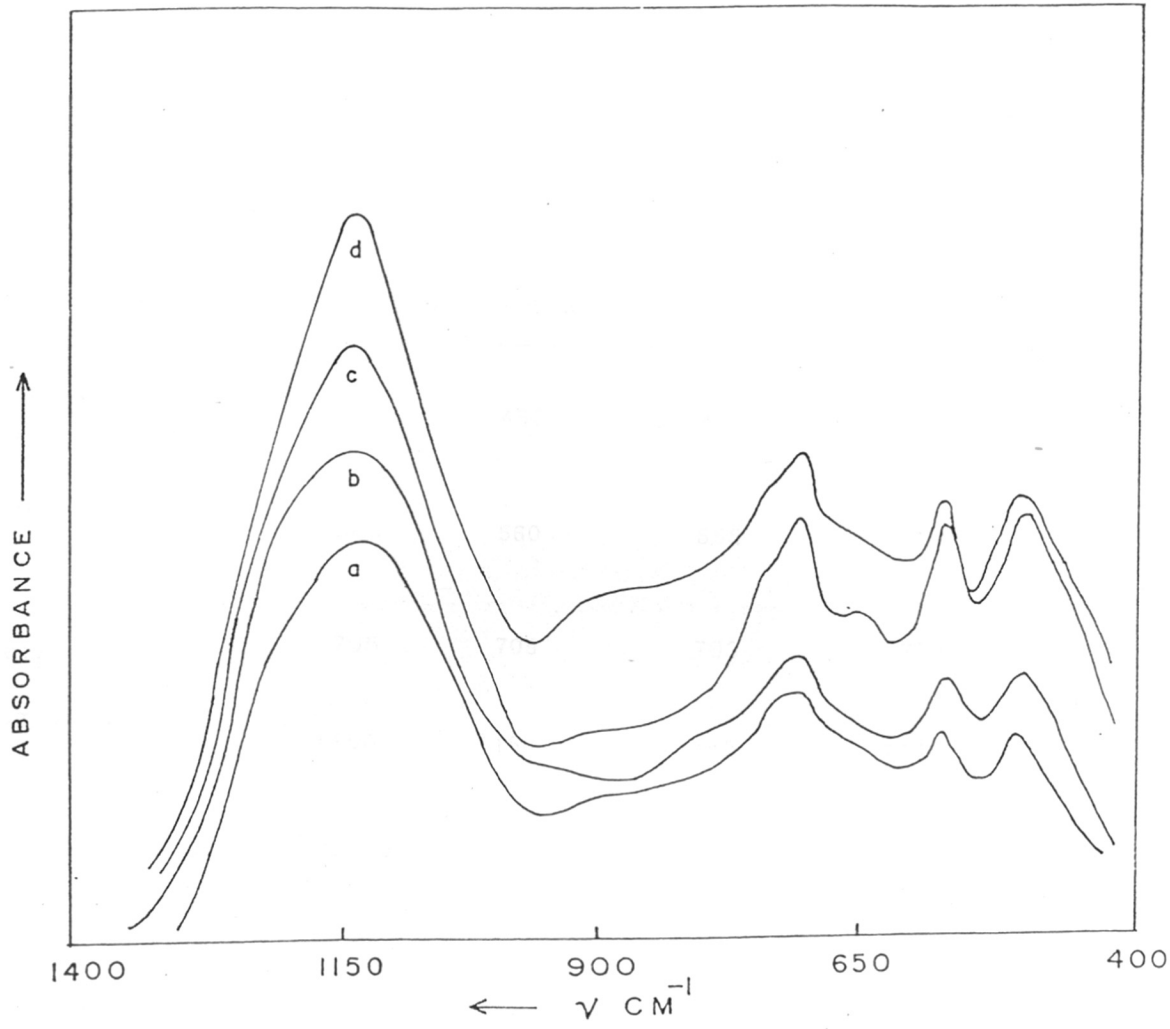

FIG. 4·14 : F.T.I.R. SPECTRA OF a) SAPO-5(I), b) SAPO-5(II), c) SAPO-5(III), d) SAPO-5(IV).

Table 4.6

Infrared assignments for framework vibrations (ν cm^{-1})

Mode of vibrations	$AlPO_4$-5	SAPO-5(I)	SAPO-5(II)	SAPO-5(III)	SAPO-5 (IV)
T-O-T bending (T = Si, Al, P)	480	482	476	474	474
Double 4,6 rings (D6R, D4R)	560	560	558	554	554
T-O-T symm. stretch	705	705	703	702	702
T-O-T asymm. stretch	1150	1150	1145	1140	1137

numbers. Indeed, we have observed such a decrease. For example, the band at 1150 cm^{-1} for $AlPO_4$-5 has shifted to 1137 in SAPO-5 (IV). The shift is small because the differenece in mass of P (31) and Si (29) is very small. This is in agreement with the results reported by Pitz et al (134).

In the Fig. 4.15 (curves c, d, e and f) are presented the diffuse reflectance spectra of ET_3N-SAPO-5 (IV) which was pre -treated in situ in the sample cell in the identical manner as that for Et_3N-$AlPO_4$-5 sample. Curves c,d and e in the figure demonstrate the room temperature spectra of Et_3N-SAPO-5 (IV) preevacuated at 473, 573 and 673 K respectively. The sample was further exposed to flowing dry air at 825 K for 10 hrs., cooled down to 673 K and evacuated for 4 hrs and finally cooled to room temperature to record the spectrum of pure SAPO-5 (IV) (curve f). The curves 'b' and 'a' are the spectra of Et_3N-$AlPO_4$-5 and of pure $AlPO_4$-5 respectively which are presented for comparison. The absorption bands at 2985, 2950, 2885 and 2800 cm^{-1} in the spectra c, d and e can be assigned to C-H stretching vibrations of tri-ethylamine in comparison with those present in Et_3N-$AlPO_4$-5 spectrum (curve b). In the region of N-H stretching vibrations, relatively broad bands at 3350, 3165 and 3055 cm^{-1} are seen. These bands in the region of N-H and C-H stretching vibrations disappear in the curve 'f' because occluded triethylamine has been completely removed by oxidative decomposition in air before recording the spectrum. Instead, in this spectrum, the weak bands at 3800, 3740 and 3670 cm^{-1} and strong bands at 3620 and

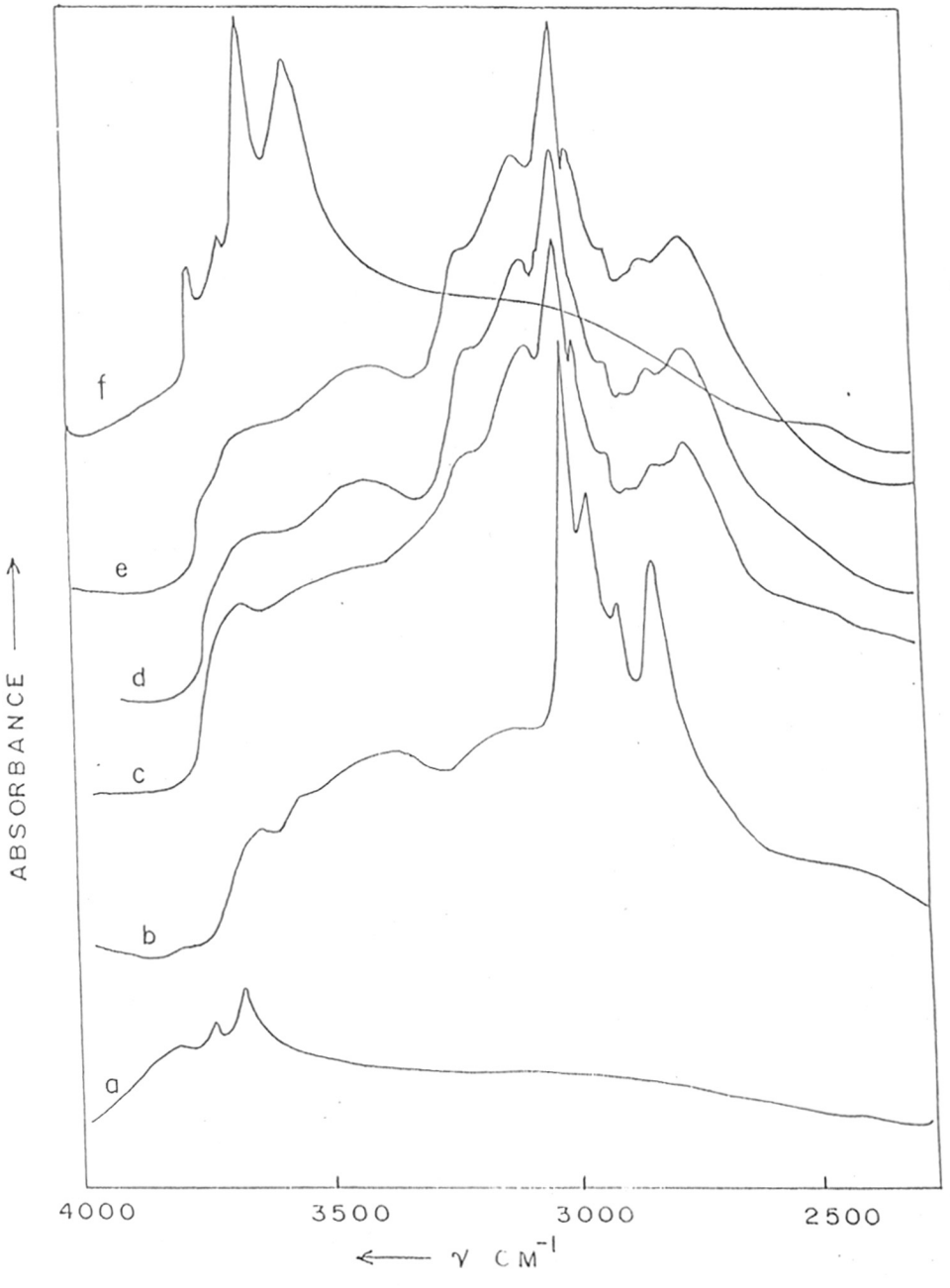

FIG. 4·15 : DIFFUSE REFLECTANCE F.T.I.R.SPECTRA OF
a) $AlPO_4$-5, b) Et_3N– $AlPO_4$-5(573), c) Et_3N-SAPO-5(375)
d) Et_3N-SAPO-5(475), e) Et_3N-SAPO-5(575),
f) SAPO-5

3525 cm^{-1} are observed in the region of O-H stretching vibrations. Therefore, the origin of these O-H groups can be unambigiously attributed to the removal of triethylamine from the sample.

If we compare the spectrum of Et_3N-$AlPO_4$-5 (curve b) and Et_3N-SAPO-5 (IV) (curve e), the following differences can be noted (i) the bands at 3350, 3165 and 3055 cm^{-1} which are present in the spectrum of Et_3N-SAPO-5(IV) are absent in Et_3N-$AlPO_4$-5 spectrum. (ii) The prominent band at 2800 cm^{-1} assigned to C-H stretching vibrations present in the spectrum of Et_3N-$AlPO_4$-5 is weak in intensity in the spectrum of Et_3N-SAPO-5(IV). (iii) An additional band of medium intensity at 2730 cm^{-1} is present in the spectrum of Et_3N-SAPO-5(IV) which is not seen for Et_3N-$AlPO_4$-5. The band in this region is generally attributed to protonated R_3-N^+-H species (138). These experimental facts indicate that triethylamine in Et_3N--$AlPO_4$-5 and Et_3N-SAPO-5 is present in different states. This difference can be understood more clearly if we compare the spectra of Et_3N-SAPO-5 having increasing mole fraction of Si in the sample. Fig. 4.16 presents the spectra of Et_3 N-SAPO-5 (I to IV) containing 0.09, 0.21, 0.29 and 0.39 mole fractions of Si (curves b-e) in the region of 4000-2400 cm^{-1}. The curve 'a' is the spectrum of Et_3N-$AlPO_4$-5 included for comparison. From the figure it should be noted that as the Si content in the sample increases, (i) the intensity of the bands at 3350, 3165 and 3055 cm^{-1} which are attributed to hydrogen bonding increases and (ii) that of the band at 2800 cm^{-1} assigned

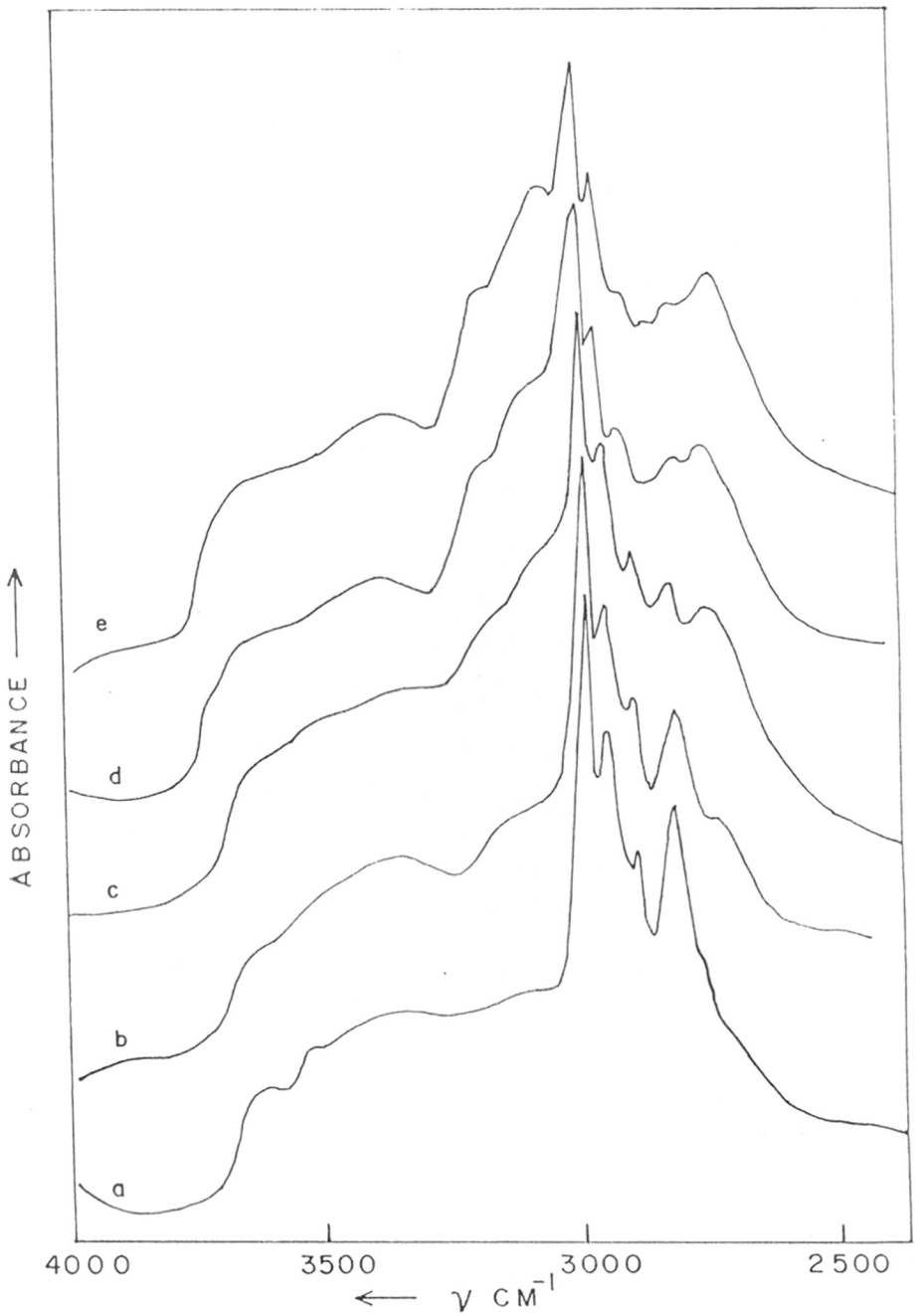

FIG. 4·16 : DIFFUSE REFLECTANCE F.T.I.R. SPECTRA OF a) Et_3N-$AlPO_4$-5, b) Et_3N-SAPO-5 (I), c) Et_3N-SAPO-5 (II) d) Et_3N-SAPO-5 (III), e) Et_3N-SAPO-5 (IV).

to C-H stretching vibrations decreases, (iii) and the intensity of the band at 2730 cm^{-1} which is assigned to protonated amine ($C_2H_5N^+H$) species increases gradually. Therefore, it can be stated that triethylamine species are only polarised and held strongly in the polar channels of $AlPO_4$-5 whereas in SAPO-5 in addition to polarization, it is strongly hydrogen bonded and proto-nated also. These two different states of occluded triethylamine in SAPO-5 can be compared with the two different peaks in the oxidative decomposition observed in the DTA curves (Fig.4.4)

The strength of the hydrogen bonds depends on the difference in the average electronegativity of the donor and acceptor groups. The average electronegativity of SAPO-5 is intermediate between that of the $HAlSiO_4$ and SiO_2. Brunner et al. (139) have used ^{1}HMASNMR to investigate the nature of acid sites in SAPO-5 and concluded that it is similar to that of HY zeolite. Hegde et al. (41) have employed diffuse reflectance infrared spectroscopy to investigate acid strength of $AlPO_4$-5, SAPO-5, HY and HZSM-5.The acid strength of SAPO-5 was found to be intermediate between HY and HZSM-5. HY zeolite has a wide range of acid strength distribution from pK_a + 608 to -8.2. Therefore, it is reasonable to presume that the range of acid strength of SAPO-5 should be wider than this. Triethylamine is a strong organic base with the ionization constant pK_b, 11.5. Therefore, the difference between the ionization constant of triethylamine and acidic hydroxyl groups in SAPO-5, ΔpK_{ba} should be, at least in the range 4.7 (11.5-6.8) and 19.7 [11.5- 8.2)]. It is generally observed (140) that this

difference of about 4.0 to 4.5 is sufficient for triethylamine to form strong hydrogen bond and the protonation of amine to take place. Therefore, the strong hydrogen bonding of triethylamine template with Brönsted acidic hydroxyl groups, producing the surface species $[(Et_3NH)^+ (Si-O-Al)^-]$ as a result of complete proton transfer from (Si-O(H)-Al) groups to triethylamine molecule is not surprising. Thus, the concept of protonated triethylamine playing structure directing role in SAPO-5 synthesis is experimen-tally evidenced. It may be mentioned here that previous IR studies on cyclohexylamine-SAPO-5 (141) and XRD studies on pype-ridine-$AlPO_4$-17 (142) systems have also provided experimental evidence to show that protonated template is indeed the structure directing species in $AlPO_4$-n molecular sieves.

The IR spectra in the region of fundamental stretching vibrations of O-H bonds in SAPO-5 (I to IV) are shown in Fig. 4.17 (curves f, g, h, i), curve 'e' is the spectrum of $AlPO_4$-5 which is included for comparison. In the spectrum of $AlPO_4$-5 there are only low intensity absorption bands with maxima at 3800, 3740 and 3670 cm^{-1}. These are assigned to P-OH and Al-OH hydroxyls on the external surface of $AlPO_4$-5 (41). Amorphous aluminophosphate materials also exhibit similar bands in the same region (143). These bands are also present in the spectra of SAPO-5 samples (curves f,g, h and i). Two additional strong bands at 3620 and 3525 cm^{-1} are also seen in these spectra. The inten-sity of these bands is considerably higher. It increases signi-ficantly on increasing mole fraction of Si in SAPO-5 from 0.09

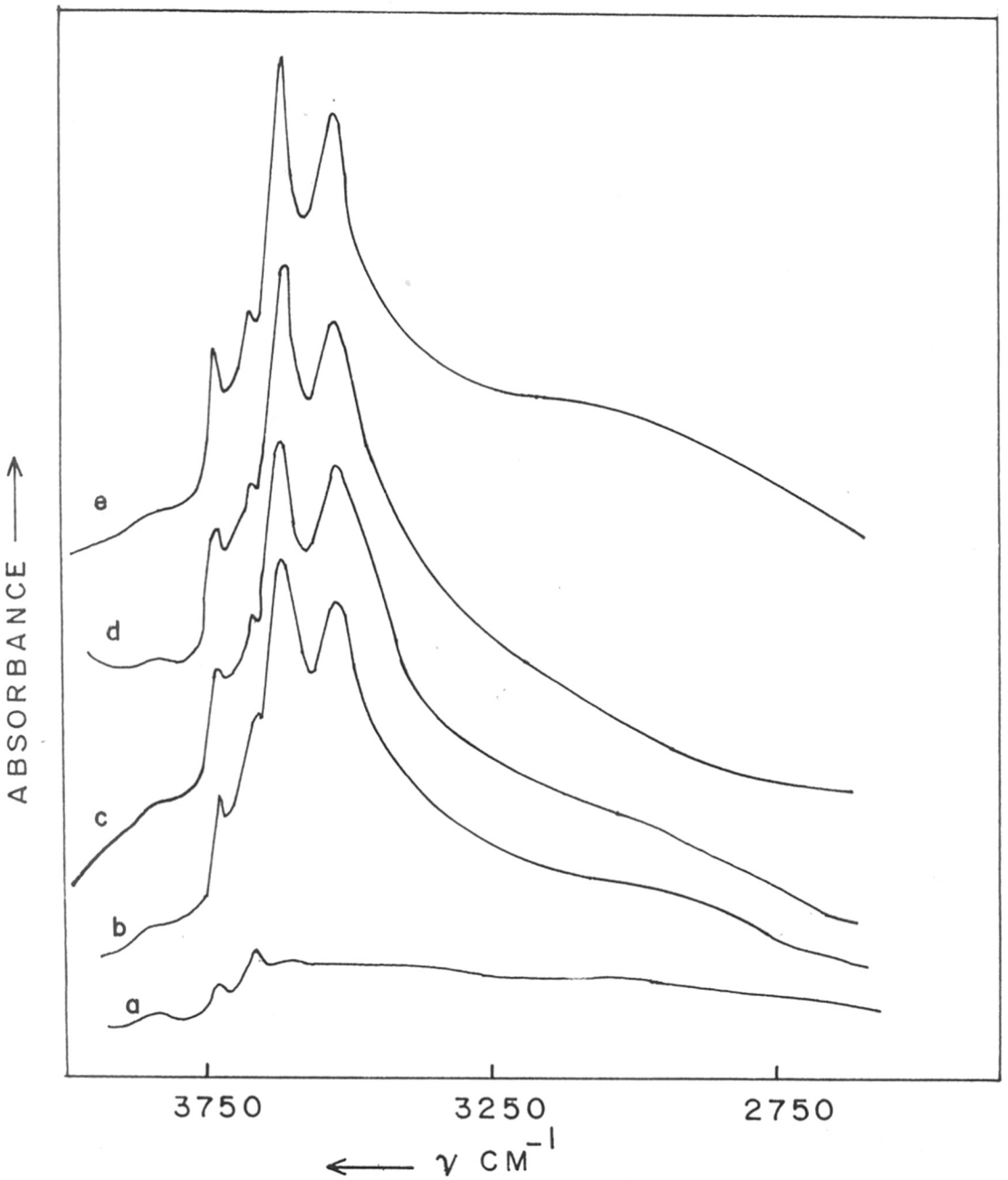

FIG. 4·17 : DIFFUSE REFLECTANCE F.T.I.R. SPECTRA OF a) $AlPO_4$-5, b) SAPO-5 (I), c) SAPO-5 (II), d) SAPO-5 (III), e) SAPO-5 (IV).

to 0.39. Brunner et al. (139) have studied the nature of these hydroxyl groups using MASNMR and Hegde et al. by IR (41) and compared these with high and low frequency bridging (Si–O(H)–Al) hydroxyl groups of HY zeolites. The band at 3620 cm^{-1} is assigned to OH groups vibrating in larger 12-membered channel systems and that at 3525 cm^{-1} to OH groups situated inside the 6-membered ring channels, respectively. The lower frequency of OH groups vibrating inside 6-membered ring channels can be attributed to the fact that these OH groups are attached strongly by neighbour-ing lattice oxygen very close in the channel.

SAPO-5 molecular sieves can have different types of surface hydroxyl groups (144) which are depicted below:

(1) Zeolites : 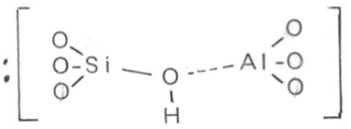 $SiO_2(HAlO_2)_X$

(2) SAPO-5 :

(i) 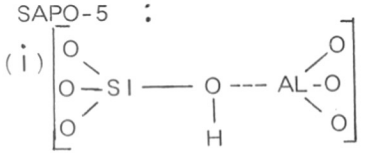 $AlPO_4$

(ii) 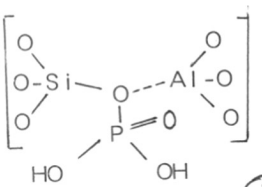 $AlPO_4$

(iii) 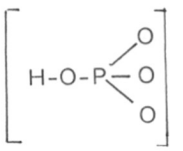 $AlPO_4{\cdot}SiO_2{\cdot}HAlO_2$

(iv) 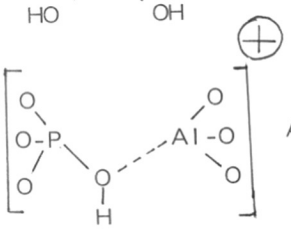 $AlPO_4$

(v) 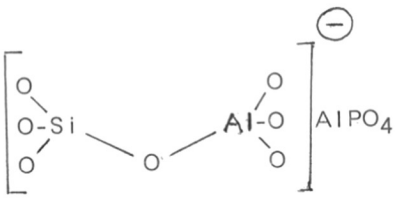 $AlPO_4$

If the active sites formed are bridged Si-O(H)-Al groups, because the mean electronegativity (145) of $AlPO_4$-5 [$1/2(x_p + x_{Al})$] = 2.11] is almost equal to that of SiO_2 (x_{Si} = 2.14), they should be as acidic as high silica zeolites. If Si is incorporated uniformly in the neutral framework of $AlPO_4$-5 without forming zones rich in Si only, the associated bridging hydroxyls can be sufficiently isolated similar to high silica zeolites. The terminal P-OH groups of type (iii) in the above scheme should be weakly acidic similar to terminal Si-OH groups of zeolites. But if they are of type (ii) as phosphoric acid ester of SAPO-5 framework, they can be moderately acidic. The groups P-O(H)-Al as in (iv) will not create stronger acidity. If we assume that they are more acidic than Si-O(H)-Al sites (Scheme i), then the equilibrium proton transfer would establish and neutralise the framework as follows

$$\gtrless P\text{-}\overset{H}{O}\text{-}Al\lesssim + \gtrless Si\text{-}O\text{-}Al\lesssim \rightleftharpoons \gtrless P\text{-}O\text{-}Al\lesssim + \gtrless Si\text{-}\overset{H}{O}\text{-}Al\lesssim$$

In order to further understand the nature of acidity in SAPO-5 molecular sieves, adsorption of D_2O, benzene and pyridine was studied by IR spectroscopy. Experimental procedure was similar to that adopted for $AlPO_4$-5. Sample was activated by evacuating at 673 K in the sample cell, cooled down to 373 K and adsorbate vapour was admitted at 10 mm presure. It was allowed to equilibrate for one hr and loosely adsorbed vapour was pumped out by evacuating at the same temperature. The diffuse reflectance infrared spectrum was then recorded. From this

spectrum, the spectrum of pure sample before adsorption of vapour was subtracted. The difference spectra obtained by this was for D_2O, benzene and pyridine are presented in Fig. 4.18 (curves a, b and c). The curve 'a' in the figure shows that on adsorption of D_2O, the bands at 3800, 3740, 3670, 3620 and 3525 cm^{-1} due to O-H stretching vibrations have disappeared (negative peaks in the spectrum) and those due to O-D stretching vibrations appeared (positive peaks in the spectrum). The exchange of deuterium in OH groups for bands at 3620 and 3525 cm^{-1} was very fast which shows that these hydroxyl groups are highly acidic.

On adsorption of benzene, stretching vibrations of acidic hydroxyl groups are shifted to lower wave numbers due to hydrogen bonding which can be depicted as follows :

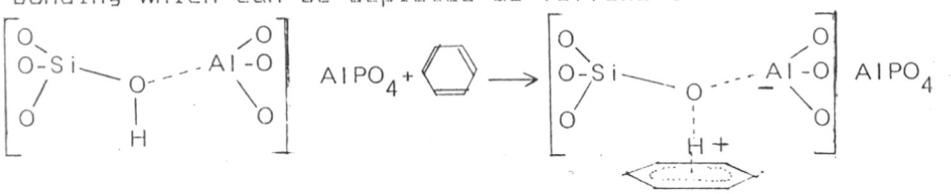

The extent of the shift is proportional to the strength of the acidic group. It should be noted that benzene is not accessible to O-H groups corresponding to the band at 3525 cm^{-1} because they are situated in 6-membered channels of SAPO-5. All other bands at 3800, 3740, 3670 and 3620 cm^{-1} are shifted to 3620, 3650, 3425 and 3395 cm^{-1} respectively (curve b). From the extent of this shift for SAPO-5, HY and HZSM-5 samples (325, 280-320 and 350 cm^{-1} respectively) (41), we can conclude that the acid strength of SAPO-5 is intermediate to that of HY and HZSM-5 zeolites.

Bielanski et al (146) have reported that on dealumination of HY zeolite, the high frequency band at 3640 cm^{-1} shifts to lower frequency to a small extent whereas for SAPO-5, we have not observed any change in frequency of 3625 cm^{-1} band on increasing Si mole fraction from 0.09 to 0.39. On adsorption of benzene, the shift of this band was also the same for all the samples. Even if the concentration of acidic hydroxyl groups increases on increaisng Si content, it is diluted in the neutral $AlPO_4$-5 framework. Therefore all OH groups must experience maximum freedom, similar to OH group;s in high silica zeolites. Therefore, it can be concluded that Si in the SAPO-5 framework must have been uniformly distributed. However, Martin et al. (141) have indicated the possibility of patches of Si enriched framework, zeolitic in nature in SAPO-5 material.

In the Fig. 4.18 (curve c) difference IR spectrum of SAPO-5 on adsorption of pyridine is shown. The spectrum shows the strong bands at 1635, 1622, 1550, 1495, and 1455 cm^{-1} characteristics (142) of C-C stretching vibrations of adsorbed pyridine. The bands of 1550 and 1635 cm^{-1} which are assigned to pyridinium ions formed on Brönsted acid sites, which are comparatively intense than those at 1622 and 1455 cm^{-1} due to coordinatively bound pyridine on Lewis acid sites. The strong band at 1495 cm^{-1} is common to both types of adsorbed pyridine.

From these studies it can be concluded that SAPO-5 molecular sieves have strong Brönsted sites due to bridging hydroxyl groups Si-O(H)-Al and Lewis sites which may be due to P-OH and Al-OH groups

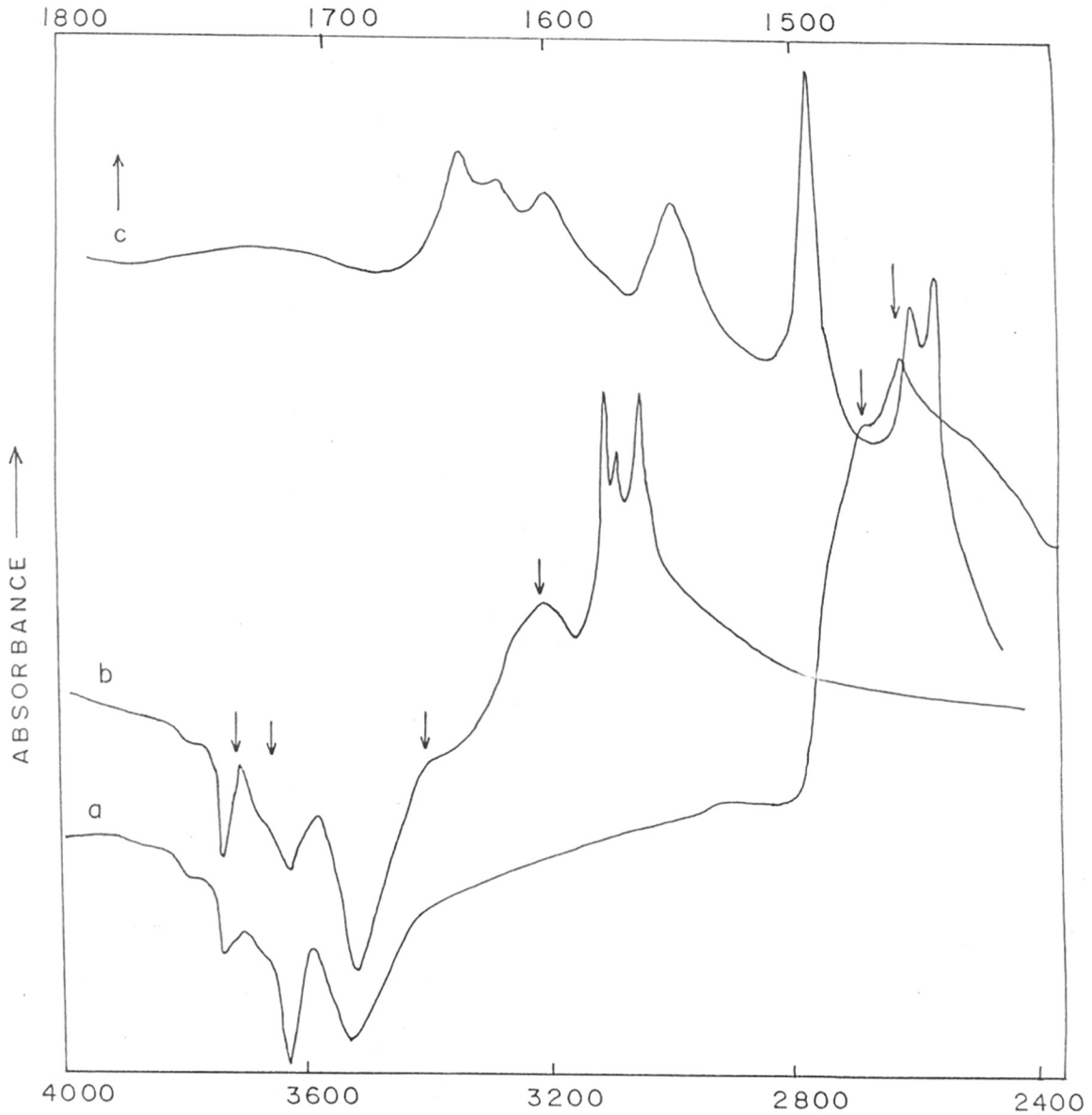

FIG.4·18 : DIFFERENCE F.T.I.R. SPECTRA OF SAPO-5 ON ADSORPTION OF a) D_2O, b) BENZENE, c) PYRIDINE

and they are stronger than that of HY but weaker than that of HZSM-5 zeolites.

4.3.3. Modified $AlPO_4$-5 (MeAPO-5) molecular sieves

IR spectra of Mg, Zn, Co, Fe, modified $AlPO_4$-5 molecular sieves in the region of framework vibrations are presented in Fig. 4.19.The main features of the spectra are similar to that of $AlPO_4$-5 except some shift in the positions of the bands. Considering the framework vibrations of tetrahedral primary units as T-O-T harmonic oscillators, the positions of the asymmetric, symmetric, bending and pore opening vibrations are assigned which are listed in Table 4.7. As the atomic weights of the substituting elements Mg (24.3), Co(59.0), Zn(65.4) and Fe(56) are considerably more than Al(27) and P(31), the asymmetric and symmetric vibrations of Al(or P)-O-T groups will obviously shift to lower wave numbers. For example, T-O-T bending vibrations at 480 cm^{-1} for $AlPO_4$-5 has shifted to 456 cm^{-1}, T-O-T asymmetric stretching vibration at 1140 cm^{-1} shifted to 1120 cm^{-1} for CoAlPO$_4$-5.

Bennet and Marcus (36a) have determined the structure of CoAlPO-44, CoSAPO-4, MgSAPO-46, CoSAPO-47 and CoAlPO-50 by x-ray diffraction and have reported the conclusive evidence for the complete tetrahedral framework substitution of various metal atoms incorporated. But Hong Xin et al. (142) while studying the nature of Fe species in FeAlPO-5 found that these samples contain iron mostly as Fe^{3+} in the lattice and partly as hydroxide or oxide extra lattice species. It was reported by Bond et al. (40)

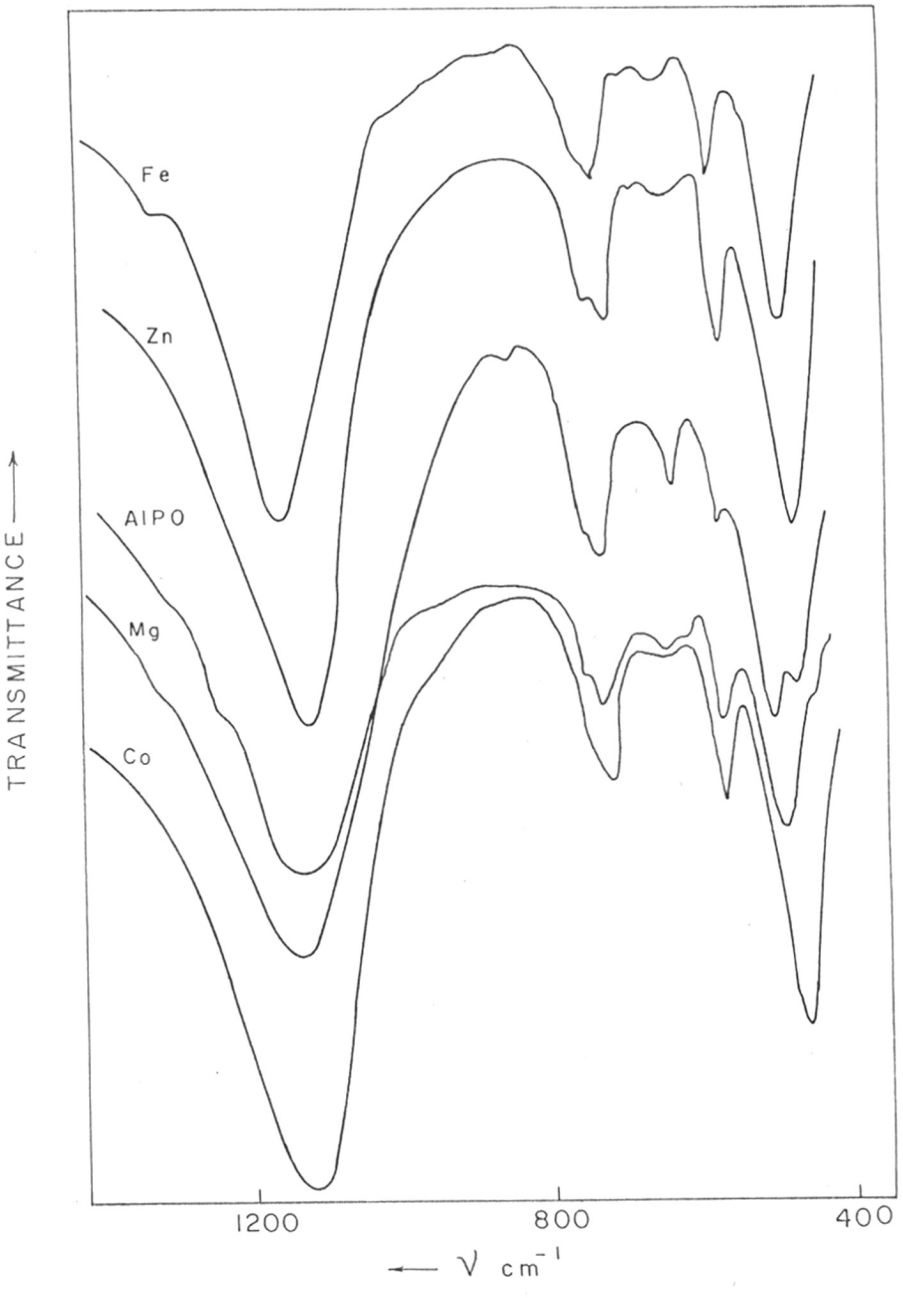

FIG. 4·19 - FT IR SPECTRA OF a) CoAlPO - 5 , b) MgAlPO - 5 , c) AlPO - 5 , d) ZnAlPO - 5 e) FeAlPO - 5

Table 4.7 : Infrared assignments for framework vibrations (νcm^{-1})

Mode of vibration	$AlPO_4$-5	MgAlPO-5	ZnAlPO-5	CoAlPO-5	FeAlPO-5
T-O-T bending (T = Si,Al,P)	480	475	460	456	455
Dopuble 4,6 rings (D6R, D4R)	560	557	550	550	550
T-O-T symm. satretch	705	705	703	700	700
T-O-T asymm. stretch	1150	1130	1125	1120	1115

that on introducing Zn in $AlPO_4$-5, surface hydroxyl groups of $AlPO_4$-5 are altered and Brönsted acidity is produced. These studies strongly corroborate our results that Mg, Zn, Co and Fe have been substituted in the $AlPO_4$-5 framework. As per TO_2 stoichiometry, the framework can be anionic if these metals are substituted as divalent atoms or it can be neutral if metal ions are substituted in trivalent form for Al . This problem was investigated by studying the nature of their surface hudroxyl groups.

In the Fig. 4.20 (curves a, b, c and d), FTIR spectra of Mg,Co, Zn and Fe incorporated $AlPO_4$-5 samples in the region of fundamental vibrations of structural hydroxyl groups are presented. Those for SAPO-5 and $AlPO_4$-5 (curves e and f) are also reproduced for comparison. The absorption bands around 3800, 3740 and 3670 cm^{-1} assigned to P-OH and Al-OH groups on $AlPO_4$-5 and SAPO-5 samples are also seen in the spectrum of Mg,Co, Zn and Fe modified samples. However, the two prominent bands at 3620 and 3525 cm^{-1} observed for SAPO-5 and assigned to Brönsted acid sites seem to have overlapped in the spectrum of these samples (curves a, b, c, and d, Fig.4.4). Instead, broad bands at 3558, 3571, 3520 and 3516 cm^{-1} are obtained as can be clearly seen in the spectra a,b,c and d, respectively. Bond et al.(40) have also reported identical spectrum for Zn modified $AlPO_4$-5 sample. The reasons for this behaviour are not known. The nature of these hdroxyl groups were further investigated by adsorption of pyridine (Fig.4.21). The experimental procedure was identical to that for

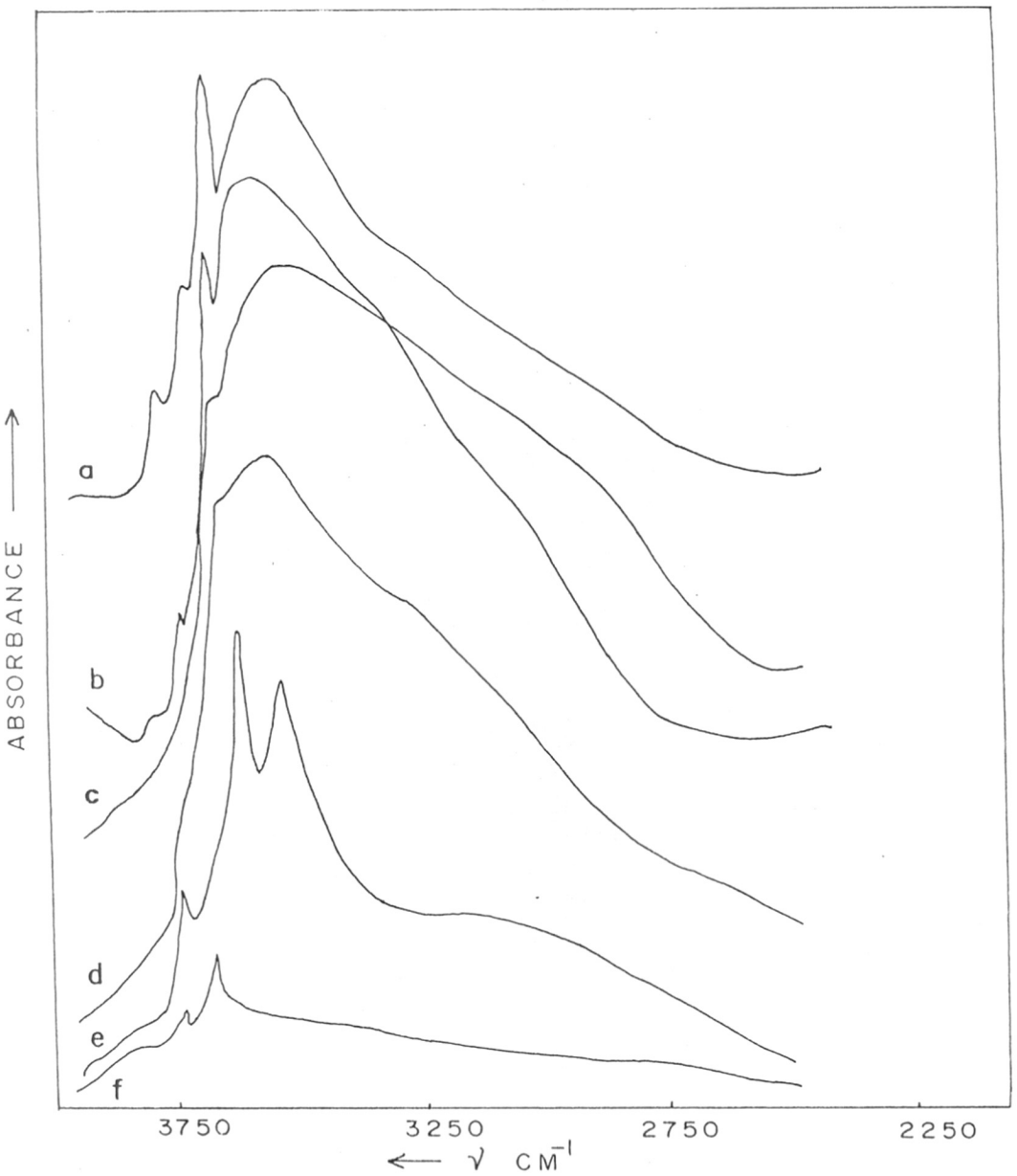

FIG. 4·20 : DIFFUSE REFLECTANCE F.T.I.R. SPECTRA OF a) MgAlPO-5, b) CoAlPO-5, c) ZnAlPO-5, d) FeAlPO-5, e) SAPO-5, f) $AlPO_4$-5

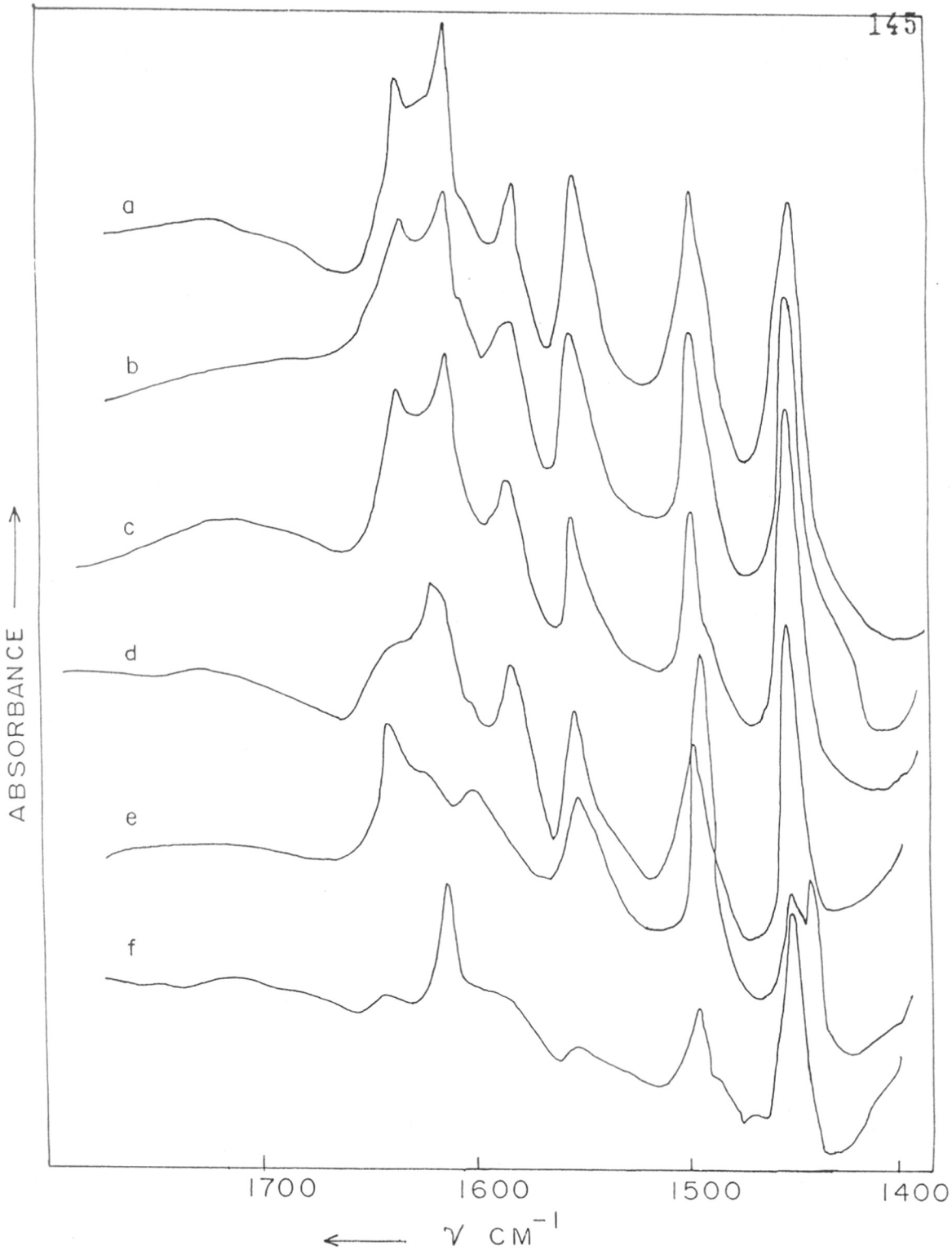

FIG. 4.21 DIFFERENCE F.T.I.R SPECTRA FOR ADSORPTION OF PYRIDINE ON a) MgAlPO-5, b) CoAlPO-5, c) ZnAlPO-5, d) FeAlPO-5, e) SAPO-5, f) AlPO4-5

$AlPO_4$-5. Two types of adsorptions were observed, one strong hydrogen bonding forming pyridinium ion and another coordination with Lewis acid sites. The bands around 1633 and 1545 cm^{-1} arise due to pyridine adsorbed on Brönsted acid sites and those at 1620 and 1450 are due to coordinatively bound pyridine on Lewis acid sites. The band at 1490 is common to both types of adsorptions.

Therefore we can see from the figure that Mg, Zn, Co and Fe modified $AlPO_4$-5 molecular sieves contain Brönsted and Lewis acid sites and that Lewis acid sites are relatively more than Brönsted acid sites.

4.4. TEMPERATURE PROGRAMMED DESORPTION OF AMMONIA (T.P.D. OF NH_3)

4.4.1. $AlPO_4$-5 molecular sieves

Temperature programmed desorption (TPD) of pyridine (pK_b = 8.75), n-butylamine (pK_b = 3.23) and NH_3 (pK_b = 4.75) have been used extensively to determine site energy distribution of acidic catalysts. NH_3 is preferred basic probe molecule because of its small size, enough to enter smallest pores in the sample. Energetics of this process can be determined by methods based on adsorption (calorimetry) and desorption (TPD). During adsorption, NH_3 enters the pores and adsorbs at the first available sites. This is not necessarily the strongest one. During desorption starting with all sites covered, NH_3 will first desorb from the weakest sites. Therefore, TPD is the most appropriate method for determining acid strength distribution. A satisfactory theory for determination of the heat of desorption from the TPD is developed by Cvtanovic and Amenomiya (149). Gorte (150) and Alnot (151) reported that the method based on heating rate variation gave the most reliable values for the heat of desorption.

The desorption process can be represented as

$$\frac{d\Theta}{dt} = K_d \Theta^n \qquad \ldots(1)$$

where Θ = degree of coverage,

K_d = rate constant,

n = order of desorption process.

In the heating rate variation method for a non-porous

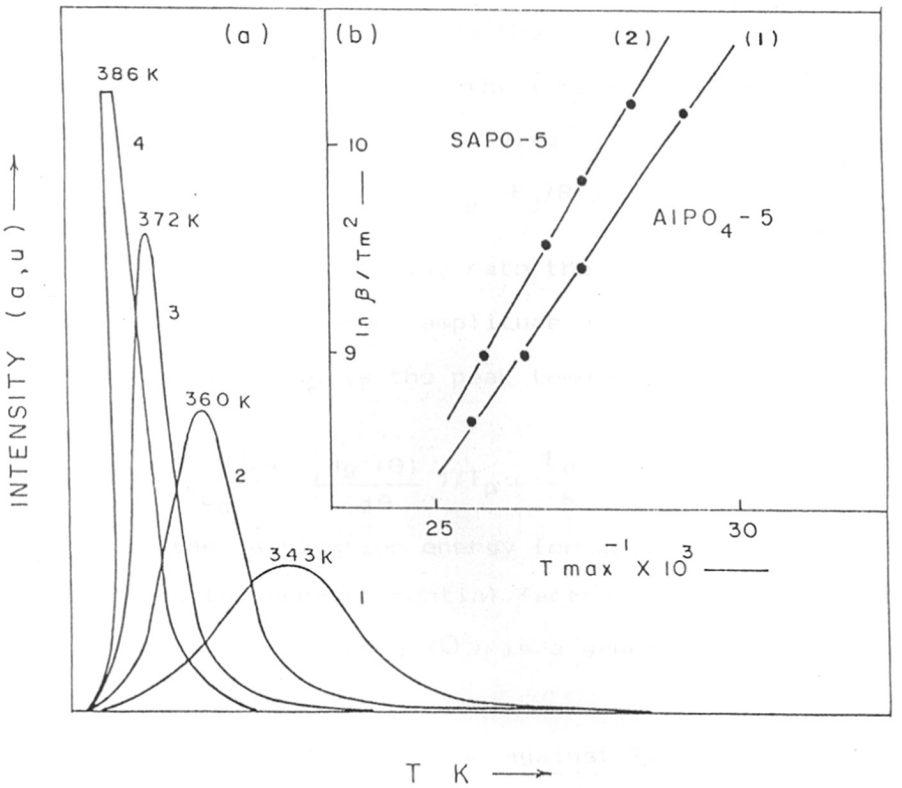

FIG. 4·22- a) T.P.D. CURVES OF NH_3 FOR HEATING RATE 1) 4, 2) 10, 3) 20 AND 4) 30 K MIN^{-1}

b) AMENOMIA – CVTENOVIC PLOT FOR (1) $AlPO_4$-5 (2) SAPO-5

energetically homogeneous surface on which n = 1, it is possible to apply Arrhenius equation which can be represented as

$$K_d = A e^{[-Ed/RT]} \qquad \ldots (2)$$

where A is the preexponential factor.

If $T = T_o + \beta$ where T_o and T are the initial temperature and temperature at time t, and β is the linear heating rate. Equation (1) and (2) can be combined to give

$$-(d\Theta/dt) = (A/\beta)\,\Theta^{n} e^{(-E_d/RT)} \qquad \ldots (3)$$

Therefore with increasing heating rate, the peaks shift to higher temperatures and show larger amplitude but reach a maximum rate in a shorter time. If T_p is the peak temperature at heating rate β, then

$$\ln \frac{\beta}{T_p^2} = \ln \frac{R\nu n}{E_d} \left(\frac{dg(\Theta)}{d\Theta}\right)/T_p + \frac{E_d}{R} \times \frac{1}{T_p} \qquad \ldots (4)$$

where E_d is the activation energy for desorption, Θ is coverage, νn is the pre-exponential factor for desorption of order n, R is the gas constant and $g(\Theta)$ is a general form of desorption dependance on coverage.

Hence, if $\ln(\beta/T_p^2)$ is plotted against T_p^{-1}, the slope is $-E_d/R$.

TPD curves of NH_3 for $AlPO_4$-5 molecular sieve obtained at heating rate of 4, 10, 20 and 30 K per minute are shown in Fig. 4.22 (a). The temperatures at peak maximum are 343, 360, 372 and 386 K respectively. The activation energy was calculated from the plot shown in Fig. 4.22(b). It is 47.00 KJ $mole^{-1}$ which agrees with isosteric heat of adsorption of NH_3 (ΔH) obtained by Janchen

et al. (152), but is significantly higher than that for silicalite (30 KJ mole^{-1}) which is a silica end member of pentasil zeolite. This is because the channels of $AlPO_4$-5 are polar and P-OH and Al-OH can be mildly acidic as per our IR studies. Pyridine adsorption on $AlPO_4$-5 shows some Lewis acidity as has been discussed earlier.

4.4.2. SAPO-5 molecular sieves

TPD curves of NH_3 for SAPO-5[(I to IV)] obtained by heating rate 10 K min^{-1} are presented in Fig.4.23. The amount of NH_3 strongly adsorbed as determined volumetrically before starting desorption is tabulated in Table 4.8. It is at once noticeable that unlike $AlPO_4$-5 which has only one peak at Tmax 373 K, all SAPO-5 samples have three peaks with Tmax 373, 463 and 593 K. The area under the first peak is almost equal for all SAPO-5 samples whereas that under second and third peak increases significantly on increasing Si mole fraction in SAPO-5.

On the basis of TPD curves it is clear that three groups of different states of adsorption can be identified as corresponding to three peak maxima at 373, 463 and 593 K. The activation energy for desorption for the three different states were determined as follows. Adsorption sites for NH_3 were saturated every time at 298, 348 and 423 K before performing TPD to determine activation energy for desorption by heating rate variation method. The typical plot of $\ln(\beta/Tm^2)$ vs $1/Tm$ is shown in Fig. 4.22 (b). E_d calculated for different states are given in Table 4.8. As the mole fraction of Si increases from 0.09 to 0.39, in SAPO-5, there

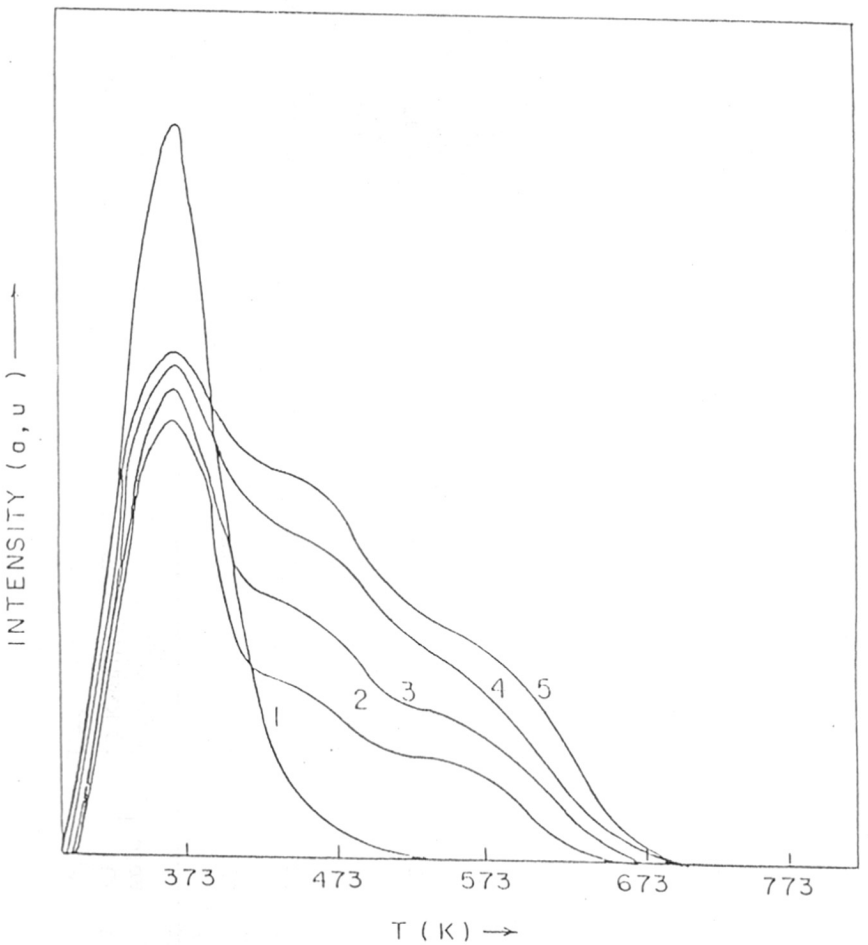

FIG. 4·23 – T.P.D. OF NH_3 FOR (I) $AlPO_4$–5
(2,3,4,5) SAPO – 5 (I TO IV)

Table 4.8

Acid strength distribution and ion-exchange capacity of $AlPO_4$-5, SAPO-5 and MeAPO-5.

Sample	Ion-exchange capacity Na^+ m.mol/g.	NH_3 saturated at 298 K			NH_3 saturated at 373 K			NH_3 saturated at 473 K		
		NH_3 m.mol/g.	E_d KJ $mole^{-1}$	T_{max} 10 K/min.	NH_3 m.mol/g.	E_d KJ $mole^{-1}$	T_{max} 10 K/min.	NH_3 m.mol/g.	E_d KJ $mole^{-1}$	T_{max} 10 K/min.
$AlPO_4$-5	0.25	1.2	47.0	372	0.20	-	443	-	-	-
SAPO-5 I	0.90	1.5	54.0	373	0.80	70.0	458	0.20	85.0	577
SAPO-5 II	1.10	1.8	55.5	370	1.00	69.0	463	0.33	86.0	573
SAPO-5 III	1.20	2.15	56.0	371	1.14	71.0	461	0.42	88.2	582
SAPO-5 IV	1.40	2.5	57.0	372	1.25	72.0	464	0.56	87.5	583
MgAlPO-5	1.50	1.5	58.0	383	-	-	-	-	-	-
ZnAlPO-5	1.10	1.6	59.0	378	-	-	-	-	-	-
CoAlPO-5	1.20	1.35	61.0	378	-	-	-	-	-	-
FeAlPO-5	0.50	1.25	53.0	370	-	-	-	-	-	-

is definite increase in the number of acid sites belonging to all the three groups (weak, medium and strong) whereas the E_d values for all of them corresponding to any group does not change. The weak, medium and strong acid sites have E_ds about 55, 70 and 87 KJ mole respectively. Therefore, in comparison with isosteric heat of adsorption of NH_3 on HY zeolites (153) we can conclude that SAPO-5 molecular sieves studied have stronger acid sites than in HY zeolites.

In the Fig. 4.24 the number of NH_3/UC, irreversibly adsorbed at 298, 373 and 453 K are plotted against Si atoms/unit cell. From the figure, it can be seen that the number of acid sites linearly increase with increase in number of Si atoms for all the three groups of acid sites but the slope of the line (0.42, 0.19 and 0.15 respectively) decreases in the order weak + medium + strong > medium + strong > strong acid sites. Therefore, it is to be concluded that more number of weaker acid sites are formed compared to number of strong acid sites when Si mole fraction is increased in the framework. In such framework compositions, simultaneous substitution of one aluminium and one phosphorous by two Si cations may be more probable than the substitution of aluminium only, by silicon atoms. (170).

4.4.3. MeAPO-5 molecular sieves

TPD curves of NH_3 for Mg, Zn, Co and Fe modified $AlPO_4$-5 molecular sieves are presented in Fig. 4.25. At 298 K, the irrever-sibly adsorbed NH_3 (Table 4.2) were 1.47, 1.56, 1.34 and 1.25

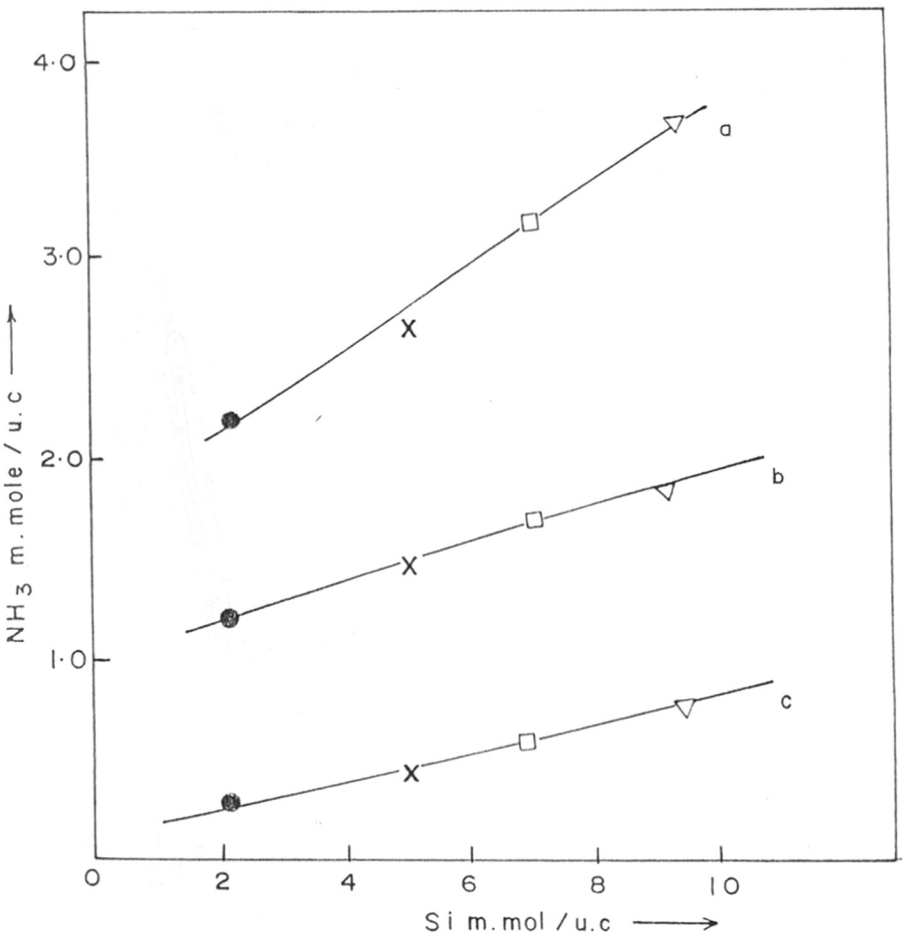

FIG. 4·24 : VARIATION OF ACID AMOUNT WITH Si MOLE FRACTION IN SAPO-5 (I to IV) (MARKS ●, X, □, △, RESPY.) CHEMISORBED AT a) 298, b) 373 & c) 453 K.

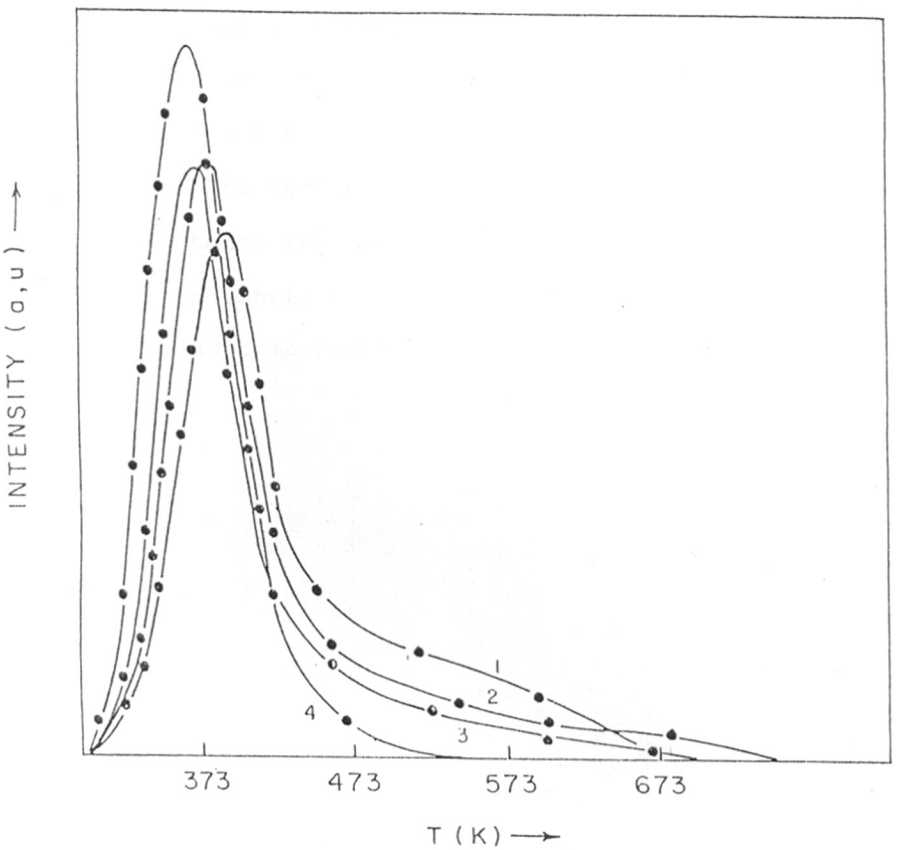

FIG. 4·25 - T.P.D. OF NH_3 FROM MgAlPO-5 (1), ZnAlPO-5 (2), COAlPO-5 (3) AND FeAlPO-5(4)

m.mole/gm respectively. From the nature of the TPD curves, it is seen that only one major peak is obtained at around 373 K for all these samples. In FeAlPO-5, no acid sites capable of retaining NH_3 beyond 473 K is observed. The amount of NH_3 retained beyond 473 K in MgAlPO-5 is greater than that in ZnAlPO-5 which is greater than that in CoAlPO-5. which is clearly seen from the figure (4.24). For all these, the activation energy for desorption which was found out by heating rate variation method was about 60 KJ $mole^{-1}$. The number of strong acid sites for these samples are less than those for SAPO-5. This is because of lower amount of isomorphous substitution and somewhat lower crystallinity of these samples as compared to SAPO-5 molecular sieves.

CHAPTER - V

CATALYTIC PROPERTIES

5.1 CATALYTIC PROPERTIES

5.2. O-XYLENE ISOMERIZATION

5.2.1. $AlPO_4$-5 MOLECULAR SIEVES

5.2.2. SAPO -5 MOLECULAR SIEVES

5.2.3. MeAPO-5 MOLECULAR SIEVES

5.2.4. O-XYLENE REACTION MECHANISM

5.2.5. CATALYST DEACTIVATION IN O-XYLENE ISOMERIZATION

5.3. CATALYTIC CRACKING OF n-HEXANE

5.3.1. INFLUENCE OF TEMPERATURE

5.3.2. INFLUENCE OF METAL SUBSTITUTION IN $AlPO_4$-5

5.3.3. THE REACTION MECHANISM

5.4. ALKYLATION OF TOLUENE WITH METHANOL

5.4.1. TOLUENE METHYLATION OVER MeAPO-5

5.4.2. INFLUENCE OF TIME ON STREAM

5.3.3. THE REACTION MECHANISM

5.1. CATALYTIC PROPERTIES

Aluminophosphates are interesting materials because of their high and intermediate electronegativity. Perry (154) classified them as strongly acidic catalysts with very weak basic sites. However, studies of Wendt (155) and mechanistic investigations by Thomke (156) and Bouer (157) suggested that it has rather moderate acid strength. A review by Moffat (143) summarises these characteristics. It was assumed that they contain both Brónsted and Lewis acid sites. Indeed, the catalytic activity of phosphates in isomerization (158) and alkylation (159) suggests that acid centers of moderate strength are present in these compounds. However, considering the IR data (154), it is evident that acid centers in aluminophosphates are weaker than those of aluminosilicates.

Microporous aluminophosphates discovered by Wilson et al. (9) have in many respects properties similar to zeolites. Therefore, it is not surprising that studies of these materials on variety of catalytic applications are appearing. Choudhary et al, (55) have investigated the site energy distribution and catalytic properties of $AlPO_4$-5, for cracking of hydrocarbons, isomerization of o-xylene and disproportionation of toluene on $AlPO_4$-5 and concluded that they have much higher acidity and catalytic activity than amorphous aluminophosphates. The activity of $AlPO_4$-5 for methanol conversion was attributed (9) to extra lattice aluminium species. Castrin (161) studied the reaction of aromatics over SAPO-5 and $AlPO_4$-5 for xylene isomerization and

found that the reaction was intramolecular showing similar types of catalytic behaviour as ZSM-5. Martin et al.(141) characterized the pore structure of SAPO-5 by n-decane test reaction. Pyke et al. (23) studied the isomerization of o-xylene and related the activity of catalysts based on $AlPO_4$-5 to their electronegativity.

Several novel silicoaluminophosphate molecular sieves having a range of pore sizes, acidities and compositions were tested (29) for propylene oligomerization and toluene alkylation and it was found that $AlPO_4$-5 catalysts are not shape selective. From these observations we came to the conclusion that the activity of $AlPO_4$-5 and modified $AlPO_4$-5 depends mostly on chemical compositions. Therefore, we thought to study some acid catalysed reactions over these catalysts and relate them to the acidic properties described earlier. We have chosen o-xylene isomerization, toluene alkylation by methanol and n-hexane cracking reactions because these are well characterized acid catalysed hydrocarbon reactions. Catalytic reactions were carried out in a downflow tubular reactor at atmospheric pressure according to the procedure described earlier.

5.2. O-XYLENE ISOMERIZATION

5.2.1. $AlPO_4$-5 molecular sieves

The conversion of o-xylene and product distribution over $AlPO_4$-5 molecular sieves is shown in Table 5.1. The conversion first increases with increasing temperature between 573-823 K (Fig.5.1) attains a maximum (13.00 %) at 823 K and then remains

steady between 773-823 K. It is observed from the product distribution data given in Table 5.1 that at lower temperatures (573-623 K) no disproportionation products are formed, the main reaction products being xylene isomers. With increasing the reaction temperature, xylene disproportionation increased from .24 to.86 wt % .

Table 5.1 : Influence of temperature on product distribution for o-xylene isomerization over $AlPO_4$-5 WHSV = 4.4.

Temp. K	573	623	673	723	773	823
Product composition wt. %						
Aliphatics	0.013	0.010	0.06	0.12	0.11	0.10
Benzene	0.040	0.026	0.15	0.25	0.21	0.20
Toluene	0.15	0.20	1.31	0.63	0.56	0.78
Ethyl benzene	0.70	0.66	0.54	0.62	0.61	0.60
p-Xylene	0.25	0.30	0.40	0.86	1.40	1.50
m-Xylene	1.12	1.50	1.70	4.01	9.60	9.80
o-Xylene	97.20	96.60	95.06	92.41	86.50	85.12
*T.M.B.(C_9 arom.)	0.24	0.25	1.52	0.77	0.70	0.86
Total xylenes	98.57	98.40	97.16	97.28	97.50	96.42
o-Xylene conv.	0.62	1.24	2.81	5.50	11.60	13.00
C_7/C_9	0.82	1.04	1.12	1.07	1.03	1.18
PATE*	0.17	0.38	0.82	2.80	5.2	5.64
MATE*	0.40	1.12	1.54	6.10	17.23	17.62

* T.M.B. : Trimethyl benzene
* PATE : Para-xylene approach to equilibrium
* MATE : Meta-xylene approach to equilibrium

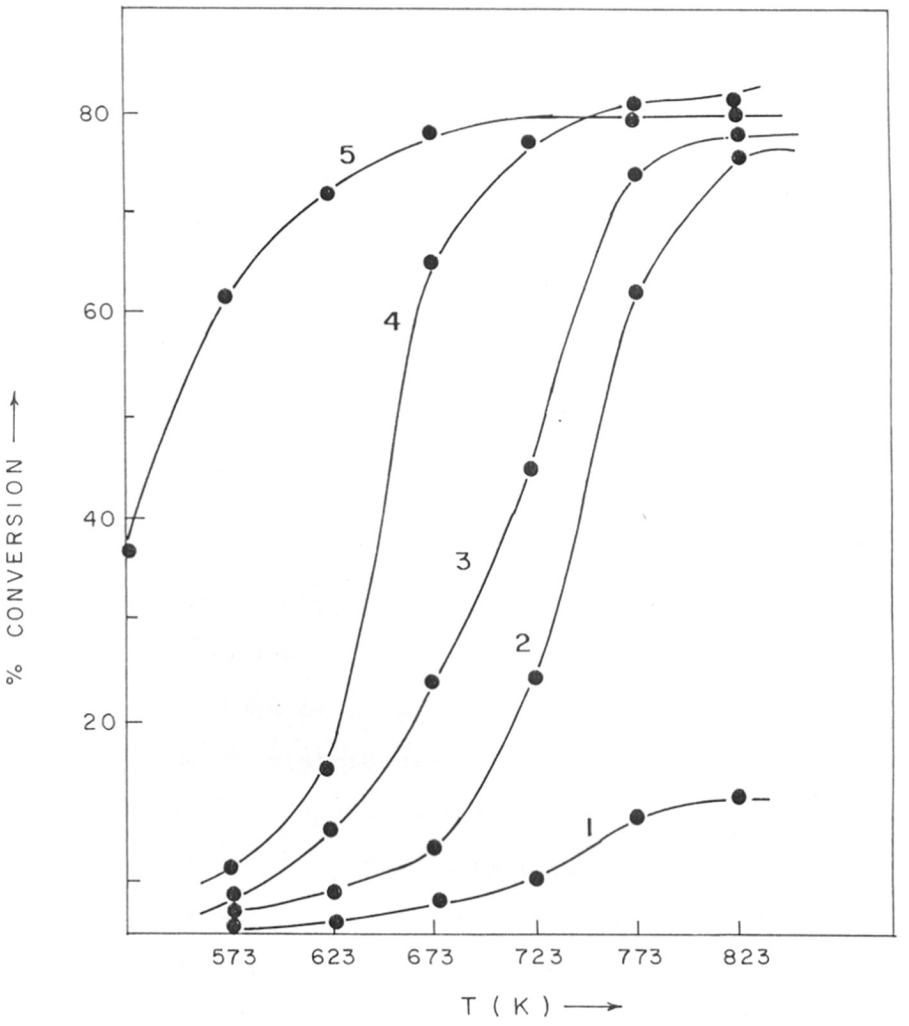

FIG. 5·1 INFLUENCE OF TEMPERATURE ON O-XYLENE CONVERSION OVER 1) $AlPO_4$-5 2) SAPO – 5 3) CoAlPO – 5 4) MgAlPO – 5 AND 5) HZSM – 5, W.H.S.V = 4·4

The equilibrium approach to p- and m-xylenes varied from 0.17 to 5.64 and 0.4 to 17.62 respectively in the temperature range 573 to 823 K. Above 723 K the percentage of liquid condensate decreased indicating demethylation of xylenes to give toluene and methane. Dealkylation to toluene occurred at 723 to 823 K and the mole ratio of toluene/trimethyl benzene observed was greater than 1.0 due to dealkylation. Our results are comparable to those of Choudhary et al. (55) who have reported about 12 % conversion at 673 K with poor selectivity, whereas Pyke et al. (23) and Qinhua et al. (54) did not find any activity for isomerization.

5.2.2. SAPO-5 molecular sieves

O-xylene isomerization on SAPO-5 (I to IV) samples with 0.09 to 0.39 mole fractions of Si were carried out at 4.4 g/hr WHSV at 723 K. The product distribution is tabulated in Table 5.2. As mole fraction of Si increases from zero in $AlPO_4$-5 to 0.39 in SAPO-5(IV) the following trend in product distribution has been noticed (i) conversion increases from 5.5 to 40.2, (ii) % xylene selectivity increases along with the approach to equilibrium of m-xylene to p-xylene (euilibrium value is 20.2 at 673 K), (iii) ratio of C_7/C_9 decreases with the increase in Si content, selectivity to p-xylene increases slightly with simultaneous dealkylation and disproportionation. The shape selectivity in fact should not be expected because it is a wide pore zeolite (pore dia $\sim$ 0.8 nm). It has been established that Si substitution

Table 5.2 : O-xylene isomerization on SAPO-5 molecular sieves

Reaction Temperature 723 K, WHSV = 4.4

Catalyst	$AlPO_4$-5	SAPO-5(I)	SAPO-5 (II)	SAPO (III)	SAPO-5 (IV)
Product dist. wt. %					
Aliphatics	0.12	0.16	0.29	0.22	0.20
Benzene	0.25	10.31	1.4	1.3	1.6
Toluene	0.63	2.01	3.9	4.9	7.5
Ethyl benzene	0.62	0.56	0.45	0.51	0.40
p-Xylene	0.86	1.94	1.62	5.94	7.10
m-Xylene	4.01	18.51	20.5	19.2	17.6
o-Xylene	92.41	73.81	66.50	61.60	57.6
Trimethyl benzene TMB	0.77	1.15	4.8	6.33	8.9
Total xylene	97.28	94.26	89.62	86.74	82.3
% o-Xylene conversion	5.5	24.54	31.3	36.2	40.2
C_7/C_9 ratio	1.07	1.22	1.06	1.02	0.95
% p-xylene	0.90	2.06	4.00	6.84	8.60
Turn over number(TON)	8.2×10^{-4}	4.1×10^{-3}	5.1×10^{-3}	5.9×10^{-3}	6.52×10^{-3}

indeed has taken place in SAPO-5 samples and Brönsted and Lewis acid sites have been identified. O-xylene isomerization is known to be catalysed by Brönsted acid sites. Therefore, the turn over number (TON) calculated as a number of o-xylene molecules converted per unit cell of SAPO-5 per second was related to the acid sites per gram determined by TPD of NH_3.

TPD curve of NH_3 (Fig. 4.22, Table 4.2) for $AlPO_4$-5 is comparable to that of SAPO-5 samples only in the region below 448 K. There are no strong acidic OH groups on $AlPO_4$-5 which can hold NH_3 beyond this range. Therefore, acid groups contributing to NH_3 desorption below this temperature can be presumed not to be important for o-xylene isomerization, because $AlPO_4$-5 has little activity for o-xylene isomerization. Therefore, NH_3 chemisorbed at and above 448 K as per TPD is only taken for the above correlation. A plot of this amount of NH_3 per gram vs TON is shown in Fig. 5.2. A linear relation passing through the origin is indeed obtained. Therefore, it can be concluded that acid sites of strength about 70 KJ/mole and above are active sites for o-xylene isomerization on SAPO-5 molecular sieves.

5.2.3. MeAPO-5 molecular sieves

Of recent interest in modified $AlPO_4$-5 material are MeAPO-5 containing alkaline earth and transition metal elements to induce better acid-base properties. Many publications (23) have appeared in this field, yet very little is known in the open literature about the nature of acid sites and catalytic activity

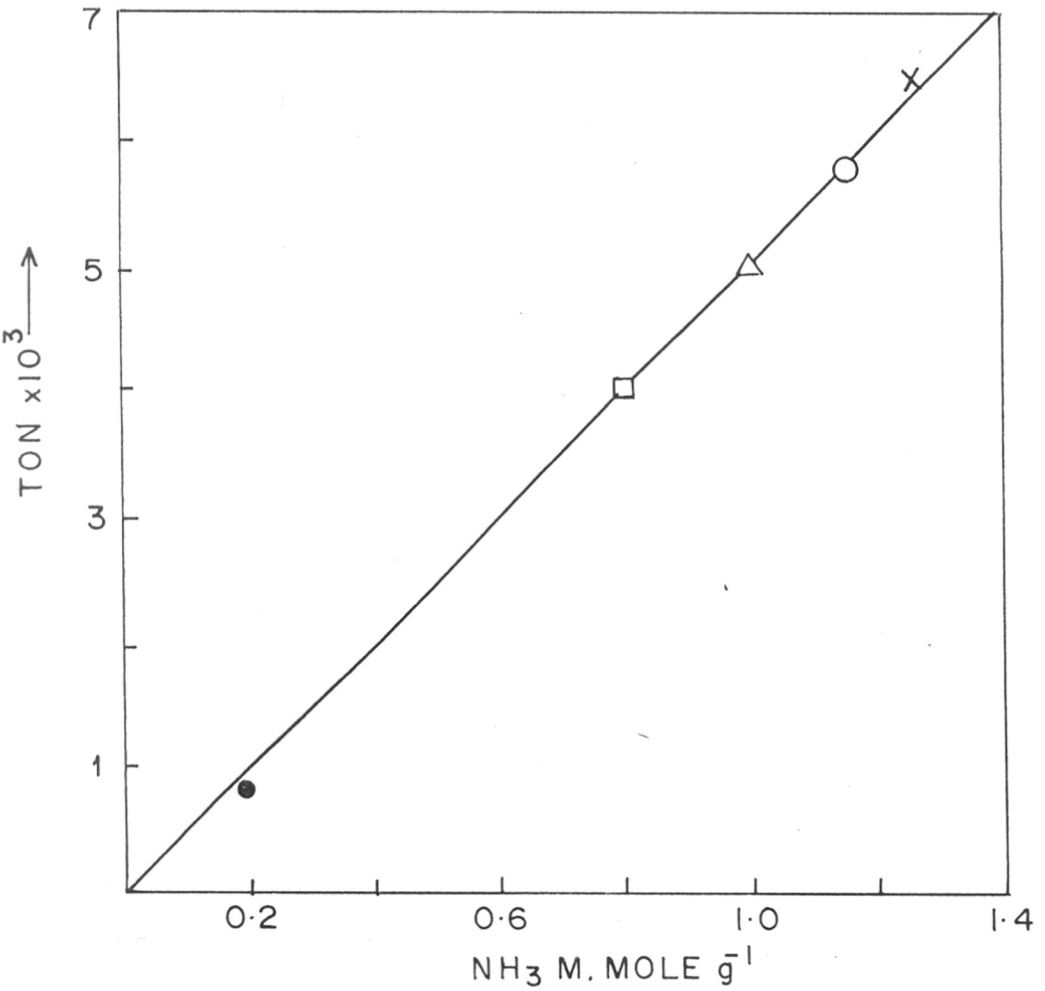

FIG.5·2 VARIATION OF O-XYLENE ISOMERIZATION ACTIVITY WITH ACIDITY FOR (●) $AlPO_4$-5, (□, △, ○, X) SAPO-5 (I TO IV).

Table 5.3 : Influence of metal substitution in $AlPO_4$-5 molecular sieves on o-xylene isomerization reaction and their product distribution

Reaction Temperature = 723 K, WHSV = 4.4

Catalyst	$AlPO_4$-5	SAPO-5	MgAlPO -5	ZnAlPO-5	CoAlPO-5	FeAlPO-5
Product dist.wt.%						
Aliphatics	0.12	0.16	0.50	0.25	0.2	0.16
Benzene	0.25	0.31	1.80	0.51	0.46	0.33
Toluene	0.63	2.01	17.00	7.11	3.91	3.22
Ethyl benzene	0.62	0.56	0.60	0.50	0.55	0.54
p-Xylene	0.86	1.94	9.50	5.44	3.82	2.0
m-Xylene	4.01	18.51	29.21	23.93	19.40	14.10
o-Xylene	92.41	73.81	21.92	53.43	67.10	75.22
Trimethyl benzene	0.77	2.51	18.01	8.54	4.43	4.15
Total xylene	97.28	94.26	60.63	82.8	90.32	91.32
% o-Xylene conversion	5.50	24.54	77.54	45.30	31.25	22.90
C_7/C_9 ratio	1.07	1.22	1.23	1.10	1.15	1.01
% p-Xylene selectivity	0.90	2.06	15.70	6.60	4.23	2.20

about these materials (170). While characterizing Mg, Zn, Co and Fe incorporated $AlPO_4$-5 materials by IR, we have detected Brönsted and Lewis acid sites on such catalysts. The catalytic activity for o-xylene isomerization was therefore carried out and the results are tabulated in Table 5.3. The results for $AlPO_4$-5 and SAPO-5 are included in the table for comparison.

The conversions over Mg^{2+}, Zn^{2}, Co^{2} and Fe^{3+} incorporated $AlPO_4$-5 were 77.54, 45.3, 31.25 and 22.9 % respectively which are higher than that for $AlPO_4$-5 and SAPO-5 materials, even though the level of incorporation of metal in the samples is 0.055, 0.025, 0.035 and 0.035 for Mg, Zn, Co and Fe, respectively as against 0.09, for Si (Table 3.12). Likewise, dealkylation and dis--proportionation reactions are also increased. The p-xylene selectivity in xylene isomzerization is found to be higher as compared to SAPO-5. The order of activity is Mg > Zn > Co > Si > Fe.

In order to understand the influence of contact time, CoAlPO-5 was selected and WHSV was varied from 4.425 to 8.85. The results are tabulated in Table 5.4. O-xylene conversion decreased from 31.25 to 9.73 when the WHSV was increased from 4.425 and 8.85 and the percentage p-xylene in total xylenes is also decreased from 3.8 to 1.5 % which is as expected. Dealkylation and disproportionation reactions also decreased as shown by C_7/C_9 ratio.

Fig. 5.[illegible] shows typical plots for the variation of o-xylene conversion with temperature of the reaction over $AlPO_4$-5, SAPO-5, CoAlPO-5, MgAlPO-5 and HZSM-5. The salient feature which comes

Table 5.4 : Influence of WHSV for o-xylene isomerization over CoAlPO-5 at 723 K

WHSV (hr^{-1} [a])	4.425	6.64	8. 85
Product comp.wt.%			
Aliphatics	0.2	0.3	0.09
Benzene	0.46	0.24	0.20
Toluene	3.91	1.54	1.30
Ethyl benzene	0.55	0.57	0.65
p-Xylene	3.82	2.10	1.40
m-Xylene	19.40	8.5	6.10
o-Xylene	67.10	84.2	88.10
TMB (C_9^+ arom.)	4.43	1.95	1.60
Total xylenes	90.12	94.80	95.60
o-Xylene conv.	31.25	13.73	9.73
C_7/C_9 ratio	1.15	1.03	1.07
% p-x in xylene	3.80	2.20	1.50

a = weight of o-xylene per hour per gm of catalyst

out from this figure is that at temperature higher than 823 K, conversion reaches to about 80% for all samples except $AlPO_4$-5.

5.2.4. O-xylene reaction mechanism

O-xylene isomerization is unimolecular reaction (162) and follows a single site reaction model involving the adsorption of xylene molecules on the protonic sites of the catalyst surface and subsequent, intramolecular, 1,2-methyl shift to form the isomers. The apparent activation energy is evaluated from the pseudo first order kinetics equation

$$K = F/W \ln(1/1-x) \quad \ldots (1)$$

and the Arrehenius equation

$$K = K_o e^{-E/RT} \quad \ldots (2)$$

where F is the hydrocarbon flow rate, W is the weight of the catalyst, K is the rate constant, x is the fraction of o-xylene converted, K_o is the initial rate constant when t is 0, E is activation energy, T is the absolute temperature and R is the gas constant (163)

The plots of log K vs 1/T (Fig. 5.3) for the absolute values of rate constants are linear between 573-773 K. The average value of the activation energy calculated from the above data for AlPO-5, SAPO-5 and MgAlPO-5 are listed in Table 5.5. It is observed that MgAlPO-5 has highest catalytic activity amongst all these molecular sieves. However, it is less than that for the high silica zeolite like HZSM-5 as reported by Babu et al (164).

It is observed from our experimental data (Table 5.1) that at low conversion level (0.62 %) of o-xylene, the product con-

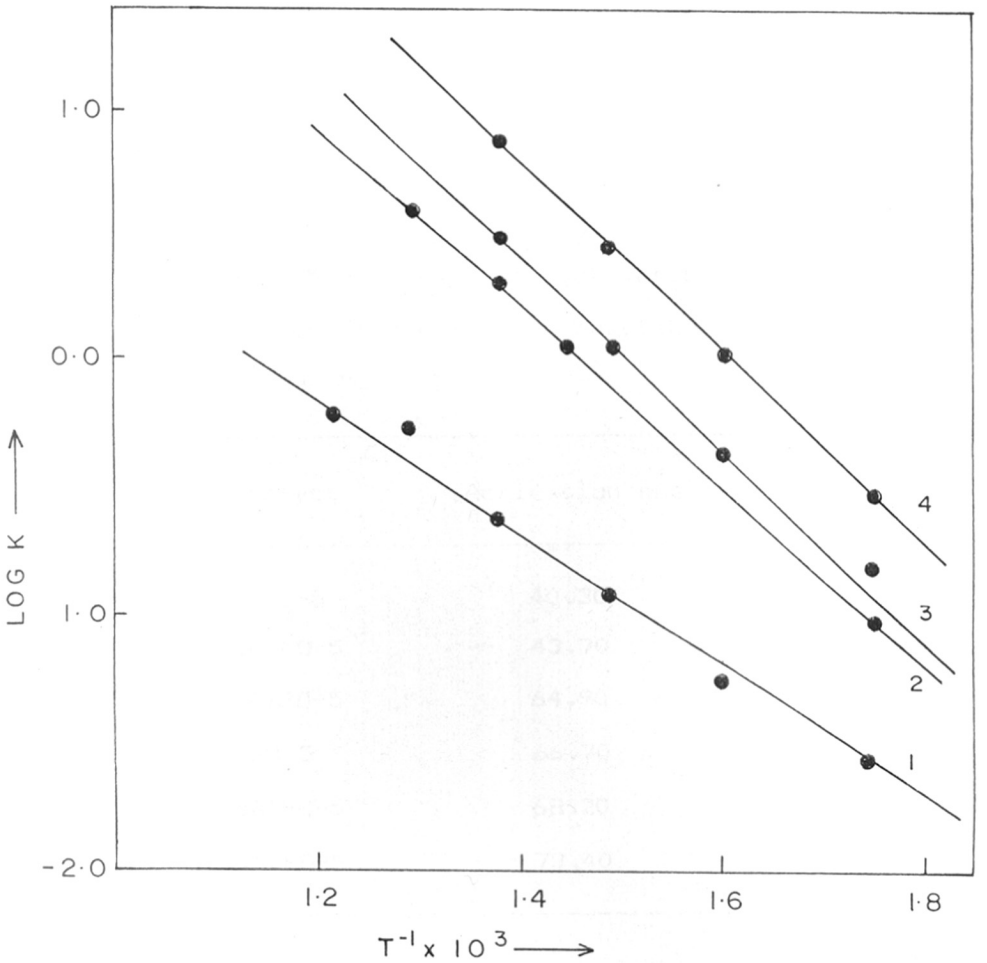

FIG. 5·3 : ARRHENIOUS PLOTS FOR O-XYLENE ISOMERIZATION 1) $AlPO_4$-5, 2) SAPO-5, (3) COAlPO-5 4) Mg AlPO-5

Table 5.5 : Apparent activation energies for o-xylene isomerization reaction over $AlPO_4$-5 and MeAlPO-5.

Catalyst	Activation energy, KJ $mole^{-1}$
$AlPO_4$-5	40.30
FeAlPO-5	43.70
ZnAlPO-5	64.90
SAPO-5	66.70
CoAlPO-5	68.20
MgAlPO-5	73.40

tains larger amount of m-xylene while at the same conversion level, isomerisation of pure m-xylene results in approximately equal amounts of o- and p-xylenes.

Isomerisation of xylenes can occur by two different reaction mechanisms (160, 165-168) namely (1) intramolecular rearrangement (1,2-methyl shift) requiring only one Brönsted acid site, (2) intermolecular reaction involving a Lewis site, or a Brónsted-Lewis pair. The reaction scheme can be represented as a series in which meta-xylene is the intermediate:

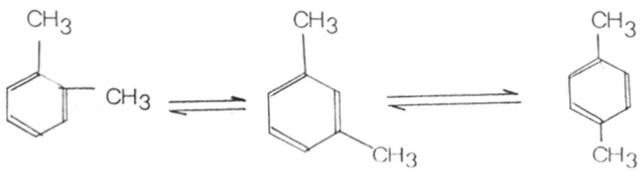

A direct ortho to para-xylene conversion has been considered for reaction in the pores of zeolites with large crystallite size (169).

According to Collins et al (170) the reactions of xylene can be represented as shown below :

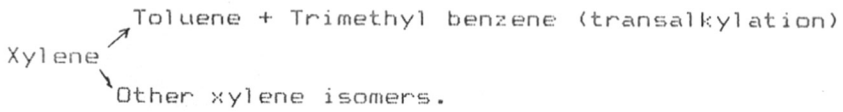

On a conventional zeolite (LaY zeolite) they observed ortho-xylene to give 1,2,3 and 1,2,4 trimethyl benzenes (TMBs) and para-xylene to give 1,2,4 TMB as expected from the directing effect of CH_3 groups. In contrast, C_9 aromatics from ZSM-5 zeo-

lite catalysed isomerization contain predominantly 1,2,4 trimethyl benzene. Transalkylation on the external surface gives rise to other isomers also.

Dealkylation of xylene also takes place as a side reaction. For a very active catalyst the mole ratio of toluene to C_9 aromatics is greater than one (Table 5.3). Dealkylation of toluene also takes place. Thus the side products observed are toluene, benzene and trimethyl benzene. It is generally accepted that isomerisation needs acid sites of weaker strength compared to the sites required for disproportionation and cracking (171, 172). In agreement with this observation, SAPO-5 and MeAPO-5 which possess broad range of acid sites show good activity for isomerization whereas $AlPO_4$-5 with no strong acid sites show least activity for this reaction.

5.2..5. Catalyst deactivation in o-xylene isomerization

The coke deposition over the catalyst is responsible for the loss in activity. Voorhies (173) was the first to derive an expression for catalyst deactivtion. Weekman and Nance (174) and Ozawa et al. (175) studied the catalyst deactivtion in detail. The diffusivities of the compounds (hydrocarbons) inside the zeolite channels are restricted and because of such restricted movements, the access of reactant molecules to the active sites and the diffusion of polyalkylated aromatic hydrocrbons are hindered. The deactivation by diffusional restrictions (at low temperatures) and coking (at higher temperatures) over modified $AlPO_4$-5 catalysts are discussed in the following studies.

To determine the deactivation constants, and to estimate the amount of coke deposits, o-xylene isomerisation was carried out in the temperature range 573 to 823 K over SAPO-5 catalyst. The product distribution is illustrated in Table 5.6.

The deactivation constant (α) was evaluated from the equation

$$K = K_o . e^{\alpha Y} \qquad \ldots (3)$$

where K is the reaction rate, Y is cumulative o-xylene conversion and K_o is initial reaction rate.

Linear plots of lnK vs Y are shown in Fig. 5.4. The deactivation constant (α) was obtained from the slope of the linear plot and the initial value of the reaction rate (K_o) was obtained from the intercept. Values of α and K_o calculated at each temperature are given in Table 5.7. From the table, it can be seen that the percentage fall in activity compared to the initial activity is higher at high temperature, and the deactivation constant.

α is high at low temperature. Due to thermal cracking and formation of polyalkylated benzenes (1,2,4-trimethylbenzene), maximum coke was deposited at high reaction temperatures 773 to 823 K. It is observed that the $AlPO_4$-5, SAPO-5 and MeAPO-5 molecular sieves are active only over a very short period of ($\sim$4 hours).

The amount of coke deposited was analysed by thermal analysis (DTA/TG). Typical thermograms for $AlPO_4$-5 and SAPO-5 are

Table 5.6 : Deactivation of SAPO-5 with time on stream; WHSV = 4.4

Temp. K	723				773			
Time on stream(hr)	1	2	3	4	1	2	3	4
Product comp. (wt. %)								
Aliphatics	0.16	0.14	0.13	0.12	0.24	0.23	0.30	0.23
Benzene	0.31	0.30	0.30	0.30	0.39	0.36	0.34	0.33
Toluene	2.01	1.34	1.12	1.12	5.05	3.30	2.54	2.34
Ethyl benzene	0.56	0.60	0.60	0.65	0.46	0.55	0.60	0.62
p-Xylene	1.94	1.31	1.10	0.91	0.96	6.64	5.60	5.24
m-Xylene	18.51	12.90	10.70	9.98	40.30	33.33	32.40	31.55
p-Xylene	73.81	81.40	84.46	86.44	37.30	51.50	54.92	56.75
TMB (C_9 arom)	2.15	1.60	1.64	1.44	4.44	3.51	2.90	2.66
Total xylene	94.26	95.61	96.26	96.33	87.56	91.47	92.92	93.34
o-Xylene conv.	24.54	16.80	13.65	11.62	61.90	47.35	43.85	42.00
C_7/C_9 ratio	1.22	1.10	0.90	1.00	1.50	1.22	1.14	1.14

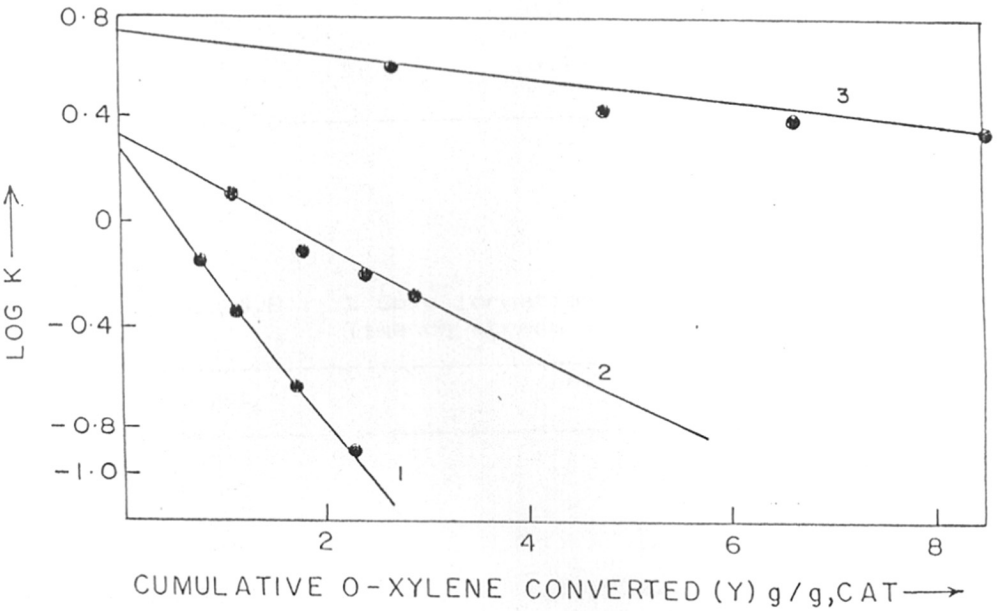

FIG.5·4 : DEACTIVATION RATE CURVES FOR, SAPO-5, W,H,S,V-4·4 AT 1) 673 K 2) 723 K 3) 773 K.

Table 5.7 : Deactivation constant and initial rate constant K_o of SAPO-5 at different temps.

Reaction Temp. K	K_o	α
673	0.26	0.54
723	0.32	0.2
773	0.74	0.044

Table 5.8 : % Coke formation in MeAPO -5 at 723 K
Time on stream : 4 hrs.

Catalyst	% Coke formed
MgAlPO-5	0.5
ZnAlPO-5	2.0
CoAlPO-5	2.1
SAPO-5	2.5
FeAlPO-5	3.0
$AlPO_4$-5	3.5

shown in Fig. 5.5. An exotherm in the DTA peak due to the oxidation of trapped organic matter was observed at 793 and 783 K for $AlPO_4$-5 and SAPO-5 respectively. It was observed that MeAPO-5 catalysts are deactivated very slowly and the amount of coke deposited is very much smaller (Table 5.8) as compared to $AlPO_4$-5.

From the above data, it can be concluded that

(1) Values of the deactivation constant are higher at lower temperatures due to the low diffusivity of trapped molcules. This restricts the accessibility of the reactant to the active sites.

(2) Coke deposition increases with temperature.

(3) The catalytic active samples deactivate slowly and the amount of coke deposited during the reaction is very much smaller on such catalysts compared to the inactive catalysts.

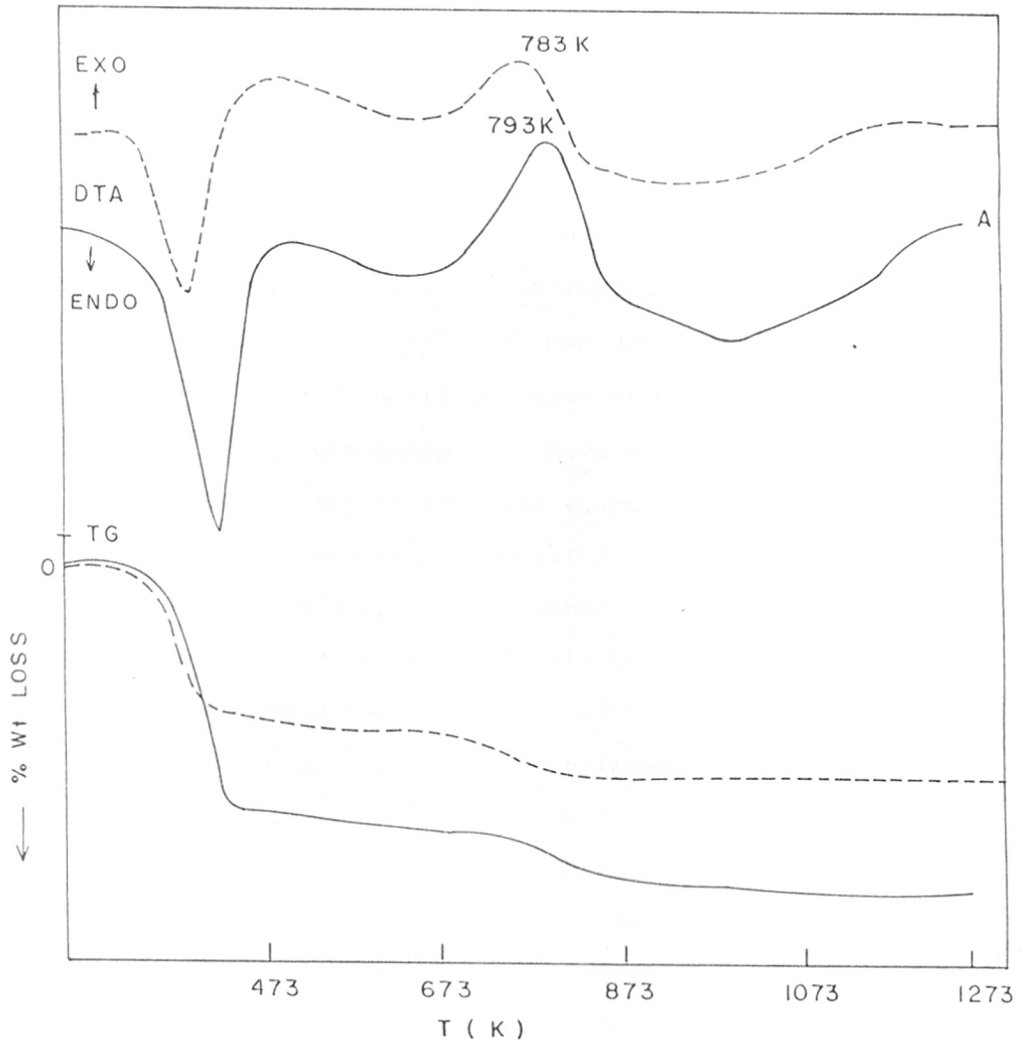

FIG. 5·5 : TG / DTA OF COKED $AlPO_4$-5 (—) AND SAPO-5 (--). IN O-XYLENE ISOMERISATION

5.3 CATALYTIC CRACKING OF n-HEXANE

Cracking of hydrocarbons having higher molecular weight to produce lower molecular weight hydrocarbon is an important industrial process which permits the conversion of heavy natural oils to lighter products, such as gasoline, increasing thereby the yield of motor fuels. Gasoline (boiling between 300-483 K and having a C_{11} to C_{13} range) comprises only of about 15-25% of natural petroleum. The straight run gasoline consists of normal and slightly branched paraffins, some naphthenes and a few aromatics and most of these components have low octane number.

Cracking of heavier petroleum fraction over selective catalyst enhances the yield of gasoline.The zeolite cracking catalysts have many advantages over conventional silica alumina amorphous catalysts. Zeolite based catalysts crack heavier fractions to give a better product distribution with less amount of coke and are more stable and resistant to nitrogenous and sulphur compounds. In the industrial catalytic cracking process, large number of side reactions occur and coupled with complexity of industrial gas oil feed, interpretation of the results is very difficult. Hence researchers have sought a pure reactant which could undergo typical cracking reaction in order to correlate the activity and the surface acidity. Therefore, n-hexane received considerable attention.

In recent years microporous modified aluminophosphates have opened up a new area of investigation for such reactions. It is because they represent a large group of zeolitelike materials

having novel crystallographic structures and varying pore sizes and pore volumes. This activity can be compared in terms of n-butane cracking rate constant K_a, which was reported by Lok et al. (22).

In this chapter, we report the influence of the reaction temeprature and surface acidity on the catalytic activity and product selectivity for n-hexane cracking over $AlPO_4$-5 and SAPO-5. The influence of metal substitution in $AlPO_4$-5 is also studied for this reaction.

5.3.1. Influence of temperature

The n-hexane cracking reaction was studied at atmospheric pressure and at 3.3 WHSV over a temperature range 573 K to 823 K for $AlPO_4$-5 and SAPO-5 catalysts, and at 723 K for MeAPO-5 catalyst . The data given in Table 5.9 and in Fig. 5.6 illustrate the influence of the reaction temperature on product distribution in the catalytic cracking of n-hexane over SAPO-5. It is observed that conversion of n-hexane gradually increases with increase in temperature and formation of C_3 and C_4 paraffins also increases simultaneously. This demonstrates that product behaviour is depen-dent on the temperature. At lower temperature the light products which can be formed by simple scission of n-hexane molecules is not detected. In conventional thermal cracking an abundance of C_1 and C_2 was observed and no saturated hydrocarbons such as propane and butane were formed (175). On the other hand, the product obtained from cracking of n-hexane over $AlPO_4$-5, SAPO-5 and MeAPO-5 contain large amount of C_3, C_4 and saturated hydroca-

Table 5.9

Influence of temperature on n-hexane conversion and product selectivity over SAPO-5 (IV)

WHSV = 3.3

Temperature	573	623	673	723	773	823
Conversion wt.%	6.5	7.8	10.20	12.50	14.25	15.60
Product selectivity	wt.%					
CH_4	0.0	0.0	0.05	0.09	0.20	0.35
C_2H_4	0.10	0.12	0.16	0.20	0.25	0.30
C_2H_6	0.10	0.10	0.11	0.12	0.20	0.60
C_3H_6 + C_3H_8	3.55	4.00	4.56	5.50	5.80	6.10
1-C_4H_{10}	1.20	1.50	2.20	2.80	3.00	3.10
n-C_4H_{10}	1.12	1.30	2.15	2.50	2.65	2.80
C_5H_{10}	0.30	0.35	0.42	1.10	1.30	1.50
C_5H_{12}	0.50	0.60	0.62	0.70	0.80	1.00
C+ aliphatics	0.83	0.90	1.10	1.30	1.38	1.50
n-C_6	90.85	89.60	87.30	85.00	83.32	82.01
Benzene	0.17	0.21	0.25	0.28	0.31	0.35
Toluene	0.01	0.01	0.02	0.02	0.03	0.03
C_9+ aromatics	0.10	0.11	0.14	0.15	0.20	0.22

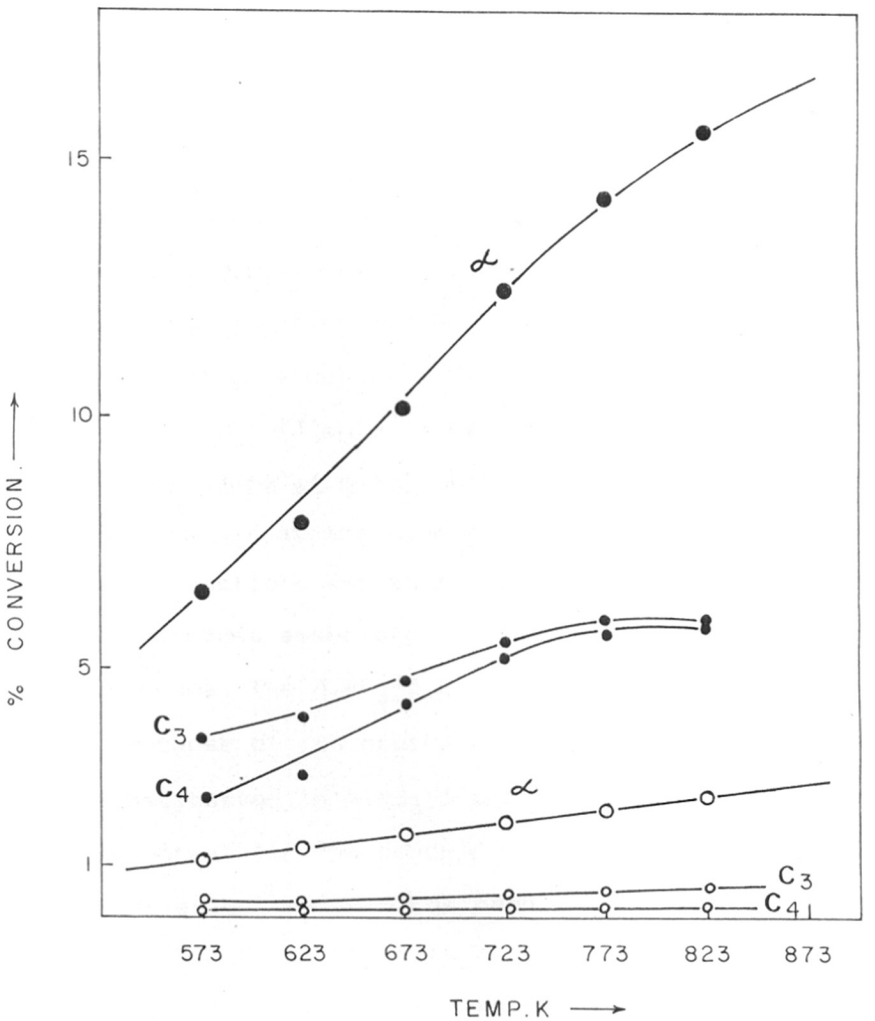

FIG. 5·6 - INFLUENCE OF TEMPERATURE ON PRODUCT DISTRIBUTION IN n – HEXANE CRACKING REACTION OVER $AlPO_4$ – 5 (o—o) AND SAPO – 5 (•—•)

rbons and traces of C_1 and C_2 at lower temperatures. The appearance of these products indicates that the reaction pathway in the cracking is different than the simple C-C bond scission reaction (175).

These new class of molecular sieves behave like zeolites but have lower catalytic activity due to their mild acidity. The apparent activation energies for $AlPO_4$-5 and SAPO-5 in n-hexane cracking reaction were calculated (Fig.5.7) and were found to be 5.65 KJ $mole^{-1}$ and 7.00 KJ $mole^{-1}$ respectively.

5.3.2. Influence of metal substitution in $AlPO_4$-5

It is well known that the hydrogen forms of zeolites promote acid catalysed reactions and that the acid activity generally originates with protons associated with the negatively charged aluminium tetrahedra. The $AlPO_4$-5 molecular sieve is catalytically inactive because of its neutral framework. It is reported that metal substitution in $AlPO_4$-5 creates Brönsted acid sites which are essential for the cracking reaction. The catalytic activity of series of MeAPO-5 has been determined for cracking of n-hexane at 723 K and the data is illustrated in the Table 5.10. The conversion of n-hexane increases depending upon the activity of substituted metal. For example, the n-hexane cracking activity of $MgAlPO_4$-5 is much higher than SAPO-5 and $AlPO_4$-5.

5.3.3. n-Hexane cracking reaction mechanism

Cracking reactions are mainly C-C bond ruptures, which are endothermic and hence favoured at high temperatures. Two types of reactions have been proposed (177) for the cracking of paraffins :

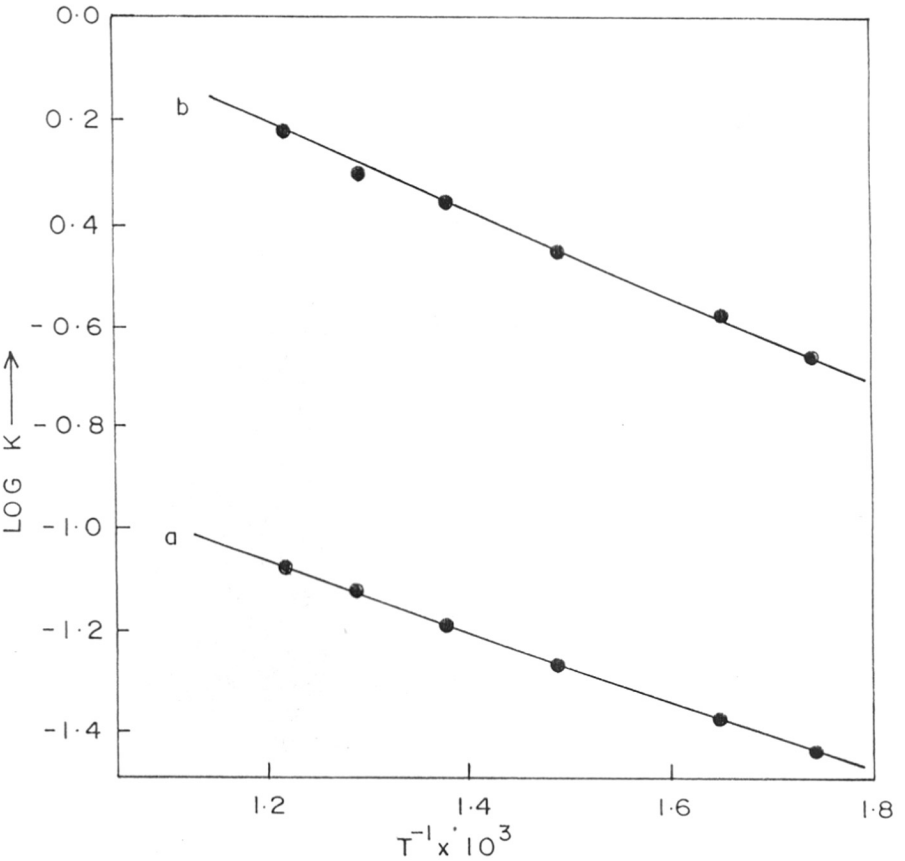

FIG. 5·7 : TEMPERATURE DEPENDANCE OF CRACKING ACTIVITY OF - a) $AlPO_4$-5, b) SAPO-5 (IV)

Table 5.10

Product distribution of n-hexane cracking reaction over MeAlPO-5 at 723 K temperature and WHSV = 3.3

Catalyst	MgAlPO-5	ZnAlPO-5	CoAlPO-5	FeAlPO-5	SAPO-5	$AlPO_4$-5
Conversion wt.%	44.00	35.30	34.00	14.00	26.52	2.0
Product distribution wt.%						
CH_4	0.50	0.30	0.21	0.12	0.09	0.01
C_2H_4	0.80	0.62	0.50	0.28	0.20	0.05
C_2H_6	1.30	0.40	0.40	0.15	0.12	0.04
C_3H_6 + C_3H_8	17.20	14.80	12.90	5.10	13.50	0.20
1-C_4H_{10}	10.50	9.80	9.33	2.90	8.10	0.13
n-C_4H_{10}	7.00	6.80	7.40	2.20	2.50	0.15
C_5H_{10}	5.40	4.10	3.90	1.25	1.10	0.02
C_5H_{12}	1.80	1.60	1.35	0.80	0.70	0.08
C_6+ aliphatics	1.00	0.10	0.08	0.70	0.60	1.50
n-C_6	54.41	62.86	64.30	83.70	74.23	95.00
Benzene	0.50	0.21	0.16	0.30	0.28	0.23
Toluene	0.20	0.02	0.03	0.01	0.01	0.01
C_9 aromatics	0.10	0.01	0.02	0.01	0.01	0.0

(1) Non-catalytic or thermal cracking, and

(2) Catalytic cracking

Non-catalytic thermal cracking proceeds by Rice-Kossiakoff (177) radical chain decomposition reaction. The first step is abstraction of hydrogen from the substrate by a small radical species formed during the initial period. Thus the mixture of alkyl radical formed may undergo β-scission to produce olefins and smaller radical. The latter may undergo further β-scission or may abstract hydrogen from substrate forming a paraffin and new long chain radical. The chain decomposition of n-hexane proceeds through formation of free radicals which decompose according to following reaction (177) :

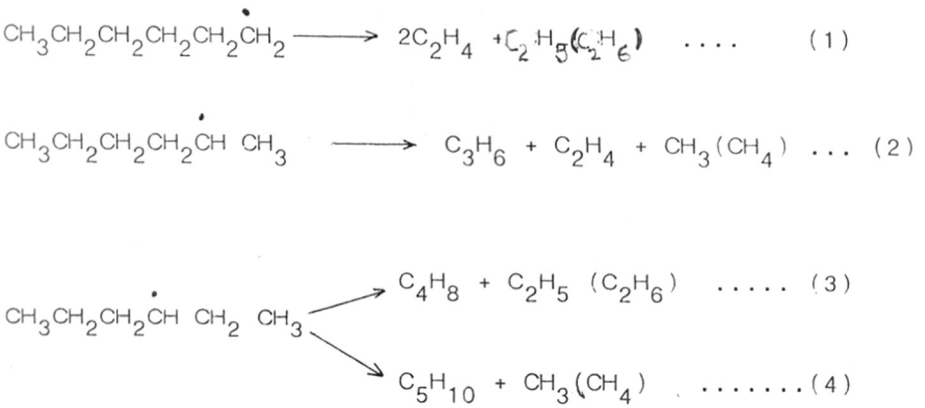

It is well known by now that cracking catalyst are acids and catalytic activity is related to the acidity of the catalyst. Carbonium ion reactions are known to occur in the presence of acids (176, 178). It has been proposed that the hydrocarbon reactions catalysed by the cracking catalyst are carbonium ion reacitons (178). The formation of carbonium ion from unsaturated hydrocarbon may occur by addition of proton to unsaturated molecule to form carbonium ion or saturates loose a hydride ion to form a carbonium ion. In alkane cracking hydrogen is first removed from the moelcule leaving a hydrogen deficient entity (179, 180), which then cracks at carbon-carbon bond, β, to the hydrogen deficient atom, producing an α-olefin and new hydrogen difficient entity. The latter repeats the process until a small uncracked group is left which then becomes saturated by acquisition of hydrogen. The product distribution with respect to carbon number and paraffin to olefin isomers is thereby greatly altered from that of thermal cracking

$$C_6H_{14} + \overset{+}{H} \longrightarrow C_6\overset{+}{H}_{13} + H_2 \qquad \text{.....} \quad (5)$$

$$CH_3\text{-}\overset{+}{C}H\text{-}CH_2\text{-}CH_2\text{-}CH_2\text{-}CH_3 \rightarrow CH_3\text{-}CH{=}CH_2 + \overset{+}{C}H_2\text{-}CH_2\text{-}CH_3$$

The cracking activity of acid zeolite has also been interpreted by a dynamic theory. It is assumed that hexane molecules are sufficiently polarized by surface field to impart themselves

ionic characteristics. For simplicity, representing surface field by a dipole, the reaction mechanism may be written as (140, 144)

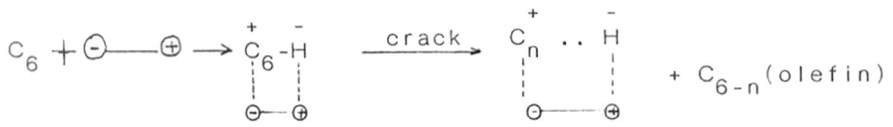

$$\longrightarrow C_6 + C_{6-n}\ (olefin) + \ominus\!\!-\!\!-\!\!\oplus$$

where C_6 and C_6^+ denote n-hexane and carbonium ion and C_n, C_{6-n} refer to olefins respectively.

From the present study it is observed that

(1) The reaction product is a complex mixture of olefins, paraffins of carbon number greater than three and negligible amounts of C_1 and C_2 products formed at low temperature.

(2) The cracking activity increases as the metal cation substitution takes place in $AlPO_4$-5 framework.

These obserations lead us to conclude that n-hexane cracking reaction over $AlPO_4$-5, SAPO-5 and MeAPO-5 proceeds via carbonium ion mechanism.

5.4 ALKYLATION OF TOLUENE WITH METHANOL OVER $AlPO_4$-5 AND MeA PO-5

This reaction provides yet another route for p-xylene production. In the alkylation of toluene by methanol, the first step in the reaction involves methyl substitution to form the kinetically favoured ortho- and para-xylene. Subsequent methylation steps yield multi-substituted benzenes. In addition, isomerization and transalkylation reactions are superimposed on the primary alkylation step. Since alkylation of aromatics needs only medium acid sites (172) $AlPO_4$-5 with no acidity, SAPO-5 and MeA PO-5 having mild acidity were therefore tested for the activity and selectivity to p-xylene with respect to this reaction. High selectivity to para-xylene using this relatively simple and practical process has been claimed in several publictions (181-184). Early work with zeolite type X and Y revealed that in the acidic form they are effective catalysts in the alkylation of benzene and toluene with methanol (185). With these large pore zeolites, molecular sieving effects on product distribution were attributed to diference in zeolite acidty and structures (186). Kaeding et al (182) have shown that over fresh, unmodified ZSM-5 and ZSM-11 catalysts, the xylene isomers produced are essentially at thermodynamic equilibrium with no evidence for shape selectivity favouring the para-isomer. However, when these zeolites were used under conditions where coke deposition became significant, a large rise in para-isomer was observed presumably resulting from a decreease of the effective pore size. It is important to note that improvements in selectivity obtained by

chemical modifications or by coking is accompanied by a substantial reduction in the catalytic activity.

5.4.1. Toluene methylation over MeAPO-5

A mole ratio of 5:1 (toluene:methanol) was chosen for the reactant mixture in order to minimise contribution from methanol reaction towards products. Also it was expected that larger amount of toluene would prolong stable activity of the catalyst so that the observed changes in product distribution could be attributed to changes in experimental parameters such as feed rate and temperature. The amount of gaseous products formed during reaction were in traces. For comparative study, few runs were carried out over selected catalysts . $AlPO_4$-5 molecular sieve with neutral framework show very poor toluene conversion (0.90 %) while SAPO-5 and MeAPO-5 (i.e. CoAlPO-5 and MgAlPO-5) show comparatively higher toluene conversion at 723 K (Table 5.11). Selectivity to para-xylene is slightly above thermodynamic equilibrium (22.6% para-xylene) due to the product selectivity effect. The formation and diffusion of the smaller para-xylene isomer is favoured by the restricted pore-size. Significantly, the shape selectivity required for para-xylene production is missing in the large pore SAPO-5 and MeAPO-5 catalysts.

5.4.2. Influence of time-on-stream

Influence of time-on-stream on product distribution in alkylation reaction over MgAlPO-5 is shown in Table 5.12. It is observed that as time on stream increases, conversion decreases and para-selectivity increases slightly due to coking effect.

Table 5.11 : Toluene methylation over MeAPO-5

(toluene/methanol mole ratio = 5:1) at 723 K

Catalyst	SAPO-5	CoAlPO-5	MgAlPO-5
WHSV hr^{-1} [a]	3.68	3.68	3.68
Conv.wt.% of toluene	12.24	6.20	17.60
Product dist.[b] wt.% (organic liquid)			
Aliphatics	0.013	0.01	0.01
Benzene	5.16	1.25	6.34
Toluene	85.17	91.05	79.99
Ethyl Benzene	-	-	-
p-Xylene	2.21	1.20	2.87
m-Xylene	4.52	1.70	6.10
o-Xylene	2.13	1.10	2.90
TMB	0.66	0.64	0.98
Xyl.comp.(%)			
Para	24.94	30.00	24.20
Meta	51.02	42.50	51.35
Ortho	24.04	27.50	24.45

a = Weight of (toluene + methanol) perhour per gm. catalyst.

b = Traces of gas were formed.

Table 5.12 : Influence of time on stream for toluene methylation over MgAlPO-5

Reaction Temp. 723 K. Toluene/Methanol = 5:1

WHSV	3.68			
Time on stream (hrs)	I	II	III	IV
Toluene conv.	17.60	15.70	12.20	9.70
Product dist.wt.% organic liquid				
Aliphatics	-	0.13	0.13	0.02
Benzene	7.0	6.34	5.16	4.40
Toluene	78.00	81.90	85.20	87.70
p-Xylene	2.90	2.64	2.21	1.9
m-Xylene	6.10	5.60	4.52	3.72
o-Xylene	2.90	2.60	2.13	1.80
TMB	0.98	0.84	0.66	0.44
Xyl.comp. %				
Para	24.20	24.50	24.94	25.71
Meta	51.35	51.67	51.02	50.34
Ortho	24.45	23.84	24.04	23.95
% Xylene selectivity	53.03	48.20	34.62	33.20
% TMB formed	7.74	6.64	5.21	3.51

This has been attributed to reduction in effective channel size due to internal coking (182) or partial blocking of the channel opening by external coke deposit (187) which reduces the outward diffusion rate of the o- and m-xylene resulting into further isomerization to p-xylene and thus increases selectivity to p-xylene. Product selectivity effect is thus enhanced by coking.

5.4.3. Reaction mechanism

The mechanism of alkylation of toluene is via electrophilic substitution; besides the xylene isomer, polyalkylated products are also formed. Isomerisation and transalkylation also take place in addition to the above reactions. Also, the conversion of methanol itself has to be considered when it is in large exess in the reactants.

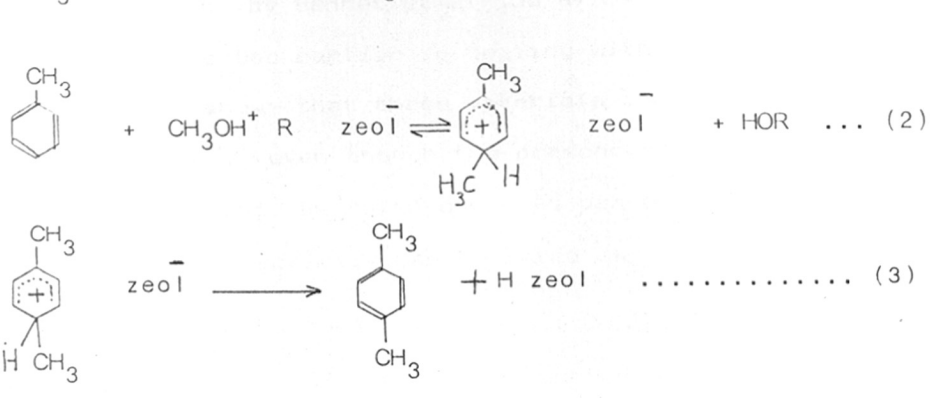

R = H or CH_3

(Scheme for alkylation (Ref.182)).

Metal incorporated $AlPO_4$-5 may be considered as (i) pure MeAPO-5 phase having isomorphous substitution of Me^{2+} and Me^{3+} for Al, or Me^{4+} for P. gives rise to neutral or anionic framework and associated Brönsted acid sites, (ii) $AlPO_4$-5 microporous matrix incorporated with metal hydroxyl species in the pores, or (iii) partly metal substituted $AlPO_4$-5 with rest of the metal in charge compensating sites.

Pyke et al.(23) have presented experimental evidence viz. ion exchange capacity, chemical stoichiometry, catalytic activity and XRD to show that these metals can be really incorporated in $AlPO_4$-5 lattice. There are many studies elucidating the true isomorphous substitutions, for example, those of Bond et al.(40) for Zn, Hangmuir et al (142) for Fe^{3+} and single crystal studies on $CoAlPO_4$-5 by Bennet et al.(36 a) may be sighted. Our own results presented earlier in dealing with physicochemical characterization show that these materials are indeed substituted in the framework, even though the presence of some extra framework impurities cannot be ruled out. As per o-xylene isomerisation is considered the activity can be rated as

$AlPO_4$-5 << FeAlPO-5 << SAPO-5 < CoAlPO-5 << ZnAlPO-5 < MgAlPO-5

This reaction is influenced by Brönsted acidity, which itself is dependent on average electronegativity of constituent T atoms in the framework.

This novel concept of electronegativity was proposed by Sanderson (145) who defined the average electronegativity of a

compound 'S' made up of 'i' atoms with S_i electronegativity as

$$\bar{S} = \left[\prod S_i^{n_i}\right]^{1/\sum n_i}$$

where n_i is the stoichiometric coefficient of the i^{th} atom participating in the compound. This concept of intermediate electronegativity has been successfully correlated with some surface properties of zeolites and aluminophosphates, namely their catalytic activity (23, 188, 189). Such correlations can be explained by taking into account the fact that the protonic activity (activity of Brönsted sites) of zeolites and molecular sieve aluminophosphates, which is mostly responsible for their catalytic activity is related to the partial charge developed on the proton. This charge is defined as (145)

$$q^i = (\bar{S} - S_i) \quad (2.08\ S_i^{0.5})^{-1}$$

However, for such calculations, n_i, the fraction of the element in framework should be exactly known. It is not possible to determine precisely this fraction in $AlPO_4$-5 and modified $AlPO_4$-5 materials. Still such correlations can be made by considering the relative electronegativities calculated from electrostatic forces (190). The values of relative electronegativities for Al, Si, O, P, Mg, Zn, Co and Fe are 1.47,, 1.74, 3.5, 2.06, 1.23, 1.66, 1.7 and 1.64 respectively. The negative charge on Al^{3+} in zeolite framework can be dissipated equally over $4Si^{4+}$ ions of greater electronegativity (Si-Al) = (1.74-1.47)=0.27). However, in SAPO-5, in which P is replaced by Si, negative charge on Si^{4+} centre should be dissipated over 4 surrounding Al^{3+}

centres of lower electronegativity (Al-Si =(1.47-1.74)= -0.27) which is less favourable. Therefore, acid strength of SAPO-5 is expected to be less than that of zeolites. Similarly, substitution of Fe^{3+} for P (Fe-Al =(1.64-1.74)= 0.17) should be less favourable than substitution of Si for P (Si-Al = + 0.27).

In the case of Mg, Zn and Co the substitution is thought to be at Al sites. Therefore, change in average electronegativity becomes 0.83, 0.40 and 0.36 respectively. Therefore, the order of electronegativity difference (which is a measure of favourable situation) is Mg > Zn > Co > Si > Fe. Our results of IR, TPD and catalytic activity for o-xylene isomerization, toluene alkylation and n-hexane cracking are in agreement with this expectations.

REFERENCES

1. D.W.Breck,"Zeolite Molecular Sieves", Wiley, New York,1974.
2. R. M. Milton, U.S. Pat., 2,882,243 and U.S.Pat. 2,882,244 (1959)
3. D.W.Breck, U.S.Pat., 3,130,007 (1964).
4. L.B.Sand, U.S.Pat., 3,436,174 (1969).
5. R.L.Wadlinger, G.T.Kerr and E.J. Rosinski, U.S.Pat., 3,308,069 (1967).
6. R.J. Argauer and G.R.Landolt, U.S.Pat.,3,702,886 (1972).
7. R.W.Grose and E.M.Flanigen, U.S. Pat., 4,061,724 (1977).
8. Eur.Pat. (Union Carbide Corpn.) Appl.No.0043562 (1981).
9. S.T.Wilson, B.M.Lok & E.M.Flanigen, U.S.Pat.,4,310,440 (1982).
10. S.T.Wilson,B.M.Lok,C.A. Messina, T.R.Cannon and E.M. Flanigen, J.Amer.Chem.Soc., 104, 1146, 1982.
11. B.M.Lok, C.A.Messina, R.L. Patton, R.T. Gajek, T.R. Cannon and E. M.Flanigen, U.S. Pat., 4,440,871 (1984).
12. C.A. Messina, B.M. Lok and E.M.Flanigen, U. S.Pat.,4,544,143 (1985).
13. S.T.Wilson and E.M.Flanigen, Eur.Pat., 132, 708 (1985), U.S. Pat., 4,567,029 (1986).
14. E.M. Flanigen, B.M. Lok, R.L. Patton and S. T. Wilson, Pure and Applied Chem., 58, 1351, 1986.
15. S.T. Wilson, B.M.Lok, C.A.Messina, T.R. Cannon and E.M. Flanigen, A.C.S. Symp. Ser., 218, 79, 1983.
16. J.M.Bennett, J.P.Cohen, E.M. Flanigen, J.J. Pluth and J.V. Smith, A.C.S. Symp. Ser., 218, 109, 1983.
17. R. D. Shannon, Acta.Cryst., 32A, 751, 1976.
18. A. Dietzel, H.J.Poegel, Die Naturwissonschaffen, 40,604, 1953.
19. R. Kniep, D. Mootz, Acta Cryst., B29, 2292, 1973.
20. R. Kniep, D.Mootz, A. Vegas, Acta Cryst., B-33, 263, 1977.
21. S.T. Wilson,B.M. Lok, C.A. Messina and E.M. Flanigen, Proc.of 6th Internatl. Zeolite Conf., 1984, p.97.
22. B. M. Lok,, C.A.Messina, R.L. Patton, R.T. Gajek, T.R. Cannon and E.M.Flanigen, J.Amer.Chem.Soc., 106, 6092, 1984.
23. D.R.Pyke, P.Whitney and H.Houghton, Appl.Cat., 18,173,1985.

24. K.R.Kamble,S.B.Kulkarni, P.N.Joshi, S.G.Hegde and P.Ratnasamy, Proc. Adv.Cat. and Cat.React.Eng. Ed. P. Kantarao, p. 129, 1986.

25. B.M.Lok, B.K.Marcus and E.M.Flanigen, Eur.Pat. Appl. E.P. 161,488; 161,489; 161,490; (1985). B.M. Lok, L.D.Vail and E.M.Flanigen, Eur.Pat.Appl., E.P. 158,976 (1985); 158,977; 158,348; 158,349 and 159,624 (1985).

26. B.M. Lok, M.T. Marcus, B.Kristofforse and E.M.Flanigen, U.S. Pat. Appl., 604,155 (1984) and U.S.Pat.Appl., 600, 170.

27. B.M. Lok, B.K. Marcus, L.D. Vail, E.M. Flanigen, R. L. Patton and S.T. Wilson, Eur.Pat.Appl. E.P. 159,624 (1985).

28. B.M. Lok, B.K.Marcus and E.M. Flanigen, U.S.Pat.,4,500,651 (1985).

29. E.M. Flanigen, B.M. Lok, R.L. Patton and S.T.Wilson, Stud. Surf.Sci. Catal., 28, 103, 1986.

30. B.M. Lok, B.K.Marcus and E.M.Flanigen, Eur.Pat. Appl. E.P. 158, 350 (1985).

31. L. M. Parker, D.M.Bibby and J.E. Patterson, Zeolites, 4, 168, 1984.

32. K.J.Chao, T.C. Tasi, Chen and I.J.Wang, Chem.Soc. Faraday Trans. I, 77, 547, 1981.

33. E. Denpsey, G.H. Kuhl, & D.H.J. Olson, Phys.Chem., 387,1969.

34. J.V.Smith, Acta Cryst., 15, 835, 1962.

35. J.B. Parise, J.Chem.Soc.Commun. 605, 1985.

36. P.R.Rudolf, C.S. Molina, & A.Clearfield, J.Phy.Chem., 90, 6122, 1986.

36a. J.M.Bennet and B.K. Marcus, "Innovation in Zeolite Material Sci., 37, 269, 1988.

37. E.M.Flanigen, H.Khatami,H.A.Symanski, "Molecular Sieve Zeolites" Adv.Chem.Ser. 101, Amer.Chem.Soc. Washington D.C. p. 201, 1971.

37a Lohodny-Sorac D. and J.L.White, J.Phy.Chem., 75, 1408, 1971.

38. J.R.Whyte and R.A.Dalla Betta, Cat.Rev.Sci.Eng. 24(4), 580 1982.

39. J.W.Ward, "Zeolite Chemistry and Catalysis", Chapter 2, ed. J.A.Rabo, A.C.S. Monograph, 171, 1976.

40. G.C.Bond, M .C.Gelsthorpe, S.W. Kenneth, Sing and C.S. Theocharis, J.Chem.Commun, 1056, 1985.

41. S. G. Hegde, L.M. Kustov, P.Ratnasamy and V.B. Kazansky, Zeolites, 8, 137, 1988.

42. I.P.Aplpleyard, R.K.Harris and F.R.Fitch, Chem.Letters, 1747, 1985.

43. C.S.Blackwell and R.L.Patton, J.Phy.Chem., 88, 6135, 1984.

44. D.Muller, E.Jahn,B.Fahlke, G.Ladnig and U.Hanbenreisser, Zeolites, 5, 1985.

45. W. Loewenstein, Amer. Mineral, 39, 92, 1954.

46. I.P. Appleyard, R.R.Harris & F.R.Fitch, Zeolites, 6, 428, 1986.

47. Ligia Siena de Saldarriaga, C. Saldarrage and M.C.Davis, J. Am.Chem.Soc., 109, 2686, 1987.

48. K.Tanabe, "Solid Acids and Bases", Chap.II,Acad.Press, New York, p.5.

49. P.A.Jacobs, "Carboniogenic Activity of Zeolites" Chapter II, Elsevier Sci.Publishing Co., Amsterdam, Oxford, New York, p. 33, 168, 1977.

50. J.R.Anderson, F.K.Mole, R.A. Rajadhyaksha and J.V.Sanders, J.Cat., 58, 114, 1979.

51. P.A. Jacobs, J.B.Uytterhoeven, M.Styeyns, G. Froment and J. Weitkamp, Proc. 5th Internal. Conf. on Zeolites, Napals, Italy, Heyden & Sons, London, 604, 1980.

52. N.Y.Topsoe, R. Pedersen and E.G. Derouane, J. Cat., 70, 41 (1981).

53. R.B. Borade, S.G. Hegde, S.B.Kulkarni & P.Ratnasamy, Appl. Cat., 13, 27, 1984.

54. Xu Qinhua, Yan Azhan, Bao shulin and Xu Kaijun, Proc. 7th Internal. Zeolite Conf., p.835, 1986.

55. V.R. Choudhary and D.B.Akolekar, J.Cat., 103, 115, 1987.

56. E.G.Derouane, S.Detremmerie, Z.Gabelica and N. Blom, Appl. Cat., 1, 20, 1981.
57. R. M. Barrer and D.A.Langloy, J.Chem. Soc., 3804, 3811, 1817, 1958.
58. I.G. Gal, O. Tankovic, S. Malcis, P. Raoovanov and M. Tadorovic, Trans. Faraday Soc., 67, 999, 1971.
59. E.H. Von, Broe Kavos, V. Ponee, Phy.Sur.Sci., 19, 351, 1985.
60. H. Bremer, W. Morke, R. Schodel, F. Vogt, Adv. in Chem. Ser. 121, 249 (1973).
61. P.B. Venuto and P. S. Landis, Adv. in Cat., 18, 269, 1968.
62. D. H. Olson, G.T. Kokatailo, S.L. Lowton and W.M.Meiser J. Phys. Chem., 85, 2238, 1981.
63. S. Brunauer, "The Adsorption of Gases and Vapours" Oxford Univ. Press, London, P.150, 1944.
64. E.G. Derouane and Z. Gabelica, J. Cat., 65, 486, 1980.
65. J. Valyon, J. Michalyh, H.K. Beyer and P. A. Jacobs, Workshop on Adsorption, Berlin DDR, P. 134, 1979.
66. Z. Gabelica, J. P. Gilson and E.G. Derouane, Proc. of 2nd Erup. Symp. on Thermal Catalysis, Ed. David Dollimone, Heyden, 434, 1981.
67. R. M. Barrer and R. M. Gibbson, Trans. Faraday Soc., 59, 2569, 1963.
68. R. M. Barrer, Pure & Appl. Chem., 52, 2143, 1980.
69. H. Stach, H. Thomm, K. Fiedler, B. Grauert, W. Wieker, E. Jahn and G. Ohlmann, Prod. of 7th Internal. Zeolite Conf. Ed. Y. Murakami, P. 539, 1986.
70. Genadi, Dworezkov, G. Rumplmayer, H. Mayer and J. A. Lercher "Adsorption and Catalysis on Oxide Surfaces", Ed. G.C.Bond, 1985.
71. E. M. Flanigen and H. Khatami, Molecular Sieves Zeollites, A.C.S., 101, 201, 1971.
72. T.Sato, Z. Anorg. allg. Chem., 391, 167, 1972.
73. A.Broorama, J.Thermal Analysis, 13, 341,1978.

74. B.C. Lippens and J.J. Steggerda, "Physical, Chemical Aspects of Adsorbents and Catalysis", Ed.B.G. Linsen, Acad. Press, London and New York, P. 174, 1970.

75. V. Meenakumari,Project Report, Univ. of Cochin, 1984.

76. R. M. Barrer, "Hydrothermal Synthesis of Zeolites", Acad. Press, London, 1982.

77. E.A. Paukshtis, P. I. Saltanov, E. N. Yurchenko and Kveta Jiratova, Coll. Czecho. Chem. Commun., 47, 1982.

78. H. Knoziger, P. Ratnasamy, Cat. Rev., 17, 31 (1978).

79. V. J. Frilette, P.B. Weisz and R.L. Golden, J. Cat., 1, 301, 1962. British Pat., 886, 716 (1962).

80. P. B. Weisz, Pure and Appl. Chem., 52, 2091, 1980.

81. E. G. Derouane, "Catalysis by Zeolite", Ed. B. Imelik, 1980.

82. C. Naccache & Y.Taarit, Pure & Appl. Chem., 52, 2175, 1980

83. L. B. Young, U.S. Pat., 3962, 364, assigned to Mobil Oil Corpn., 1976.

84. S.A. Butter, U.S. Pat., 400, 7231, assigned to Mobil Oil Corpn., 1977, W. D. Haag, D. H. Olson, U.S. Pat., 3856871 assigned to Mobil Oil Corpn., 1974; R.A. Morrison, U. S. Pat., 3856872 assigned to Mobil Oil Corpn., 1974.

85. N. Y. Chen, W.W. Kaeding and F.G. Dwyer, J.Amer.Chem.Soc., 101, 6783, 1979.

86. R. B. Borade, Ph.D. Thesis, Poona Univ., India, 1983.

87. R. J. Pellet, G.N. Long and J.A. Rabo, Proc. 7th Internatl. Zeolaite Conf., P. 843, 1986.

88. B. Lok, M.Tak, Marcus, Bonita, Kristoffersen, E. M. Flannigen (Union Carbide Corpn.), U.S. Pat.Appl. 600, 179 (1984) and U.S. Pat. Appl. 604, 155 (1984).

89. Kaiser, W.C. Steven, Arabian J.Sci. Eng.10, 361, 1985.

90. R.Pellet, Gortsema, Frank, Peter, J. Springer, A.Roymond, R. Jule, A. Long, G. Norman (Union Carbide Corpn)., U.S. Pat. Appl., 683,241, 1984.

91. R.Pellet, et. al. U.S. Pat. Appl., 683, 942, 1984.

92. R.Pellet, et. al. U.S. Pat. Appl., 675, 279, 1984.

93. R.Pellet, et. al. U.S. Pat. Appl., 682, 946 (1984).
94. E.G.Derouane, V.Ballmay, N. Roland (Mobil Oil Corpn.) Eur. Pat. Appl. E.P. 146, 385 (1985).
95. E.G. Derouane, et. al., Eur.Pat.Appl. E.P. 146, 386 (1985).
96. E.G. Derouane, et. al., Eur.Pat.Appl. E.P. 146, 387 (1985).
97. E.G. Derouane, et. al., U.S. Pat., 4,647,442 (1987).
98. B.M.Lok, Tak, Marcus, U. Boni, Kristoffersen, E.M.Flanigen, (Union Carbide Corpn.), Eur.Pat. Appl. E.P. 161, 488 (1985).
99. B.M.Lok, et al., U.S. Pat. Appl. 604,155 (1984).
100. B.M.Lok, et. al., Eur.Pat. Appl., E. P. 121, 232 (1984).
101. B.M.Lok, et. al., Eur. Pat. Appl., E.P. 158, 975 (1985).
102. A. Culfaz and L.B. Sand, Adv. Chem.Ser., 121, 140, 1973.
103. N.J.Tapp, N.B.Milestone and D.M.Bibby, "Innovation in Zeolite Materials Science", Vol. 37, p. 393, 1988.
104. J.P. Pariente, J.A. Martens and P.A. Jacobs, Zeolites, 8, 46, 1988.
105. W.G.Young, H. Walter, Harling and Franks, S. Crosslay, J. Am.Chem. Soc., 58, 100, 1936.
106. a : M.J. Avarami, Chem.Phys., 9, 117, 1941.
b: B.V. Erofeev, C.R.Acad. Sc. USSR, 52, 511, 1946.
107. G.V. Tsitsishvili, Adv.Chem.Ser., 121, 291, 1973.
108. J.V.Smith, Adv. Chem.Ser., 101, 171, 1971.
109. E.M. Flanigen, H.Khatami and H.A. Szymonski, Adv. Chem. Ser., 101, 201, 1971.
110. S. Brunauer, P.H. Emmett and E. Teller, Amer. Chem.Soc., 60, 309, 1938.
111. L.M. Parker,D.M.Biby and J.E. Patterson, Zeolites, 4, 168, 1984.
112. Hong-Xin Li, J.A. Martins, P.A. Jacobs, et. al., "Innovation in Zeolite Material Science", Ed. P.J. Gribet, P. 75, 1987.
113. N.J. Tapp, N.B. Milestone and D.M. Biby, ibid, P. 393.
114. W.Ward, "Zeolite Chemistry and Catalysis", A.C.S. Ser., 171, Ed. J.R. Rabo.
115. U. Lohse, M. Noack and E. John, Adsorption Science and Technology, 3, 19, 1986.

116. A.W. Coats and P. J. Redfern, Nature, 201, 68, 1964.
117. G.O. Piloyan and O.'S. Novikova, Russ. J. Inorg.Chem., 12, 313, 1980.
118. H.E. Kissinger, Anal.Chem., 19, 1702, 1957.
119. D. Kadle, Czech. Chem.Commn, 36, 2415, 1971.
120. R.L. Meville, J. Coll. Inter.Sci., 41, 371, 1972.
121. V.R.Choudhary, D.B.Akolekar and S.D.Sansare, Materials Chemistry and Physics, 18, 245, 1987.
122. S. J. Greg and K.S.W. Sing,"Adsorption, Surface area and Porosity", Acad. Press, London, 1967.
123. M.M.Dubinin, Bull. Acad.Sci., U.S.S.R., 23, 958, 1974.
124. R.M. Barrer,Quart. Rev. London, 3, 293, 1949.
125. R.M. Barrer, S. Wasilewski, Trans. Far. Soc., 57, 1153, 1961.
126. J. Hopper, Ph.D. Thesis, Univ. Microfilms Inc., Ann. Arbur. Michigan, P. 335, 1969.
127. M.M.Dubinin, Zhukovskaya and K.O. Murdama, Bull. Acad. Sci. U.S.S.R., 708, 896 (1962).
128. D.L. Paterson, F. Holfforich and G.C. Blytas, J. Phys. Chem. Solids, 26, 835, 1955.
129. A.V. Kiselev, "Molecular Sieve Zeolites II", Adv.Chem.Ser., 102, 37, 1971.
130. H. Thamm, H. Stach,E. Jahn and B. Fahlke, Adsorption Sci. and Technology, 3, 217, 1986.
131. W. Schirmer, H. Thamm, H. Stach and U.Lohse, "The Properties and Application of Zeolites", the Chemical Society London, Special Publication No. 33, P. 204.
132. I.V. Mishin, G.A. Piloyan, and G.Klychko and A.M. Rubinstein Bull. Acad. Sci. USSR, 22, 1298, 1301, 1973.
133. N. Y. Chen, J. Phys. Chem., 80, 60, 1976.
134. T.C. Vaimakis, P.J. Pomonis and A.T. Sloukos, React. Kinst. Catal. Lett., 37, 169, 1988.
a : W. Pitz, C Reuker and E. Than, Preprints of Workshop III Adsorption in Microporous Adsorbents, Vol.1, P.95, 1987.

b : P. A.Jacobs, E.G. Derouane and P. J. Weitkamp, Chem. Soc. Comm., 591 (1981).

135. P.G. Rouxhet and R.E. Sempels, J.Chem.Soc. Farad. Trans.I, 1, 70, 2021, 1971.
136. L. H. Little, "Infrared Spectra of Adsorbed Species", Acad. Press, London (1966), 195.
137. R. Szostak, T.L. Thomas, J. Cat., 101, 549, 1986.
138. L. J. Balani, "Infrared Spectra of Complex Molecule"
139. E. Brunner, H. Ernst, D.Freude, M.Hunger and Pfeifer, P.J.Grobet, et al. (edts.) "Innovation in Zeolite Material Science", Vol. 37, P.155, 1988.
140. S.P. Zhdavov, L.S.Kosheleva and T.I. Titova, Langmuir, 3, 960, 1987.
141. J.A. Martens, M. Martenes, P.J. Grobet, P.A. Jacobs, P. J. Grobet, et al. (editors), "Innovation in Zeolite Materials Science", Vol. 37, 97 (1988).
142. H.X.Li, J.A. Martens, P.A. Jacobs, et al., ibid, P.75.
143. J.B. Moffat, Catl.Rev. Sci. Eng., 18, 199, 1978.
144. J.Sauer and W. Schirmer, P.J. Grobet et. al. (editors), "Innovation in Zeolite Material Science", Vol.37, 323, 1988.
145. R. T. Sanderson, "Chemical Bonds and Bond Energy", Acad. Press, New York, 1960.
146. A.Bielanski, J.M. Borak, et.al., Bull. Acad. Pol. Sci., 23, 455, 1975.
147. W. L. James, M.N. Brennan, Eur.Pat., 0141662, 1984.
148. O.V. Kikhtyanin, V.M. Mastikhin and K.G. Ione, Applied Cat., 42, 1, 1988.
149. R.J.Cvetanovic and Y. Arrenomiya, Adv. Cat., 17, 103, 1967.
150. R.J.Gorte, J.Catal., 75, 164, 1982.
151. M. Alnot and A. Cassato, Surf.Sci., 112, 325, 1981.
152. J. Janchen, S.G. Hegade and H. Stach, Preprints of Workshop III Adsorption in Microporous Adsorbents, Vol.1, 103, 1987.
153. V. P. Shiralkar, Ph.D. Thesis, Poona Univ., India, 1980.
154. J.B Perri, J. Phy. Chem., 70, 3166, 1966.

155. G. Wendt, Z. Chem., 17, 118, 1977.
156. K. Thomke, J. Cat., 44, 339, 1976.
157. R. Bour, K. Thomke and H. Nollev, Proc. 8th Internatl. Congr. Catal. Berlin, 3, 439, 1986.
158. H. Itoh, A. Tada and K. Tanabe, Chem. Lett., 1567, 1981.
159. I.P. Kolenko and V.I. Korenskii, Izv. Akad. Nauk Ser. Khim, 7, 1460, 1979.
160. D. J. Collms, K. J. Mulrooney, K.J., R.J. Medina, J. Cat., 75, 291, 1982.
161. A. Castrin, et. al., Diss. Abst. Int., 8, 2723 B, 1988.
162. J.W. Ward, J. Catal., 38, 351, 1975.
163. S. Vishnoi, P. Ratnasamy, Proc. 4th Natl. Symp. on Catal., Hyderabad, India, P. 35, 1978.
164. G.P. Babu, S. G. Hegde, S.B.Kulkarni and P. Ratnasamy, J. Cat., 81, 471, 1983.
165. A. Cortis and A. Corma, J.Cat., 51, 338, 1978.
166. J.W.Ward and R.C. Hanford, J.Cat., 13, 154, 1969.
167. S.L. Meisel, J.P.Mcclough, C.H.Lechthaker and P.B. Weisz, Leo Friend Symp. A.C.S. Chicago,Aug. 30, 1977.
168. S.M. Csicsery, and D.A. Hickson, J.Cat., 386, 1970.
169. J. Wei, J.Cat., 76, 433, 1982.
Ibid, 1, 526, 1962.
170. E.M.Flanigen, R.L. Patton and S.T. Wilson, "Innovation in Zeolite Materials Science", P.J. Grobet (editors), Vol. 37, P. 13, 1988.
171. V.S. Nayak and V.R. Chowdhary, Appl. Cat., 4, 333, 1982.
172. P.A. Jacobs, "Carboniogenic Activity of Zeolites", Elsevier Sci. Publishing Co. Amsterdam, Oxford.
173. A. Voorhies, P. A.Bryant Jr., AIChE J., 14, 852, 1968.
174. V.W. Weekman,Jr., D.M.Nace, AIChE, J., 16, 397, 1970.
175. Y. Ozava, K. Bischoff, Ind.Eng.Chem.Pro. Disc. Dev., 7, 67, 1968.
176. J.B Peri, Disc. Faraday Soc.,52, 55, 1971.
177. A. Kossiakoff and F.O. Rice, J.Am.Chem. Soc., 65, 590,1943.

178. B.S.Greensfolder,H.H.Voge and G.M.Good, Ind.Eng.Chem., 41, 2573, 1949.
179. H. Heinemann, Cat. Rev., 15, 53, 1977.
180. F.C. Whitmanes, J.Am. Chem.Soc., 54, 3274, 1932.
181. W.W.Kaeding, U.S. Pat., 4,029,716 assigned to Mobil Oil Corpn.(1977), W.W.Kaeding and L.B. Young, U.S. Pat. 3,965,208, 1976.
182. W.W.Kaeding, C, Chu, L.B. Young, B. Wanstein and S.A. Butter, J. Cat., 67, 159, 1981.
183. L.B. Young, S.A. Butter and W.W. Kaeding, J. Cat., 76, 418 , 1982.
184. M. Derewinski, H. J. Haber, J.Ptaszynski, V.P.Shiralkar and S. Dzwgai in Structure and Reactivity of Modified Zeolites Edts. P.A. Jacobs, Elsevier Sci. Publishers Amsterdam, 1984.
185. P.B. Venuto, L.A. Hamilton, P.S. Landis and J.J.Wise, J. Cat., 4, 81, 1966.
186. T. Yashima, H.Ahmad, K. Yamazaki, M. Katsuta and N. Hora, J. Cat., 16, 273, 1970.
187. E.G. Derouane, "Molecular Shape Slective Catalysis in Zeolites selected topics of the Canadian Symp. on Catalysis, 1984.
188. W. J. Mortier, J. Cat., 55, 138, 1978.
189. S.Hocevar, B. Drzai, J. Cat., 73, 205, 1982.
190. A. Rocaov, J. Inorg. Nucl. Chem., 5, 264, 1958.
191. P. A. Jacobs, E.G. Derouane and P. Weitkamp, J. Chem. Soc. Chem. Communication, 591, 1981.

SUMMARY

Aluminophosphate molecular sieves ($AlPO_4$-n) are the first ever reported crystalline macroporous materials with framework structures composed of AlO_2^-, PO_2^+ tetrahedra. Most of the AlPOs have novel three dimensional structures. Only a few are structural -ly related to the aluminosilicate family of zeolites, like erionite-offretite ($AlPO_4$-17), sodalite ($AlPO_4$-20), faujasite ($AlPO_4$-37) and analcime type ($AlPO_4$-24). Further development in the chemistry of aluminophosphate molecular sieves has been directed towards their modifications by isomorphous substitution of Al or P in the $AlPO_4$ framework by other elements which are known to tolerate tetrahedral coordination in the oxide lattice. According to the Pauling's concept, the elements with ionic radii between 0.02 and 0.06 nm are reported to be potential candidates for incorporation into the aluminophosphate framework. However, many elements that have been substituted in the $AlPO_4$-n framework have minimum radius ratios that are not consistent with Pauling's concept. This has been explained on the basis that framework structures in molecular sieves are more flexible than dense phase oxides and that $AlPO_4$-n molecular sieves are prepared in mildly acidic conditions. Such substituted elements include Si, Mg, Zn, Co, Fe, Ni, Ti, V and their several combinations. The resulting new generation AlPO, SAPO and MAPO-n molecular sieves comprise nearly 200 compositions and cover a wide range of pore sizes e.g. very large pore (1.0 nm, VPI-5), large pore (0.8 nm,$AlPO_4$-5, 37, 46), medium pore (0.6 nm $AlPO_4$-11, 31, 41) and small pore (0.42 nm, $AlPO_4$-34, 17). These compositions, therefore, have a large

potential as selective adsorbents, catalysts and catalyst supports.

Among the various $AlPO_4$-n molecular sieves, the $AlPO_4$-5 which has a novel structure has been selected for the present study for the following reasons :

1. $AlPO_4$-5 can be synthesised in presence of a large number of organic templating agents. However, the mechanism and kinetic parameters for the nucleation and crystallization have not been reported so far.

2. The detailed information on the influence of the nature of the basic raw materials is limited.

3. $AlPO_4$-5 molecular sieve shows the least template-structure specificity. However, the nature of template species occluded in the pores is not yet fully understood.

4. The $AlPO_4$-5 is a large pore molecular sieve and has a micro-pore opening of about 0.8 nm which is interesting as a catalyst or catalyst support for hydrocarbon conversion reactions. Yet, detailed studies on such reactions are not reported in the open literature.

The present thesis reports the synthesis and characterization of pure and substituted aluminophosphates of the type $AlPO_4$-5, SAPO-5 and MeAPO-5 respectively. The feasibility of synthesis of these materials using triethylamine as an organic structure directing (templating) agent has been examined in depth. The influence of the basic raw materials on the kinetics of nucleation and crystallization of $AlPO_4$-5 as well as SAPO-5 with

varying silicon substitution in the framework lattice of AlO_2^-, PO_2^+ tetrahedra has been investigated. The basic raw materials used for the synthesis of these materials are, orthophosphoric acid, pseudoboehmite, aluminium isopropoxide, microfine silica, ethylorthosilicate, chloride or nitrates of cobalt, zinc, magnesium and iron. Tetrapropyl ammonium hydroxide, tripropyl- and triethylamine were initialy examined as organic structure directing agents. On account of low cost and easy availability, triethylamine was selected as a template for detailed studies. The influence of the composition, reaction period and temperature on the kinetics of nucleation and crystallization as well as the purity of the alumino phosphate phases has been explored.

The crystalline $AlPO_4$-5 molecular sieves were prepared by heating the aluminophosphate gel compositions prepared by mixing aqueous solutions of phosphoric acid, a source of alumina (pseudo-bochmite or aluminium isopropoxide) and the templating agent. The mixture was heated at 375 to 475 K for 24 to 48 hours under hydrothermal conditions. The most suitable gel composition was found to be 1.5 R, 1.0 Al_2O_3, 1.0 + 0.2 P_2O_5, 40-60 H_2O where R represents the organic templating agent. The optimum crystallization period and temperature were in the range 24 to 48 hrs and 423 to 473 K respectively. The reaction temperature and time play significant role in the crystallization process. Increase in the crystallization temperature above 473 K and crystallization period above 48 hrs leads to the formation of dense phase alumino-phosphates structurally similar to tridymite crystobalite and

hydrated $AlPO_4$-xH_2O. At temperatures lower than 423 K and crystallization period less than 10 hrs, the $AlPO_4$-5 samples were contaminated with unreacted boehmite or amorphous $AlPO_4$ and other unidentified impurity phases. The pH of the gel mix also plays important role.

The temperature dependence of the rate of nucleation and crystallization were analysed by employing the well known rate equations and the activation energy for nucleation (E_n) and that for crystallization (E_c) were evaluated. The values of E_n and E_c for the synthesis of SAPO-5 were higher than the corresponding values for the formation of $AlPO_4$-5 molecular sieves.

The synthesized samples were characterized by the x-ray diffraction (XRD), scanning electron microscopy (SEM), thermal analysis (DTA/TG), sorption of probe molecules (H_2O, n-hexane, cyclohexane), TPD of (NH_3), IR spectroscopy and catalytic reactions for hydrocarbon conversions.

The XRD was used for the identification and purity of the crystalline phases formed. The XRD pattern was similar to that reported in literature. the scanning electron micrographs of $AlPO_4$-5 exhibit a well defined hexagonal shaped crystals, while those for modified AlPOs consist of a mixture of hexagonal barrels, hexagonal plates and a few ill-defined crystals.

The thermoanalytical curves DTA/TG show that the decomposition of organic template occluded in the channels of modified AlPOs occurs in two stages, the the DTA exhibiting two exothermic peaks at 653 and 713 K. This indicates that the template mole-

cules exist in two different energetic states in the pores of SAPO-5 and MeAPO-5. The AlPO-5 on the other hand, shows only one exotherm. The amount of triethylamine estimated from the TG curve is about 0.1 cc g^{-1} of the pore volume. The activation energy for the desorption of zeolitic water (E_d) determined by Coats-Redfurn equation is 42.8 KJ $mole^{-1}$ for $AlPO_4$-5, and is comparable to the value reported for ZSM-5 zeolite. This shows that the $AlPO_4$-5 is moderately hydrophilic, the adsorbed water forming coordinate bonds with the polarised channel walls. The values of E_d for SAPO-5 samples containing 0.09, 0.2, 0.29 and 0.39 mole fractions of Si were 49.0, 50.4, 54.2 and 56.9 KJ $mole^{-1}$ respectively. The higher values for the SAPO-5 samples are attributed to increase in the anionic charge of the framework. In the case of Mg, Zn, Co and Fe modified AlPOs, the values of E_d are 55.4, 49.7 and 48.5 KJ $mole^{-1}$ respectively. The thermal analysis of the samples suggest that Si, Mg, Zn, Co and Fe are incorporated in the framework of aluminophosphates.

The physical adsorption of nitrogen at 77 K was used for estimating the surface areas and the % crystallinity of the synthesised samples. The sorption data are analysed by using the Langmuir, BET and Dubinin-Radhuskevich (D-R) equations. It has been found that the Langmuir equation gives better results than the BET equation. The pore volumes evaluated by employing the (D-R) equation shows linear relation with the % crystallinity of the samples. The affinity coefficinets for water estimated from the adsorption isotherms for water show an increase with increas

-ing Si substitutiion in the SAPO-5 samples. This has been attributed to the increase in the anionic charge on the framework lattice and therefore to the specific interaction of water with the framework. The pore volume estimated from the sorption of water (0.29 cc g^{-1}) is higher than that determined from the sorption of n-hexane (0.136 cc/g). Due to difference in the molecular size, smaller water molecules can enter the smaller pores while larger n-hexane molecules are excluded. The sorption properties of Mg, Co, Zn and Fe modified MeAPO-5 showed similar results.

The IR spectrum of $AlPO_4$-5 exhibits several bands in the 1300-200 cm^{-1} region due to fundamental vibrations of the different framework units. The band at 1140 cm^{-1}, due to Al-O-P asymmetric stretching vibration shifts to the higher frequency on Si substitution and to the lower frequency on Mg, Zn, Co and Fe substitution in the $AlPO_4$-5 framework. The intensity of the band at 560 cm^{-1}, attributed to the double ring vibrations increases with increasing the % crystallinity of the sample estimated from the XRD pattern.While the IR spectrum of Et_3N occluded in $AlPO_4$-5 channel was almost identical to that of pure Et_3N, that of Si and Me substituted $AlPO_4$-5 showed characteristic features of strong hydrogen bonded and protonated species ($Et_3\overset{+}{N}H$). On removal of Et_3N by oxidative decomposition, the $AlPO_4$-5 showed weak bands at 3800, 3740 and 3670 $^{-1}$. SAPO-5 on the other hand , exhibits additional strong bands at 3620 and 3525 cm^{-1}, which have been assigned to the fundamental stretching vibrations of P-OH, Al-OH

and Si-O-Al groups respectively.The origin of the above hydroxyl bands has been atributed to the removal of protonated triethyl -amine (Et_3NH) species from the channels of SAPO-5. The comparison with the IR bands of HY zeolite suggested that the OH groups exhibiting the bands at 3620 and 3525 cm^{-1} are situated in the 12 and 6 membered ring channels respectively. The MeAPO-5 samples showed only one broad band at about 3520 cm^{-1} which may be due to two overlapping bands.

The adsorption of D_2O, benzene and pyridine show that the OH groups in the $AlPO_4$-5 are due mostly to weak Lewis acid sites, whereas the SAPO-5 and MeAPO-5 exhibit the presence of both Brönsted and Lewis acid sites, their strength being intermediate between those of HY and HZSM-5 zeoalites.

The $AlPO_4$-5 sample showed only one sharp TPD (NH_3) peak with T_{max} at 373 K. The apparent activation energy for the desorption of NH_3 estimated from the heating rate variation was 47 KJ $mole^{-1}$ for $AlPO_4$-5. The SAPO-5 smaples showed three TPD(NH_3) peaks with T_{max} at 373, 463 and 593 K indicating the presence of three types of sites with different acid strengths. The apparent activation energy for the desorption of NH_3 are 55, 70 and 87 KJ $mole^{-1}$ respectively. The TPD of MeAPO-5 samples did not exhibit large number of strong acid sites.

The activity of the various aluminophosphate samples have been studied for o-xylene isomerization, h-hexane cracking and toluene methylation in order to correlate the influence of surface acidity with their catalytic activity. At 723 K and WHSV

4.4, the % conversion of o-xylene on $AlPO_4$-5, FeAlPO-5, CoAlPO-5, SAPO-5, ZnAlPO-5 and MgAlPO-5 was 5.5, 22.9, 24.5, 31.2, 45.3 and 77.5 respectively. Associated dealkylaation and disproportionation also increased in the same order. P-xylene selectivity was higher for metal substituted $AlPO_4$-5 samples. The isomerization increased linearly with the number of medium + strong acid sites estimated from the TPD(NH_3) data on SAPO-5 samples. The conversion of o-xylene increased with the temperature and decreased with the increase in the WHSV as expected. The activation energy values calculated from pseudo-first order kinetic equation $K = F/W \ln [1/(1-x)]$ were 40.3, 43.7, 64.9, 66.7, 68.2 and 73.4 KJ $mole^{-1}$ for AlPO4-5 and Fe, Zn, Si, Co and Mg modified samples respectively. The deactivation constant α, evaluated from the equation $K = K_o e^{\alpha y}$ decreased with the increase in the temperature for the SAPO-5 catalysts. Depending on the activity of the catalyst the amount of coke in the samples varied from 0.5 to 3.5 %.

The activity of the catalyst samples for n-hexane cracking at 3.3 WHSV was studied in the temperature range of 573 to 823 K. The conversion on SAPO-5(IV) increased from 6.5 to 15.6 % when the temperature was increased from 573 to 823 K with simultaneous increase in the formation of C_3, C_4 paraffins in the product. The values of apparent activation energy for the n-hexane cracking on $AlPO_4$-5 and SAPO-5(IV) were 5.65 and 7.0 KJ $mole^{-1}$ repsectively. The MeAlPO-5 samples showed higher activities than the $AlPO_4$-5 or SAPO-5 samples. It may be suggested that the n-hexane cracking occurs via carbonium ion mechanism.

The toluene methylation was studied at 723 K and 3.68 WHSV and toluene:methanol ratio 5:1 over SAPO-5, CoAlPO-5 and MgAlPO-5 catalysts. The convesion with respect to methanol was 100 % and that with respect to toluene was 12.2, 6.2 and 17.6 respectively on SAPO-5, Co and Mg substituted $AlPO_4$-5. The selectivity to p-xylene was not significant initially and was enhanced by coking of the catalyst. The product distribution followed the known mechanism for the acid catalysed toluene alkylation via electrophilic substitution.

The isomorphous substitution of dvivalent or trivalent atoms for Al in the $AlPO_4$-5 gives rise to anionic or neutral framework. Similarly, the substitution of P by M^{4+} leads to anionic sites in the framework. The nature of OH groups thus created depends on the charge on the proton which can be calculated by Sanderson's electronegativity or from electrostatic forces. The electronegativity difference resulting on the substitution of Mg, Zn, Co, Si and Fe in the $AlPO_4$-4 framework is 0.83, 0.40, 0.36, 0.27 and 0.17 respectively. The charge on the proton resulting from such substitution is expected to follow the same trend. The results reported on the IR, TPD and catalytic activity data are in agreement with these expectations.

CONCLUSIONS

1. The experimental parameters for the synthesis of pure single phase alumino phosphate molecular sieves and the substituted samples have been established.

2. The kinetic parameters for the hydrothermal synthesis have been evaluated and reported for the first time.

3. The role of polarised and protonated triethylamine species in the synthesis of these molecular sieves is clearly illustrated.

4. The nature of OH groups and the acid strength distribution in $AlPO_4$-5, SAPO-5 and MeAPO-5 samples are characterized in detail by combination of FTIR, TPD and thermogravimetric techniques for the first time.

5. The carboniogenic activity of the SAPO and MeAPO-5 samples are exemplified from the study of o-xylene isomerization, n-hexane cracking and toluene methylation reactions.